TECHNISCHE UNIVERSITÄT MÜNCHEN

Fakultät für Medizin

Forschungszentrum für krebskranke Kinder

Klinik und Poliklinik für Kinder- und Jugendmedizin

Functional characterization of the protein STEAP1 for the development of specific biomarkers and targeted therapeutics for Ewing tumors

Dr. med. Thomas Georg Philipp Grünewald

Vollständiger Abdruck der von der Fakultät für Medizin der Technischen Universität München zur Erlangung des akademischen Grades eines

Doctor of Philosophy (Ph.D.)

genehmigten Dissertation.

Vorsitzender: Univ.-Prof. Dr. Florian R. Greten

Prüfer der Dissertation:

1. Univ.-Prof. Dr. Stefan Burdach
2. apl. Prof. Dr. Achim Krüger

Die Dissertation wurde am 12.06.2012 bei der Fakultät für Medizin der Technischen Universität München eingereicht und durch die Fakultät für Medizin am 21.08.2012 angenommen.

For my wife, Barbara

1 Introduction

1.1 Ewing tumor nosology and epidemiology

Ewing tumors (ET) comprise the second most common group of bone and soft tissue sarcomas in children and young adults after osteosarcomas (incidence about 3.2 in $1x10^6$ under the age of 15) [1, 2]. The American pathologist James Ewing initially described this entity in 1921 as "diffuse endothelioma of the bone" [3]. Although ET indeed display, besides a neuroectodermal, an abrogated endothelial differentiation [4], their precise histogenesis is still enigmatic [5]. This is also reflected by the fact that albeit ET commonly arise in bones, they may as well arise at any other site of the body, arguing against a pure osseous histogenesis [5].

Clinically, ET are highly metastatic sarcomas that feature about 25% rates of metastasis at primary diagnosis [2, 6]. Although great advances in the treatment of localized disease have been achieved in past decades [7], established therapies still have limited success in advanced stages of the disease despite high toxicity [2, 8].

As a unifying hallmark all ET express chimeric EWS/ETS (Ewing sarcoma breakpoint region 1 / E-twenty-six) fusion proteins derived from chromosomal translocations, with EWS/FLI1 (Ewing sarcoma breakpoint region 1 / friend leukemia virus integration 1) being the predominant one (85%) [9-11]. *EWS/FLI1* encodes an oncogenic transcription factor that determines the complex and highly malignant phenotype of ET [4].

Even though there is still an ongoing debate whether ET might arise from neural crest-derived mesenchymal stem cells (MSCs) [12], recent transcriptomic and functional evidence suggests that ET most likely descend from a mesoderm-derived mesenchymal progenitor cell possibly providing ET with stem cell features [13, 14]. In accordance, apart from human primary fibroblasts, murine and human MSCs are to date the only cells to be found that tolerate the artificial expression of the EWS/FLI1

oncoprotein [15, 16]. However, EWS/FLI1 expressing MSCs do not fully transform into ET [15, 17, 18], suggesting that additional factors might be necessary to create, apart from mere cellular survival, a "permissive milieu" that fully enables malignant transformation.

Although experimental inactivation of classical tumor suppressor genes like p53 and p16 in primary cells can induce tolerance to EWS/FLI1 [19, 20], genetic mutations in these tumor suppressors are present in only a small fraction of clinical ET (about 10%) [20, 21]. Thus, alternate mechanisms of tumor suppressor gene inactivation may exist in the “true” ET cell of origin.

One appealing concept is that there might be underlying genetic variants in specific genes in a minority of individuals that ultimately create such a permissive milieu for the establishment of the EWS/FLI1-induced oncogenic transformation [22].

In line with this idea are strong epidemiological data proving that the incidence of ET is up to ten times higher in European Caucasians compared to African and Asian populations [23-26]. Similar findings have been obtained from the recent analysis of the US National Cancer Institute (NCI) Surveillance Epidemiology and End Results (SEER) database, which are reinforced by the observation of cumulative ET incidence in relatives, especially in twins, and the fact that ET incidence is not modified among migrated populations [27-29] (for review see [22] and references therein).

Of note, a recent genome-wide association study could identify three individual genomic regions on chromosomes 1, 10, and 15 harboring single-nucleotide polymorphisms that are strongly associated with the onset of ET [30]. As ET do not appear to be a component of known cancer susceptibility syndromes, these potentially underlying genetic risk alleles or variants, which possibly set the stage for full EWS/FLI1-mediated oncogenic transformation, may alter the function of hitherto unknown cancer predisposition genes, which are possibly relevant for tumorigenesis of other malignancies, too [22, 30].

1.2 Clinical and biological markers for outcome prediction

Combined modality treatment is crucial for successful therapy of patients with ET [31]. Various studies have identified metastatic state, tumor volume, tumor site, age, gender, and histological response to chemotherapy as major risk factors, with primary metastasis as the most unfavorable one [31-34]. Although there is agreement that clinical management will benefit from biological markers that can guide therapeutic decisions [34], currently available biomarkers for ET are very limited [33-35]. In fact, apart from the proliferation marker Ki67 [36], there is no robust immunohistological marker for outcome prediction of ET patients [32, 33].

As mentioned above, all ET are defined by *EWS/ETS* translocations [10] encoding aberrant transcription factors that are necessary to initiate and drive this disease [4]. Even though different variants of EWS/ETS fusion proteins exist, they fail to provide robust biomarkers for individual risk stratification [11, 37].

Nevertheless, the discovery of novel biomarkers that have prognostic and/or predictive value would potentially lead to a better understanding of tumor heterogeneity, allow individual risk stratification and ultimately serve as guidance for the development and personalized use of targeted therapeutics [38-40].

1.3 Targeted therapy of Ewing tumors

While multimodal treatment of ET has been improved dramatically in past decades, metastatic ET are still associated with dismal prognosis and can only rarely be cured by conventional highly toxic therapies [8]. Hence, the development of more potent and in particular more specific drugs is a prerequisite to reduce the toxic burden of cure [41].

To date, numerous studies have been carried out to identify ET specific proteins and pathways that might yield *bona fide* drug targets for a specific anti-ET therapy [4, 42].

For instance, various studies have pointed out the impact of EWS/FLI1 on the activation of the insulin-like growth factor 1 (IGF1) pathway, suggesting that targeting this pathway may have therapeutic potential [43, 44]. Moreover, Erkizan *et al.* recently showed that a small-molecule compound that specifically interferes with the heterodimerization of EWS/FLI1 and the RNA helicase A significantly slows, but not completely prevents ET growth [45]. Although these data are certainly promising, much more work is needed to develop additional strategies for targeted therapy of ET.

Another approach, apart from the direct targeting of *EWS/FLI1*, is to search for specifically expressed proteins, which are possibly transcriptional targets of EWS/FLI1, and that might constitute promising novel drug targets due to their localization at the plasma membrane and, hence, surface of ET cells. Moreover, the detailed functional characterization of the EWS/FLI1-induced transcriptome may be key to understand the underlying mechanisms of the disease and ultimately to halt its progression [4, 46].

Previously, Staege *et al.* identified a specific expression signature of 37 genes that are highly up-regulated in ET compared to benign tissues [4]. Part of this signature is the six-transmembrane epithelial antigen of the prostate 1 (STEAP1) – a membrane-bound protein possibly contributing to transmembrane electron transfer [47, 48].

1.4 Current state of knowledge on STEAP1

The discovery of the six-transmembrane epithelial antigen of the prostate 1 (STEAP1) as a prostate-specific cell-surface antigen highly expressed in prostate carcinoma and many other cancers in 1999 and the subsequent identification of three other STEAP proteins (STEAPs) initiated a rapidly expanding research field [48].

The human STEAP family contains at least four homologous proteins (STEAP1, -2, -3, and -4). All STEAPs share a characteristic transmembrane region that is flanked by intracellular amino- and carboxy-terminal domains. This domain architecture is

reminiscent of channel- and/or transporter-proteins [49-52]. At their N-termini, STEAPs are highly homologous to archaeal and bacterial F420:NADPH oxidoreductases (FNO) and to human NADPH oxidoreductases (NOX) such as NOX1 [49-52]. This FNO-like domain is predicted to enable STEAPs to bind flavins as electron donors for their oxidoreductase activity [49, 50]. Accordingly, in close vicinity to the FNO-like domain, STEAPs share a structural GXGXXG/A motif (Rossman-fold), which is found in proteins that bind nucleotides like nicotinamide adenine dinucleotide (NAD) and flavin mononucleotide (FMN) [49, 50]. The absence of these domains in STEAP1 is believed to cause its deficient metalloreductase activity, which was so far reported for STEAP2, -3, and -4 [49, 50].

In addition, all STEAPs share a striking similarity at their C-terminal ends to the transmembrane domains of the yeast FRE metalloreductases, which have heme-binding capabilities and are involved in electron transfer chains [49-52] (Figure 1). This domain forms a ferric oxidoreductase (amino acids 118-265 in STEAP1), which is why a general role of STEAPs in cellular iron homeostasis is assumed [49, 53]. However, in contrast to STEAP2, -3, and -4, STEAP1 does not facilitate iron uptake and reduction, suggesting another distinct function [50, 53].

STEAP1 (alias STEAP) is the founding member of the STEAP family [48]. STEAP1 is a six-transmembrane protein of 339 amino acids in length (Uniprot-ID: Q9UHE8) encoded by a single gene on chromosome 7q21.13 (RefSeq: NM_012449, exon count: 5; coding exon count: 4) [48]. The N- and C-termini of STEAP1 are both located within the cytoplasm and the six transmembrane domains are ordered in a ring-like structure possibly allowing STEAP1 to act as a channel-protein [47, 48, 50, 51]. The third and fifth transmembrane domain of STEAP1 contain each an evolutionarily conserved histidine residue (H175 and H268, respectively), which are predicted to act as heme-binding motifs (Figure 1).

Among STEAPs, especially STEAP1 (and to a far lesser extent STEAP2 and -4) are overexpressed in many carcinomas including prostate, breast, and bladder cancer, where they locate to plasma and endosomal membranes [48, 50]. However, their precise cellular function remains elusive.

Recently, STEAP1 was validated as an excellent marker for MSCs [54] supporting the relationship of ET to MSCs [13]. Moreover, mRNA of STEAP1 circulates in peripheral blood of cancer patients [55] and its detection in bone marrow of ET patients is indicative for occult ET cells [56]. In contrast, STEAP1 mRNA is not detectable in blood of healthy donors and is only minimally expressed in normal tissues, except for low amounts in urothelium and prostate [48, 55, 57].

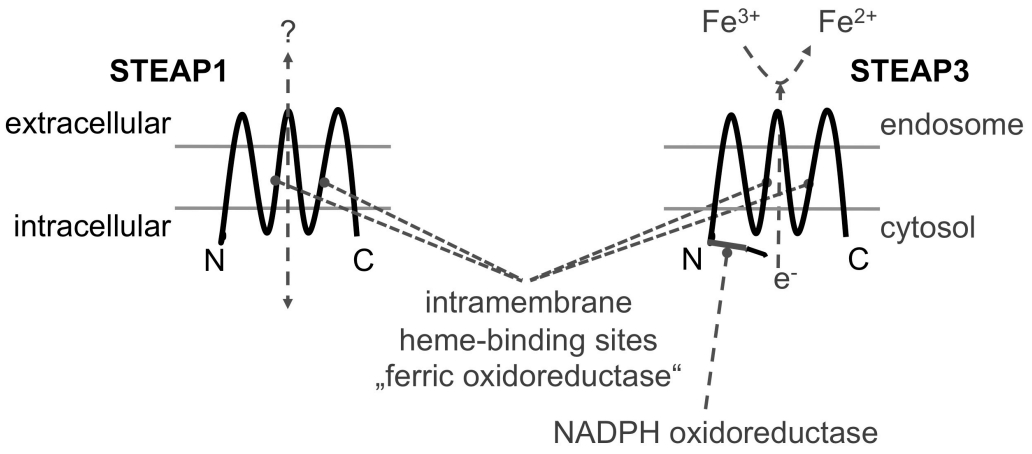

Figure 1: STEAP1 in comparison to STEAP3:
Both proteins locate to membranes, with STEAP1 being predominantly located at the plasma membrane, whereas STEAP3 predominantly locates to endosomal membranes. In both proteins the C- and N-termini are placed within the cytoplasm. STEAP1 and -3 contain intra-membranous heme binding-sites constituting the ferric oxidoreductase. However, STEAP1 lacks the NADPH oxidoreductase present in other STEAPs such as STEAP3.

Due to its high tumor-specificity and membrane-bound localization, STEAP1 might serve as a promising candidate for targeted therapy [48, 55, 56]. In accordance, monoclonal antibodies against STEAP1 were reported to inhibit growth of xenografted prostate and bladder cancer cells in mice [58]. Moreover, STEAP1 has been used as a novel immunotherapeutic target for various carcinomas *in vitro* and *in vivo* [59-65].

Interestingly, STEAPs are homologs of NOX [51, 52], which are involved in cellular ROS (reactive oxygen species) metabolism and frequently overexpressed in highly proliferative cancers [66]. Consistently, a recent study of Pan *et al.* could demonstrate that artificial overexpression STEAP1 in thyroid epithelial cells increases their proliferation and intracellular ROS levels [67], suggesting a role of STEAP1 in cellular ROS metabolism.

1.5 The dual role of reactive oxygen species in cancer

ROS are naturally occurring byproducts of normal cellular metabolism [68] and important mediators in physiological cell signaling [69], differentiation and organ development [70, 71]. However, increased ROS levels expose cells and organisms to oxidative stresses, which activate a variety of mechanisms enabling them to cope with these changes [72].

The study of ROS in cancer has been subject of intensive research for decades: multiple studies proved that oxidative stress conditions play important roles in initiation, promotion and progression of many malignancies e.g. by regulating DNA synthesis, enhancers, transcription factors, and cell cycle regulators [73, 74]. Accordingly, other studies demonstrated a possible beneficial effect of (nutritional) antioxidants in cancer prevention, which is still matter of controversial debates (for review see [75] and references therein).

Owing to these numerous studies it is becoming increasingly clear that ROS are indeed intimately involved in oncogenic signaling and that elevated ROS levels are a salient feature of highly invasive cancers [76, 77], possibly including ET [78]. Mounting evidence suggests that many malignancies take advantage of a permanently active oxidative stress phenotype leading to increased invasiveness, which has been recognized as an additional hallmark of cancer [79]. Moreover, recent data

demonstrate that ROS are produced in a highly site-specific manner within a given cellular compartment and that ROS can oxidize signaling proteins at defined residues, thereby initiating and/or facilitating further downstream signaling, e.g. by protein phosphorylation [80]. These specific effects of ROS are mediated in large part by covalent post-translational modifications of cysteine residues within redox-sensitive proteins [73]. In synopsis, although ROS have been historically regarded as mere unspecific and potentially harmful byproducts of cell metabolism, they are now viewed as rather specific and essential components of signaling cascades [81], which may be malfunctioning in cancer.

These oncogenic effects of ROS seem to operate in a highly dose-dependent fashion: while low or intermediate ROS levels are very effective in triggering mutagenesis and proliferation of cancer cells, high levels of oxidative stress may inhibit proliferation and can have cytotoxic effects [74]. In this regard, endogenously elevated levels of ROS may also represent the “Achilles’ heel” of cancer cells, because ROS are well known to be potent intrinsic radio- and chemosensitizers [82-84]. This concept has been recently proven in ovarian cancer [85]. Cancer cells with elevated ROS levels are particularly vulnerable to irradiation and other oxidizing agents [82, 84], which possibly might apply to ET since these sarcomas are highly sensitive to irradiation as compared to e.g. neuroblastoma or osteosarcoma [86].

In accordance, there are several experimental approaches under investigation trying to increase oxidative stress selectively in cancer cells prior to treatment with ROS-dependent therapeutics (tumor-targeted induction of oxystress for cancer therapy; also referred to as “oxidation therapy”) [74]. However, it is challenging to specifically enhance ROS-production in cancer cells and to keep ROS – once they are specifically produced – within tumor cells.

Therefore, other approaches aim to identify critical factors that contribute to excess ROS-production, which are *a priori* overexpressed in certain cancer entities [74]. The

knowledge about these intrinsic ROS-enhancers, especially if they constitute robust biomarkers, may provide new avenues for the design of personalized anti-tumor strategies based on ROS-dependent therapeutics.

2 Research objectives and scientific aims

2.1 Research objectives

Based on its homology to NOX, its possible association with ROS metabolism, and its overexpression in highly metastatic cancers, the underlying hypothesis of this Ph.D. thesis was that STEAP1 is involved in the invasive behavior and oxidative stress phenotype of ET. In the present study the author investigated the putative oncogenic function of STEAP1 *in vitro* and in a preclinical xenotransplantation model *in vivo* to assess the endogenous effects of STEAP1 on the ET phenotype.

Moreover, the author performed a retrospective tissue microarray (TMA) study to assess whether STEAP1 protein expression can serve as an immunohistological marker for outcome prediction of ET patients. In addition, this patient study aimed to explore intertumor heterogeneity and expression patterns concerning STEAP1 and whether STEAP1 expression status of the primary pre-treatment ET enables prediction on tumor response to therapy.

2.2 Scientific aims

1) Assessment of specificity of STEAP1 mRNA and protein expression in ET

2) Assessment of the mode of STEAP1 regulation and its potential dependency on EWS/FLI1 expression

3) Evaluation of the impact of STEAP1 on the phenotype of ET cell lines *in vitro*

4) Analysis of the impact of STEAP1 on the phenotype of ET cells in a xenograft model

5) Exploration of the STEAP1 expression pattern in clinical ET samples

6) Correlation of STEAP1 expression in ET with clinicopathological parameters

7) Interpretation and discussion of results and generation of consequential hypotheses for future research on STEAP1 in ET

3 Materials and methods

3.1 Materials

3.1.1 List of manufacturers

Manufacturer	Location
Abcam	Cambridge, UK
Abgent	San Diego, California, USA
AEG	Nürnberg, Germany
Ambion	Austin, Texas, USA
Amersham Biosciences	Piscataway, New Jersey, USA
Applied Biosystems	Darmstadt, Germany
ATCC	Rockyville, Maryland, USA
Autoimmun Diagnostika	Strassberg, Germany
B. Braun Biotech Int.	Melsungen, Germany
Bayer HealthCare Pharmaceuticals	Leverkusen, Germany
BD Biosciences Europe	Heidelberg, Germany
Beckman Coulter	Palo Alto, California, USA
Becton Dickinson (BD)	Heidelberg, Germany
Berthold detection systems	Pforzheim, Germany
Biochrom	Berlin, Germany
Biometra	Göttingen, Germany
BioRad	Richmond, California, USA
Biosource	Nivelles, Belgium
Biovision Research	Mountain View, California, USA
Bio Whittaker	East Rutherford, New Jersey, USA
Biozym	Hess. Olendorf, Germany
Branson	Dietzenbach, Germany
Carestream Health Inc.	Stuttgart, Germany
Cayman Chemical Company	Ann Arbor, Michigan, USA
Cell Signaling Technology	Frankfurt a. M., Germany
Covance Inc.	Munich, Germany
Dako Pathology Products	Hamburg, Germany

Dionex	Idstein, Germany
DSMZ	Braunschweig, Germany
Eppendorf	Hamburg, Germany
Falcon	Oxnard, California, USA
Fermentas	St. Leon-Rot, Germany
GE Healthcare	Freiburg, Germany
Genomed	St. Louis, Missouri, USA
Genzyme	Neu-Isenburg, Germany
GFL GmbH	Burgwedel, Germany
GLW	Würzburg, Germany
Greiner	Nürtingen, Germany
Heidolph Instruments	Schwabach, Germany
Heraeus	Hanau, Germany
IBM Corporation	Armonk, New York, USA
ImaGenes GmbH	Berlin, Germany
Invitrogen	Karlsruhe, Germany
Jackson ImmunoResearch Laboratories	Baltimore, Maryland, USA
Kawasaki	Kanagawa, Japan
Leica	Wetzlar, Germany
Lonza	Basel, Switzerland
Mabtech	Hamburg, Germany
Macherey-Nagel	Düren, Germany
MatrixScience	London, UK
Merck	Darmstadt, Germany
Millipore	Billerica, Massachusetts, USA
Miltenyi Biotec GmbH	Bergisch Gladbach, Germany
Molecular BioProducts, MbP	San Diego, California, USA
Nalgene	Rochester, New York, USA
New England BioLabs	Frankfurt a. M., Germany
New Objective	Woburn, Massachusetts, USA
Nikon	Düsseldorf, Germany
Nunc	Naperville, USA

PAA	Cölbe, Germany
Pan Biotech GmbH	Aidingen, Germany
Pechiney Plastic Packaging	Menasha, Wisconsin, USA
Peske OHG	Munich, Germany
Phenomenex	Aschaffenburg, Germany
Philips	Hamburg, Germany
Promega	Madison, Wisconsin, USA
Qiagen	Chatsworth, California, USA
R&D Systems	Minneapolis, Minnesota, USA
Roche	Mannheim, Germany
Roche/ACEA Biosciences	San Diego, California, USA
(Carl) Roth	Karlsruhe, Germany
Santa Cruz Biotechnology	Heidelberg, Germany
Sartorius	Göttingen, Germany
SAS Institute	Cary, North Carolina, USA
Schleicher und Schüll	Dassel, Germany
Scientific Industries	Bohemia, New York, USA
Sempermed	Vienna, Austria
Sigma	St. Louis, Missouri, USA
Stratagene	Cedar Creek, Texas, USA
Syngene	Cambridge, UK
Takara Bio Europe	Saint-Germain-en-Laye, France
Teca	Crailsheim, Germany
Tecan	Männedorf, Switzerland
Thermo Scientific	Braunschweig, Germany
TKA GmbH	Niederelbert, Germany
TPP	Trasadingen, Switzerland
Thermo Fisher Scientific	Ulm, Germany
Ventana Medical System	Tucson, Arizona, USA
Whatman	Dassel, Germany
Zeiss	Jena, Germany

3.1.2 General materials

Material	Manufacturer
Cryovials	Nunc
Culture plates (100 mm ∅)	Nunc
Cuvettes	Roth
Filters for cells, cell strainer	Falcon
Filters for solutions (0.2 and 0.45 µm)	Sartorius
Flasks for cell culture (75 and 175 cm^2)	TPP
Flasks for cell culture (75 and 175 cm^2)	Falcon
Gloves (nitrile, latex)	Sempermed
Hybond-P PVDF membrane	GE Healthcare
Hypodermic needle (23 and 30G)	B. Braun Biotech Int.
Parafilm	Pechiney Plastic Packaging
Pasteur pipettes	Peske OHG
Petri dishes	Falcon
Pipettes (2, 5, 10 and 25 ml)	Falcon
Pipette tips (10, 200 and 1,000 µl)	MbP
Pipette filter tips (10, 200 and 1,000 µl)	Biozym
Plates for cell culture (6-, 24- and 96-well)	TPP
Scalpels (No. 12, 15, 20)	Feather
Tubes for cell culture (polystyrene, 15 ml)	Falcon
Tubes for cell culture (polypropylene, 15 and 50 ml)	Falcon
Tubes for molecular biology, Safelock (1.5 and 2 ml)	Eppendorf
Tubes for flow cytometry (5 ml)	Falcon
Whatman paper	Whatman

3.1.3 Instruments and equipment

Device	Specification	Manufacturer
Bacteria shaker	Certomat BS-T	Sartorius
Ice maker	AF 100	Scotsman

Cell counting chamber	Neubauer	Brand
Centrifuge	Multifuge 3 S-R	Heraeus
Centrifuge	Biofuge fresco	Heraeus
Controlled-freezing box	Mr. Frosty	Nalgene
Electroporator	Gene Pulser Xcell™	BioRad
Electrophoresis chamber		BioRad
ELISA reader	Multiskan Ascent	Thermo Scientific
ELISpot reader	AID-ELIRIFL04	Autoimmun Diagnostika
Flow cytometer	FACScalibur™	Becton Dickinson
Freezer (-80°C)	Hera freeze	Heraeus
Freezer (-20°C)	cool vario	Siemens
Fridge (+4°C)	cool vario	Siemens
Gel documentation	Gene Genius	Syngene
Incubator	Hera cell 150	Heraeus
Liquid nitrogen reservoir	L-240 K series	Taylor-Wharton
Luminometer	Sirius Luminometer	Berthold detection systems
Multichannel pipette	(10-100 µl)	Eppendorf
Heating block	Thermomixer Comfort	Eppendorf
Micropipettes	(0.5-10 µl, 10-100 µl, 20-200 µl, 100-1,000 µl)	Eppendorf
Microplate reader	Safire	Tecan
Microscope (fluorescence)	AxioVert 100	Zeiss
Microscope (electron)	Philips CM 10	Philips
Microscope	Nikon Eclipse TS100	Nikon
Microwave oven		Siemens, AEG
PCR cycler	iCycler	BioRad
Pipetting assistant	Easypet	Eppendorf
Power supplier	Standard Power Pack P25	Biometra
Rotator		GLW
Semi-dry transfer apparatus	Fastblot	Biometra

SDS-PAGE chamber	Minigel-Twin	Biometra
Shaking incubator		Eppendorf
Shaker	Polymax 2040	Heidolph Instruments
Spectrophotometer	GeneQuant II	Amersham Biosciences
Sterile bench		Heraeus
Sonifier	Digital Sonifier®	Branson
Water bath		GFL GmbH
Western blot documentation	Gel Logic 1500 imaging sytem	Carestream Health, Inc.
Real-time PCR	7300 Real-Time PCR	Applied Biosystems
Vortexer	Vortex-Genie 2	Scientific Industries
Water purification system	TKA GenPure	TKA GmbH

3.1.4 Chemical and biological reagents

Chemical/reagent	**Manufacturer**
Agar	Sigma
Agarose	Invitrogen
Ampicillin	Merck
AmpliTaq DNA Polymerase	Invitrogen
Ammonium persulfate (APS)	Sigma
β-mercaptoethanol	Sigma
BCP (1-bromo-3-chloropropane)	Sigma
BenchMark™ Prestained Protein Ladder	Invitrogen
BHA (butylated hydroxyanisole)	Sigma
Blue Juice Gel Loading Buffer	Invitrogen
Bradford reagent	BioRad
Calcein AM	Merck
Crystal violet	Sigma
DEPC (diethylpyrocarbonate)	Sigma
Deoxycholic acid	Roth
Dihydroethidium (DHE)	Invitrogen

Dimethylformamide	Roth
dNTPs	Roche
DMEM medium	Invitrogen
DMSO (dimethyl sulfoxide)	Merck
DTT (DL-dithiothreitol)	Sigma
EDTA (ethylenediaminetetraacetate)	Merck
EtBr (ethidium bromide)	BioRad
Ethanol	Merck
FBS (fetal bovine serum)	Biochrom
Formaldehyde (37%)	Merck
Gentamicin	Biochrom
Glycerol	Merck
Glycine	Merck
G418	PAA
HBSS (Hank's buffered salt solution)	Invitrogen
HCl (hydrochloric acid)	Merck
HEPES	Sigma
Hering sperm DNA, denaturated	Sigma
HiPerFect Transfection Reagent	Qiagen
Human IgG	Genzyme
Isopropanol	Sigma
KCl (potassium chloride)	Merck
L-glutamine	Invitrogen
Matrigel Matrix	BD Biocoat
Maxima™ Probe / ROX qPCR Master Mix (2x)	Fermentas
Metaphosphoric acid	Sigma
Methanol	Roth
Methylcellulose	R&D Systems
$MgCl_2$ (magnesium chloride)	Invitrogen
$NaHCO_3$ (sodium hydrogen carbonate)	Merck
NaN_3 (sodium azide)	Merck
NaOH (sodium hydroxide)	Merck

Nonidet-P40 (NP40)	Sigma
PBS 10x (phosphate buffered saline)	Invitrogen
PCR buffer (10x)	Invitrogen
Peptone	Invitrogen
PFA (paraformaldehyde)	Merck
Polyacrylamide (30% acrylamide/Bis)	Merck
Polybrene (hexadimethrine bromide)	Sigma
Propidium iodide	Sigma
Puromycin	PAA
Ready-Load 1.0 and 0.1 Kb DNA Ladder	Invitrogen
RPMI 1640 medium	Invitrogen
SDS (sodium-dodecylsulfate)	Sigma
Skim milk powder	Merck
Sodium chloride (NaCl)	Merck
TEMED (N,N,N′,N′-tetramethylethan-1,2-diamin)	Sigma
Triethanolamine	Sigma
Tris	Merck
Triton X-100	Sigma
Trypan-Blue	Sigma
Trypsin / EDTA	Invitrogen
Tween 20	Sigma
2-vinylpyridine	Sigma

All reagents were purchased from Sigma (Deisenhofen, Germany) if not otherwise specified.

3.1.5 Commercial reagent kits

Name	Manufacturer
Annexin V-PE Apoptosis Detection Kit I	BD Biosciences
Biovision Iron Assay Kit	Biovision Research
Cell Invasion Assay	BD Biosciences
DNeasy® Blood & Tissue Kit	Qiagen

ECL-Plus Western blot Detection System	GE Healthcare
EndoFree Plasmid Kit	Qiagen
Glutathione Assay Kit (#703002)	Cayman Chemicals
High-Capacity cDNA Reverse Transcription Kit	Applied Biosystems
RNeasy® Mini Kit	Qiagen
NucleoSpin® Plasmid Kit	Macherey-Nagel
QIAEX II Gel Extraction Kit	Qiagen
QIAquick PCR Pufification Kit	Qiagen
TRI Reagent RNA Isolation Kit	Ambion
TaqMan® Gene Expression Assays	Applied Biosystems
MycoAlert Mycoplasma Detection Kit	Lonza

3.1.6 Media, buffers and solutions

3.1.6.1 Cell culture media and universal solutions

Standard medium	500 ml RPMI 1640 or DMEM, 10% fetal bovine serum (FBS), 2 mM L-glutamine, 1 mg gentamicin
4% paraformaldehyde	4% PFA in 1xPBS, adjusted to pH 7.4 with NaOH
4% formaldehyde	4% Formalin, 55 mM Na_2HPO_4, 12 mM NaH_2PO_4-H_2O
LB medium	10 g peptone, 5 g Yeast extract, 10 g NaCl, ad 1000 ml distilled water
LB agar medium	10 g LB Broth Base, 7.5 g Agar, ad 500 ml distilled water

3.1.6.2 Buffers and gels for Western blot analysis

Laemmli buffer (3x)	188 mM Tris/HCl pH 6.8, 3% SDS, 45% glycerol, 0.05% Bromophenol blue, 7.5% ß-mercaptoethanol
SDS running buffer	25 mM Tris, 200 mM glycine, 0.1% (w/v) SDS
Separating buffer (4x)	1.5 M Tris, 0.4% SDS, adjusted to pH 8.8 with HCl
Separating gel (8-12.5%)	(10%): 3.33 ml 30% acrylamide/Bis, 2.5 ml separating

	buffer (4x), 4.17 ml water, 50 µl APS (10%), 20 µl TEMED
Stacking buffer (4x)	0.5 M Tris, 0.4% SDS, adjusted to pH 6.8 with HCl
Stacking gel (4.5%)	750 µl 30% acrylamide/Bis, 1.25 ml stacking buffer (4x), 3 ml water, 50 µl APS (10%), 20 µl TEMED
10% APS	ammonium persulfate 10% (w/v) in distilled water
Transfer buffer (5x)	25 mM Tris pH 8.3, 192 mM glycine
TBS (10x)	0.5 M Tris-HCl pH 7.4, 1.5 M NaCl
TBS-T	1xTBS including 0.05-0.1% (v/v) Tween 20

3.1.6.3 Buffer and gel for DNA/RNA electrophoresis

TAE running buffer	50xTAE: 2 M Tris, 10% EDTA (0.5 M), 5.71% HCl
Electrophoresis gel	200 ml TAE buffer (1x), 1% agarose, 4 µl EtBr

3.1.6.4 Buffers and solutions for flow cytometry and cell cycle analysis

Sample buffer	0.1% glucose (w/v) in 1xPBS, 0.22 µm filtration, stored at 4°C
Staining buffer	2% FBS, 0.05% NaN_3 dissolved in 1xPBS
PI staining solution	50 µg/ml propidium iodide (PI) and 100 U/ml RNAse A in sample buffer

3.1.7 Human cell lines, mouse model and bacterial strain

All human cell lines were purchased from the German Collection of Microorganisms and Cell Cultures (DSMZ), except for the human A673 ET cell line, which was purchased from ATCC (LGC Standards). The human SB-KMS-KS1 ET cell line was established in the Laboratory of Functional Genomics of Department of Pediatrics (TU München). Human MSCs lines L87 and V54.2 were immortalized with SV40 large T-antigen [46] and kindly provided by PD Dr. Peter Nelson (Department of Biological

Chemistry, Ludwig-Maximilians-Universität, Munich). Retrovirus packaging cell line PT67 was obtained from Takara Bio Europe.

3.1.7.1 Human cancer cell lines

Cell line	Description
A673	ET cell line (type 1 translocation) established from the primary tumor of a 15-year-old girl [87]
cALL2	Acute lymphoblastic leukemia (ALL) cell line established in 1993 from peripheral blood of a 15-year-old Caucasian girl
CHP126	Neuroblastoma cell line with N-MYC amplification established in 1973 from a stage III tumor of a 14-month-old girl [88]
MHH-ES1	ET cell line (type 2 translocation) established from ascites of a 12-year-old Turkish boy with a pelvic ET and peritoneal metastases
MHH-NB11	Neuroblastoma cell line established from an adrenal metastasis of a 4-year-old Caucasian boy
Nalm6	B precursor leukemia cell line established in 1976 from peripheral blood of a 19-year-old man with relapsed ALL
RDES	ET cell line (type 2 translocation) established in 1984 from the primary tumor (humerus) of a 19-year-old Caucasian man
RH-30	Undifferentiated alveolar rhabdomyosarcoma cell line [PAX3/FKHR fusion protein derived from t(2;13)(q35;q14)] established from bone marrow of a 17-year-old boy [89]
SB-KMS-KS1	ET cell line (type 1 translocation; initially designated SBSR-AKS) established from an inguinal metastasis of a 17-year-old girl
SHSY5Y	Neuroblastoma cell line established in 1970 from bone marrow of a 4-year-old girl
SIMA	Neuroblastoma cell line with N-MYC amplification established in 1991 from a stage III tumor of a 20-month-old Caucasian boy
SK-ES1	ET cell line (type 2 translocation) established in 1971 from an 18-year-old man
SK-N-MC	ET cell line (type 1 translocation) established in 1971 from a supraorbital metastasis of an Askin's tumor (ET of the chest) of a14-year-old girl
TC-71	ET cell line (type 1 translocation) established in 1981 from a locally relapsed ET (humerus) of a 22-year-old man
697	B cell precursor leukemia cell line established in 1979 from bone marrow of a 12-year-old boy with relapsed ALL

3.1.7.2 Mouse model

The *recombination activating gene 2 (Rag2)-gamma(c)* knockout (KO) mouse (*Rag2*$^{-/-}$ $\gamma_c^{-/-}$) is a severely immunodeficient model that can be used in studies addressing

vaccine development, cancer biology, or transplantation experiments. Backcrossing of two immunocompromised mouse strains (*Rag2* KO mice and *gamma(c)* KO mice) generated this double KO mouse strain. Homozygous *gamma(c)* KO mice lack the *gamma(c) receptor* gene. Therefore, lymphocyte development is markedly compromised and consequently the endogenous natural killer cell population is depleted in these mice. However, *gamma(c)* KO mice still have small numbers of B and T cells. In order to completely eliminate the B and T lymphocyte populations in this animal model, the *gamma(c)* KO mouse was backcrossed onto the *Rag2* KO mouse. Homozygous *Rag2*$^{-/-}$ mice lack several exons of the *Rag2* gene and are thus incapable of initiating somatic recombination of variable, diverse, and joining (VDJ) gene segments of the immunoglobulin and T cell receptor genes and thus cannot generate functional B and T lymphocytes [90].

3.1.7.3 Bacterial strain used for plasmid expansion

Chemically competent One Shot® TOP 10 *E. coli* (Invitrogen) with the following genotype were used: F-mcrA ∆(mrr-hsdRMS-mcrBC) φ80lacZ∆M15 ∆lacX74 recA1 araD139 ∆(ara-leu)7697 galU galK rpsL (StrR) endA1 nupG.

3.1.8 Primer assays used for quantitative Real-Time PCR (qRT-PCR)

Inventoried TaqMan Gene Expression Assays (Applied Biosystems) were used for *ALCAM* (Hs00233455_m1), *ADIPOR1* (Hs01114951_m1), *DTX3L* (Hs00370540_m1), *EMP1* (Hs00923125_g1), *EPHB2* (Hs00362096_m1), *GAPDH* (Hs99999905_m1), *GAP43* (Hs00176645_m1), *GFAP* (Hs00157674_m1), *MMP-1* (Hs00899658_m1), *NGFR* (Hs00182120_m1), *USP18* (Hs00276441_m1), *PSMB9* (Hs00160610_m1), *STAT1* (Hs01013996_m1), *STEAP1* (Hs00185180_m1), and *TAP1* (Hs00184465_m1). For EWS/FLI1 detection, the following primers 5'-TAGTTACCCACCCCAAACTGGAT-3' (sense), 5'-GGGCCGTTGCTCTGTATTCTTAC-3' (antisense), and probe 5'-FAM-

CAGCTACGGGCAGCA-TAMRA-3' were used. The concentration of primers and probes were 900 and 250 nM, respectively.

3.1.9 Sequences of small interfering RNAs (siRNAs)

EWS/FLI1 5'-GCAGAACCCUUCUUAUGACUU-3' (sense) and 5'-GUCAUAAGAAGG-GUUCUGCUUU-3' (antisense); STEAP1_2 5'-CAAUUGUUGUCCUGAUAUUTT-3' (sense), 5'-AAUAUCAGGACAACAAUUGGA-3' (antisense); STEAP1_3 5'-GAUUAGACAUGGUUGGGAA-3' (sense), 5'-UUCCCAACCAUGUCUAAUC-3' (antisense); siADIPOR1_1 5'-AAGGACAACGACUAUCUGCUA-3' (sense), 5'-UAGCAGAUAGUCGUUGUCCUU-3' (antisense); siADIPOR1_7 5'-UUGGAGGGUCA-UCCCAUAUGA-3' (sense), 5'-UCAUAUGGGAUGACCCUCCAA-3' (antisense); siDTX3L_5 5'-ACAGGAGAUAUCAGAGAUCGA-3' (sense), 5'-UCGAUCUCUG-AUACUCCUGU-3' (antisense); siDTX3L_7 5'-AUGCCUCAUGUCAGUUGAUGA-3' (sense), 5'-UCAUCAACUGACAUGAGGCAU-3' (antisense); siMMP-1_7 5'-GCUAACCUUUGAUGCUAUATT-3' (sense), 5'-UAUAGCAUCAAAGGUUAGCTT-3' (antisense); siMMP-1_12 5'-GAUGAAUAUAAACGAUCUATT-3' (sense), 5'-UAGAU-CGUUUAUAUUCAUCAT-3' (antisense); siSTAT1_6 5'-GUCUUUCUCGAACU-GUCAUUU-3' (sense), 5'-CAGAAAGAGCUUGACAGUAAA-3' (antisense).

3.1.10 Sequences of primers for chromatin immunoprecipitation (ChIP)

Relative to the transcriptional start site (TSS) of *STEAP1*: -1465 bp 5'-GGGCTTTA-AACTAATCCAAGGAA-3' (sense); -1465 bp 5'-TTAACTAGCATGCCGCCTTC-3' (antisense); -850 bp 5'-GGCAAGGAAGGGAGGGACGGA-3' (sense); -850 bp 5'-CAAACCCTGCTCCCCAGCCG-3' (antisense); -850 bp 5'-GGCAAGGAAGGGAGGGA-CGGA-3' (sense); -850 bp 5'-CAAACCCTGCTCCCCAGCCG-3' (antisense); -250 bp 5'-ACCCCATCCCAGACATACTG-3' (sense); -250 bp 5'-GATTACCCGGGGGC-TTATTA-3' (antisense).

3.1.11 Antibodies for Western blot and immunohistochemistry

Primary antibodies: polyclonal rabbit-anti-STEAP1 (1:100; H-105; sc-25514; Santa Cruz); rabbit-anti-phospho-signal transducer and activator of transcription 1 (STAT1) (Y701) (1:1,000; #9171; Cell Signaling); rabbit-anti-STAT1 (1:1,000; #9172; Cell Signaling); loading control: polyclonal rabbit-anti-hypoxanthine phosphoribosyl-transferase 1 (HPRT) (1:500; FL-218; sc-20975; Santa Cruz). Secondary antibody: horseradish peroxidase (HRP)-coupled bovine anti-rabbit IgG (1:1,000; sc-2370; Santa Cruz). Apart from STEAP1, ET xenografts were additionally stained in immunohistochemistry with primary antibodies directed against the following proteins: CD31 (1:75, Abcam), cleaved caspase-3 (1:250, Asp175, 5A1, Cell Signaling) and MAC3 (1:20, M3/84, Becton Dickinson). For these markers antigen retrieval was performed by microwave treatment in Dako target retrieval solution, citrate, pH 6.0 (caspase-3, MAC3) or by heat treatment in EDTA buffer (1 mM EDTA, 0.05% Tween 20, pH 8.0) (CD31).

3.2 Methods

3.2.1 Cell culture conditions and cell cryoconservation

Cells were grown at 37°C in 5% CO_2 in plastic flasks in a humidified atmosphere in RPMI 1640 (Invitrogen) containing 10% FBS (Biochrom), 1% L-glutamine and 100 µg/ml gentamicin (Invitrogen). The ALL cell lines and neuroblastoma cell line CHP126, which grow in suspension, were cultured in a humidified atmosphere at 37°C (5% CO_2) with 30 ml RPMI standard medium in T75 culture flasks. Approximately every 4 days, cells were split 1:4 and cultured in 30 ml fresh medium.

Depending on the given tumor cell line, cell concentrations between $1x10^6$ and $1x10^7$ cells per ml FBS/10% DMSO were frozen in liquid nitrogen (-192°C). After resuspension of cell pellets in an appropriate volume of pre-cooled FBS/10% DMSO, 1 ml aliquots of the cell suspension were transferred into pre-cooled cryovials. The cryovials were placed into controlled freezing boxes, stored for 12-18h at -80°C and were then transferred into the liquid nitrogen reservoir for long-term storage.

To re-culture the cryopreserved cells, cryovials were thawed at room temperature (RT) until only small ice crystals were seen floating inside the cryovial. The content of a vial was rapidly transferred into a 15 ml reaction tube containing 10 ml of fresh RPMI standard medium. Cells were pelletized by centrifugation at 1,300 rpm for 7 min, resuspended in pre-warmed culture medium and transferred into T75 culture flasks. Cell amounts were determined with a Neubauer hemocytometer. Cell viability was assessed by Trypan-Blue (Sigma) exclusion method.

Cell lines were checked routinely for purity by PCR and/or flow cytometry (EWS/FLI1 translocation product, surface antigen and/or HLA-phenotype) and mycoplasma contamination using the MycoAlert™ Mycoplasma Detection Kit according to the manufacturer's instructions (Lonza).

3.2.2 Transformation of competent bacteria

Transformation of TOP10 chemically competent *E. coli* was performed following the manufacturer's instructions. Vials of OneShot TOP10 competent cells (Invitrogen) were thawed at 4°C for each transformation. 2 µl of each ligation reaction (see below) were added onto competent cells, mixed and incubated for 5 min. Vials were then incubated for 30 sec at 42°C and afterwards for 2 min at 4°C (heat-shock). Then 250 µl of S.O.C. medium was added and the vials were shaken for 1h at 37°C at 300 rpm in a shaking incubator (Eppendorf). Subsequenty, 80 µl from each transformation vial were spread on separate LB agar plates containing ampicillin (Invitrogen) and incubated for 16h at 37°C. Colonies were selected and analyzed by plasmid isolation and sequencing.

3.2.3 Mini- and Maxi-preparation of plasmid DNA

Initial isolation of plasmid DNA from *E. coli* (Mini-preparation) was performed with the NulcoSpin Plasmid Kit from Machery-Nagel according to the manufacturer's instructions. DNA concentration was measured by spectrophotometry and the plasmids were analyzed by restriction enzymes and agarose gelelectrophoresis. Bacterial stocks were frozen after the addition of 15% glycerol and stored at -80°C. Maxi-preparation of DNA from *E.coli* was performed with the EndoFree Plasmid Kit from Qiagen according to the manufacturer's instructions.

3.2.4 Agarose gelelectrophoresis

Separation of DNA and RNA fragments was performed in 1% agarose gel at 10 V/cm. 2 g agarose per 200 ml TAE buffer were boiled and afterwards 4 µl EtBr were added before casting the gel. 1 µg of DNA or RNA were mixed with 6x Blue Juice Gel Loading Buffer (Invitrogen). Gel-pockets were loaded with a final volume of 20 µl. The 0.1 kb or 1 kb, respectively, DNA ladder (Invitrogen) was included as a size standard. For extraction of DNA fragments from agarose gels, the desired amplicons were cut from

the gel and purified using the QIAEX II Gel Extraction Kit (Qiagen) according to the manufacturer's protocol.

3.2.5 Annealing of oligonucleotides

For annealing, the purified oligonucleotides were resuspended in 1xTE buffer to a final concentration of 100 µM. The oligonucleotides for the top strand and bottom strand were mixed in an 1:1 ratio yielding 50 µM of ds oligonucleotides in a volume of 10 µl. The following thermal conditions were used for annealing: 95°C for 30 sec, 72°C for 2 min, 37°C for 2 min, 25°C for 2 min, and 4°C terminal hold.

3.2.6 RNA isolation using RNeasy Mini Kit

To examine gene expression by quantitative Real-Time PCR (qRT-PCR), RNA from cultured cells was isolated using the RNeasy Mini Kit according to the manufacturer's instructions (Qiagen Handbook 04/2006). This procedure provides an enrichment of mRNA since RNA molecules smaller than 200 bases are sequestered under given high-salt conditions. Up to $1x10^7$ cells were lysed in an appropriate volume of RLT buffer (containing 10 µl ß-mercaptoethanol/ml RLT), mixed with an equal amount of 70% ethanol and vortexed. The lysate was transferred onto RNeasy spin columns and centrifuged for 1 min at 10,000 rpm. This step enabled binding of the RNA to the silica-gel membrane within the RNeasy spin column. The membranes were washed three times with wash buffers with a final centrifugation step at 12,000 rpm for 2 min to dry the membranes. Elution of RNA was carried out with 30-40 µl RNAse-free water. RNA concentrations were determined photometrically at 260 nm. RNA was stored at -80°C.

3.2.7 Isolation of total RNA using TRI Reagent RNA Isolation Kit

Isolation of total RNA from frozen tissue was performed with the TRI Reagent RNA Isolation Kit according to manufacturer's instructions (Ambion Manual Version 0610).

Frozen tissue was mechanically disintegrated and homogenized in 1 ml TRI Reagent. After addition of 100 µl BCP (1-bromo-3-chloropropane) per ml TRI Reagent, samples were vigorously vortexed for 20 sec and centrifuged at 4,000 rpm for 60 min at 4°C. The aqueous RNA phase was transferred into a new reaction tube and RNA was precipitated by adding 500 µl isopropanol per ml TRI Reagent.

The sample was vortexed and centrifuged at 4,000 rpm for 30 min at 4°C. Then the RNA pellet was washed with 1 ml 75% ethanol and centrifuged at 4,000 rpm for 10 min at 4°C. After removal of ethanol the pellet was air-dried for 2-5 min and dissolved in 50-100 µl RNAse-free water. RNA concentration was determined photometrically at 260 nm. RNA was stored at -80°C. This RNA isolation procedure was also used to isolate total RNA from cultured cells for microarray experiments, because RNA isolation by RNeasy Mini Kit is not sufficient for the isolation of RNA molecules smaller than 200 bases.

3.2.8 Reverse transcription

To examine gene expression by qRT-PCR, isolated RNA was reversely transcribed into complementary DNA (cDNA) using the High-Capacity cDNA Reverse Transcription Kit (Applied Biosystems). According to the manufacturer's instructions (Applied Biosystems Insert P/N 4375222 REV A) 10 µl of 2x reverse transcription master mix containing dNTPs, MultiScribe™ Reverse Transcriptase, reverse transcription random primers and buffer were mixed with 10 µl RNA solution (containing 1 µg purified RNA). The cDNA was synthesized under the following thermal cycling conditions: 10 min at 25°C, 120 min at 37°C, 5 min at 85°C, and terminal hold at 4°C.

3.2.9 Quantitative Real-Time PCR (qRT-PCR)

Quantification of synthesized cDNA by qRT-PCR allows examination of differential gene expression as the amount of cDNA corresponds to the amount of cellular mRNA.

qRT-PCR was performed by use of Maxima™ Probe/ROX qPCR Master Mix (2x) containing Hot Start Taq Polymerase, PCR buffer, and dNTPs. Gene-specific expression assays were obtained from Applied Biosystems, which consisted of a FAM™ dye-labeled TaqMan® MGB probe and two unlabeled PCR primers. All analyses were carried out in 96-well format. 1 µl of specific primer assays and 0.5 µl of cDNA template were added to 8 µl of Maxima™ Probe/ROX qPCR Master Mix (2x) and adjusted to a final volume of 20 µl with RNAse-free water. The final concentration of primers and probe were 900 and 250 nM, respectively. Fluorescence was measured with an AB 7300 Real-Time PCR System (Applied Biosystems). Gene expression values were normalized to those of the housekeeping gene *glyceraldehyde 3-phosphate dehydrogenase* (*GAPDH*) using the 2^{-ddCt} method. Mean values and standard deviations of duplicate measurements were calculated using Microsoft Excel.

3.2.10 Detection of EWS/FLI1

There are no inventoried TaqMan Gene Expression Assays for the detection of EWS/FLI1 type 1 mRNA levels available. Thus, primers detecting EWS (sense) and FLI1 (antisense) of the fusion transcript and a probe detecting type 1 translocation were designed. The master mix was prepared by adding 10 µl of MaximaTM Probe/ROX qPCR Master Mix (2x), 0.3 µM of each primer and 0.2 µM of FAM probe to 7.6 µl RNAse-free water. To a final volume of 19.5 µl Master Mix per 96-well 0.5 µl of cDNA template were added. Fluorescence was measured with an AB 7300 Real-Time PCR System (Applied Biosystems). Gene expression values were normalized to those obtained for GAPDH and calculated using the 2^{-ddCt} method.

3.2.11 Ligation of DNA fragments, constructs and retroviral gene transfer

These methods were in part applied in cooperation with Dr. Sabine Rössler and Mrs. Colette Zobywalski (both Department of Pediatrics, Klinikum rechts der Isar, TU

München). To ligate ds oligonucleotides into expression vectors, the following reaction mix was assembled: 1 µl linearized expression vector (50 ng/ml), 1 µl annealed oligonucleotide (0.5 µM), 1.5 µl 10xT4 DNA Ligase Buffer, 0.5 µl BSA (10 mg/ml), 10.5 µl DEPC-treated H_2O, 0.5 µl DNA Ligase (400 U/ml). The reaction mix was incubated for 3h at 22°C and subsequently used for transformation of competent bacteria. The cDNA encoding *EWS/FLI1* was described previously [4]. A BglII fragment was subcloned in pMSCVneo (Takara Bio Europe). For STEAP1-overexpression *STEAP1* coding DNA was cloned into pMSCVneo. For stable STEAP1-silencing, oligonucleotides of the short hairpin corresponding to the siRNAs were cloned into pSIREN-RetroQ (Takara Bio Europe). Retroviral constructs were transfected by electroporation into PT67 packaging cells at the capacitance of 960 µF and 270 V / 0.4 cm. After electroporation, cells were incubated on ice for 10 min and subsequently seeded in cell culture flasks and grown in RPMI 1640 medium containing 20% FBS. Stable PT67 transfectants were selected with puromycin (2 µg/ml). Supernatants were harvested at 70% confluence of the cells and filtered through 0.45-µm filters. Viral infection of target cells (density: $1x10^5$/ml/well of a 6-well plate) was carried out with 1 ml retrovirus supernatant supplemented with 4 µg/ml (final concentration) polybrene. Infectants were selected in 600 µg/ml G418 (pMSCVneo) or 2 µg/ml puromycin (pSIREN-RetroQ), respectively.

3.2.12 Chromatin immunoprecipitation (ChIP)

These analyses were performed in cooperation with Dr. Rebekka Unland and Prof. Dr. Carsten Müller-Tidow (University of Münster, Germany). $2x10^7$ SK-N-MC and RH-30 cells were fixed in 1% formaldehyde for 8 min. Samples were sonicated to an average DNA length of 500-1,000 bp. ChIP was performed with 5 µg of anti-FLI1-antibody (C-19; Santa Cruz) added to 0.5 mg of precleared chromatin. Quantitative PCR of immunoprecipitated DNA was performed using SybrGreen (Thermo Fisher Scientific).

FLI1 data of the SK-N-MC cells at individual genomic loci were normalized to the control cell line RH-30 and standardized to a non-regulated genomic locus outside of the *STEAP1* locus.

3.2.13 Western blot (WB)

Procedures were essentially done as described previously [46]. Cells were lysed in 2xLaemmli buffer and equal amounts of protein were resolved by 10% SDS-PAGE. Proteins were blotted on PVDF membranes. Transfer efficacy was determined by Ponceau-S staining (0.1% w/v in 1% acetic acid). PVDF membranes were blocked with 5% nonfat dry milk in 10 mM Tris, pH 7.5, 150 mM NaCl, 0.05% (w/v) Tween 20. Protein bands were detected by ECL plus (Amersham Biosciences) and visualized with a GelLogic 1500 luminometer (Carestream Health Inc.).

Specificity of the STEAP1 antibody was assessed previously by others [63, 91] and reassessed by the author using WB and indirect immunofluorescence (IF) as previously described [92, 93]. These control experiments further confirmed the specificity of the used STEAP1 antibody (Figure 2) in agreement with published findings on the STEAP1 protein [48]. To reactivate dried PVDF membranes, membranes were incubated in methanol (~1 min), washed once with 1xTBST, and blocked for 1h in 5% skim milk/0.05% Tween 20.

3.2.14 RNA interference (RNAi)

For transient protein knockdown, cells were transfected with small interfering RNA (siRNA) using the HiPerFect transfection reagent according to standard procedures for large-scale transfection in 100 mm dishes (Qiagen Handbook 05/2008). 1-3x10^6 cells were plated into 100 mm culture dishes at a final volume of 12 ml medium containing 5 nM siRNA and 36 µl transfection reagent and incubated at least 48h at 37°C (5% CO_2)

in a humidified atmosphere. Knockdown efficacy was assessed by qRT-PCR and/or WB.

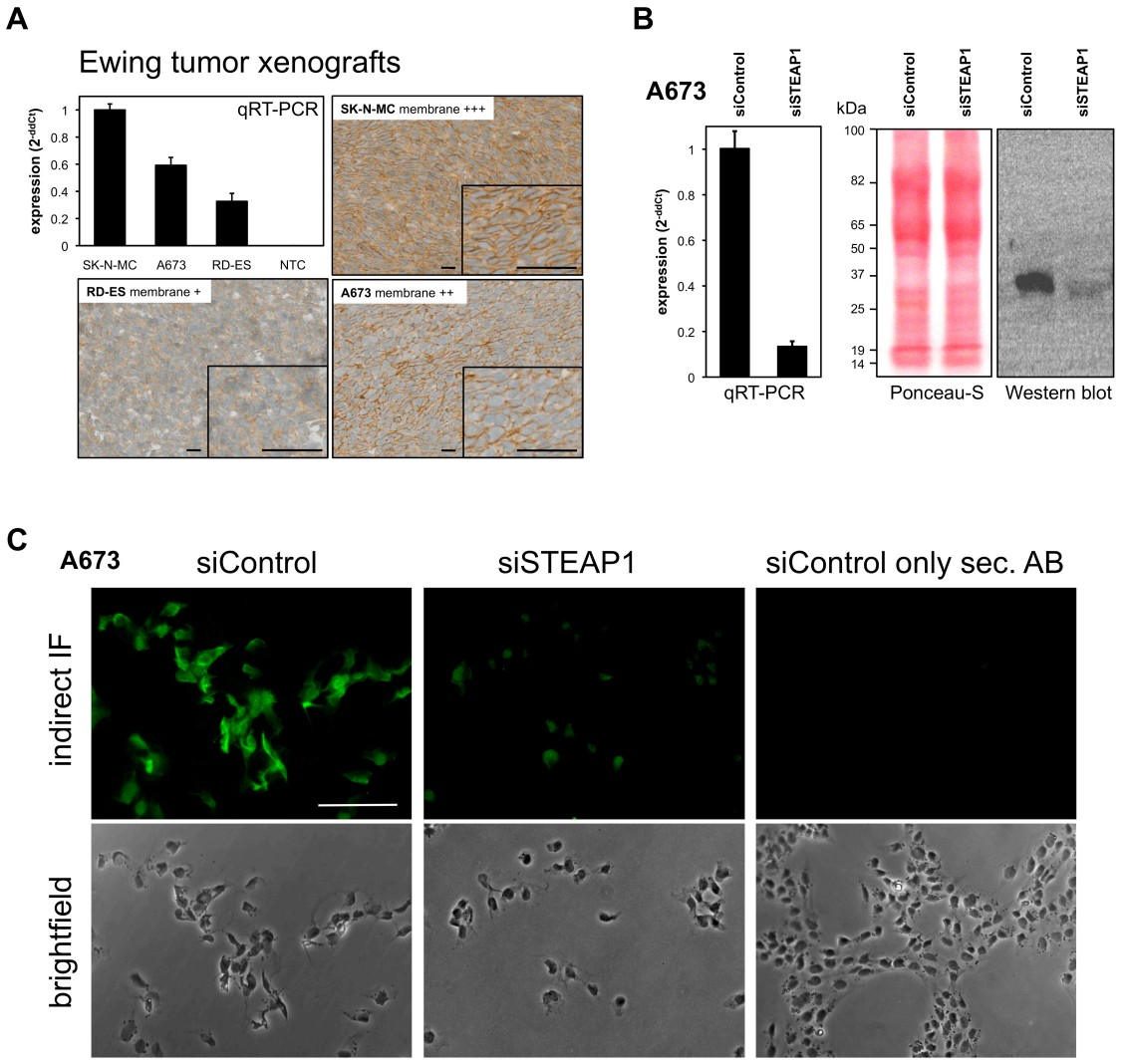

Figure 2: Confirmation of specificity of STEAP1 antibody:
A: Analysis of STEAP1 mRNA and protein expression (qRT-PCR and immunohistochemistry) of xenografted ET cell lines SK-N-MC, A673 and RDES. Scale bars = 20 µm for overview and 80 µm for detail images. NTC = no template control. B: qRT-PCR and WB for STEAP1 in A673 cells transfected with STEAP1 siRNA 48h before. Ponceau-S staining of blotted proteins served as loading control in WB. The predicted molecular weight of STEAP1 is 36 kDa. C: IF of A673 cells transfected with STEAP1 siRNA 48h before staining with STEAP1 antibody (scale bar = 50 µm).

3.2.15 Microarrays

Experiments were essentially done as previously described [46] in cooperation with Olivia Prazeres da Costa, M.Sc. (Expression Core Facility at the Institute for Medical Microbiology, Immunology and Hygiene of the TU München). A673 and SK-N-MC cells

were transfected with siRNA and allowed to grow for 48h. Thereafter cells were washed twice with PBS and harvested by trypsination. RNA was isolated with TRI Reagent RNA Isolation Kit. Total RNA (200 ng) was amplified and labeled using Affymetrix GeneChip Whole Transcript Sense Target Labeling Kit. cRNA was hybridized to Affymetrix Human Gene 1.0 ST arrays.

Arrays were RMA-normalized. Quality assessment consisted of RNA degradation plots, Affymetrix control metrics, sample cross-correlation, and probe-level visualizations. Normalization incorporated (separately for each RNA type data set) background correction, quantile normalization, and probe-level summation by RMA. Data were deposited at the Gene Expression Omnibus (GSE26422) and analyzed with independent one-sample t-test [94] and Genesis software package [95].

Transcripts were functionally assigned using gene ontology (GO)-annotations (http://www.cgap.nci.nih.gov). Gene-set enrichment analysis (GSEA) and pathway analyses were performed with the GSEA tool (http://www.broad.mit.edu/gsea) [96].

For analysis of differential regulation of micro RNA species (miRNAs) A673 and SK-N-MC ET cells were transfected with siRNA and allowed to grow for 68h. Cells were harvested by trypsination and RNA was isolated with TRI Reagent RNA Isolation Kit. Total RNA was prepared as described above and hybridized to Affymetrix GeneChip miRNA arrays 2.0. Normalization and quality checks were performed as described above. Putative targets of differentially regulated miRNAs were ranked by use of the mirSVR scoring algorithm (http://www.microrna.org) [97].

3.2.16 Measurement of ROS and mitochondrial mass

Procedures were previously described [98] and in part performed in cooperation with Dr. Isabel Diebold and Prof. Dr. Agnes Görlach (Department of Experimental and Molecular Pediatric Cardiology, German Heart Center Munich at the TU München). $1x10^4$ cells/well were plated in 96-well plates 1 day before measurements to achieve

40% confluency on the next day. Generation of ROS was detected using dihydroethidium (DHE; Invitrogen). Cells were incubated with DHE (50 µM) for 10 min. Thereafter cells were washed with HBSS and fluorescence was monitored using a Safire microplate reader (Tecan). DHE fluorescence was standardized to the number of viable cells using the alamarBlue test (Biosource) according to the manufacturer's protocol. Mitochondrial ROS and mitochondrial mass were measured by incubating $1x10^6$ ET cells with either 75 µM Mitosox Red or Mitotracker Green (both Invitrogen), respectively, dissolved in PBS for 45 min in the dark at 37°C. Fluorescence intensity was assessed with a FACScalibur flow cytometer (Beckton Dickinson).

3.2.17 Flow cytometry

Cells were stained 48-72h after transfection as previously described [92]. Briefly, cells were harvested by trypsination, washed twice with PBS and resuspended in a concentration of $2x10^6$/ml in sample buffer (see methods 3.1.6.4). Samples were blocked with human IgG (100 µg/ml) 20 min at 4°C for and afterwards incubated with specific fluorochrome-labeled antibodies (1 µg antibody/$1x10^6$ cells) for 30 min at 4°C. After washing twice with sample buffer, samples were resuspended in 500 µl sample buffer and analyzed on a FACScalibur flow cytometer (Becton Dickinson). All samples were analyzed in single-color staining and at least 30,000 events/sample were recorded. Data were saved in *.fcs format and analyzed with Cellquest software (Beckton Dickinson).

For detection of adhesion and integrin molecules anti-human CD29 (APC, MAR4), CD49a (PE, SR84), CD49b (FITC, AK-7), CD49c (PE, C3 II.I), CD49d (APC, 9F10), CD49e (PE, IIA1), CD49f (PE, GoH3), CD54 (PE, HA58), and CD56 (APC, B159) antibodies (all BD Biosciences) were used. For determination of the HLA phenotype specific biotinylated murine-anti-HLA-A1, -HLA-A2, and -HLA-A3 antibodies followed

by streptavidin-PE were used (all BD Biosciences). As controls the respective isotype control antibodies (BD Biosciences) were used.

3.2.18 Assessment of cell cycle, apoptosis and necrosis

Cell cycle phases of ET cells were analyzed using propidium iodide (PI; Sigma). $2x10^6$ cells were harvested 48h after transfection with siRNA by trypsination. Cells were washed twice with sample buffer (see methods 3.1.6.4), fixed in 70% ethanol at 4°C, and subsequently stained by resuspension in 300 µl PI staining solution (see methods 3.1.6.4) for 45 min in the dark before flow cytometry analysis. The annexin-V-PE/7-AAD apoptosis detection kit 1 (Beckton Dickinson) was used according to the manufacturer's protocol to assess apoptosis and necrosis. Samples were analyzed on a FACScalibur flow cytometer using Cellquest software (both Becton Dickinson). In addition, necrosis was assessed by Trypan-Blue (Sigma) exclusion method.

3.2.19 Proliferation assay

Cell numbers were counted in real-time with a bioelectric xCELLigence instrument (Roche/ACEA Biosciences) monitoring impedance across gold microelectrodes on the bottom of E-plates. Immediately after transfection with siRNA $1.6x10^4$ cells were seeded in wells in 200 µl medium containing 10% FBS and transfection reagents. Cellular impedance was measured periodically every 4h thereafter. Transfection efficacy was controlled by WB and/or qRT-PCR.

3.2.20 Invasion assay

$5x10^5$ transiently transfected cells were seeded in 500 µl serum-free medium into the upper chambers of Matrigel-covered transwell plates (Becton Dickinson). Bottom chambers contained 500 µl medium with 10% FBS. After 48h invaded cells were stained

with 4 µg/ml Calcein AM (Merck) in HBSS and photographed with an AxioCam MRm camera attached on an Axiovert 100 microscope (both Zeiss). The number of invaded cells was normalized to proliferation as assessed with xCELLigence (Roche/ACEA Biosciences). N-acetyl-cysteine (NAC) or hydrogen peroxide (H_2O_2) pre-treatment of Matrigel-plates did not affect invasiveness of untreated ET cells plated thereafter.

3.2.21 Colony forming assay

Procedures were described previously [46]. Cells were seeded in duplicate at a density of $5x10^3$ cells per 1.5 ml methylcellulose-based media (R&D Systems) into a 35-mm plate according to the manufacturer's instruction, and cultured for 14 days at 37°C and 5% CO_2 in a humidified atmosphere. Number of colonies was documented by photography and analyzed with NIH ImageJ software (rsbweb.nih.gov/ij/).

3.2.22 Angiogenesis assay

Cellular tube formation capability of ET cells was tested with a commercial Matrigel matrix assay (Biocoat, BD Biosciences) according to the manufacturer's instructions as previously described [46]. Briefly, $1x10^5$ cells/well were seeded in a volume of 150 µl medium in Matrigel covered wells (96-well plate) and allowed to grow for 24h in a humidified atmosphere. Then cells were stained with 4 µg/ml Calcein AM (Merck) in HBSS for 90 min at 37°C. Stained cells were photographed with a Zeiss AxioCam MRm camera on a Zeiss Axiovert 100 microscope.

3.2.23 Migration assay

Confluent monolayers of transiently transfected cells were wounded using a sterile pipette tip. Detritus was removed by washing twice with PBS. Still adherent cells were resuspended in 10 ml RPMI 1640 medium containing 10% FBS. Wound distances were photographed periodically using a Nikon Coolpix 5400 camera attached to a

Nikon Eclipse TS100 microscope (Nikon). Images and wound distances were analyzed with NIH ImageJ software.

3.2.24 Indirect immunofluorescence (IF)

IF was carried out as previously described [92]. Fixed and permeabilized cells were stained with monoclonal mouse-anti-vinculin antibody (1:4,000; VIN-11-5, Sigma) or polyclonal rabbit-anti-STEAP1-antibody (1:50, H-105, Santa Cruz) overnight followed by secondary FITC-labeled goat-anti-mouse antibody (1:100, sc-2078, Santa Cruz) or FITC-labeled goat-anti-rabbit secondary antibody (1:100, sc-2012, Santa Cruz), respectively. Images were recorded with a Zeiss AxioCam MRm camera attached on a Zeiss Axiovert 100 microscope and analyzed with NIH ImageJ software.

3.2.25 Adhesion assay

Adhesion of cells was assessed as previously described [99]. Cells were washed in serum-free medium, re-suspended at a concentration of $5x10^5$/ml and seeded in a total volume of 1.5 ml in wells of a 24-well plate. Cells were allowed to attach for 1h at 37°C. Non-adherent cells were removed by gentle washing with PBS. Attached cells were fixed in 4% (w/v) paraformaldehyde for 10 min at 4°C and stained with 200 µl 0.5% crystal-violet in 2% ethanol/PBS for 20 min at RT. Surplus crystal-violet was removed by washing with PBS. The dye was eluted in 10% acetic acid and absorbance was measured at 595 nm with a photometer.

3.2.26 Mice and *in vivo* experiments

Immunodeficient $Rag2^{-/-}\gamma_c^{-/-}$ mice on a BALB/c background were obtained from the Central Institute for Experimental Animals (Kawasaki) and maintained under pathogen-free conditions in accordance with the institutional guidelines and approval by the Regierung von Oberbayern. Experiments were performed in 6-16 week-old mice. For *in*

vivo tumor growth $3x10^6$ ET cells in 200 µl PBS were subcutaneously injected in groins. The amount of $2\text{-}5x10^6$ cells has been previously reported to be optimal for assessment of local growth of ET xenografts [46, 100]. Mice bearing tumors greater than 10 mm in diameter (determined with a caliper) were considered positive (event). To analyze metastatic potential, tumor cells were injected intravenously. Five weeks later mice were euthanized and metastasis was monitored in individual organs. All macroscopically visible metastases within dissected organs were counted. Tumors and affected tissues were excised for histology and gene expression analysis.

3.2.27 Glutathione assay

Cellular glutathione (GSH) was assessed with the colorimetric Cayman Glutathione Assay Kit using the endpoint measurement method following the manufacturer's protocol (#703002, Cayman Chemicals Europe). Briefly, $3x10^6$ cells were lysed 48h after transfection with siRNA in 300 µl DEPC-treated water with a 30G needle. Cell debris was removed by centrifugation and supernatant was deproteinated by adding an equal volume of metaphosphoric acid (final concentration 50 mg/ml; Sigma). Then 50 µl of the deproteinated supernatant were treated with triethanolamine reagent (final concentration 200 mM; Sigma), plated in wells of a 96-well plate (flat bottom), and incubated with the GSH Assay Cocktail (Cayman Chemicals Europe). For measurement of glutathione disulfide (GSSG) deproteinated samples and respective standards were preincubated in a final concentration of 5 mM with 2-vinylpyridine (Sigma) in order to derivatize GSH before GSSG measurement. Photometrical measurements were carried out at 405 nm with a plate reader (Thermo Scientific).

3.2.28 Electron microscopy

Procedures were essentially done as described [101, 102] in cooperation with Prof. Dr. Ulrich Welsch (Anatomical Institute, Ludwig-Maximilians-Universität, Munich). $3x10^6$

SK-N-MC cells transfected with siRNA 80h before harvest were fixed in 2.5% glutaraldehyde in Soerensen's buffer. For ultrastructural studies, the glutaraldehyde-fixed samples were postfixed in 2% osmium tetroxide and then embedded in araldite. Thin sections were stained with uranyl acetate and lead citrate and viewed in a Philips CM 10 electron microscope (Philips).

3.2.29 2D gelelectrophoresis, spot selection and mass spectrometry

The following procedures were performed in cooperation with Prof. Dr. Elke Butt (Institute for Clinical Biochemistry, University of Würzburg, Germany) and Dr. Katharina Lohrig, Dr. Urs Lewandrowski and Prof. Dr. Albert Sickmann (Leibniz – Institut für Analytische Wissenschaften – ISAS e.V., Dortmund; and Medical Proteome Center (MPC), Ruhr-University Bochum, Germany). 2D-IEF/SDS-PAGE were essentially done as described [93]. Differential regulation of spots in 2D gels was assessed using PDquest advanced software (BioRad). The 24 most significantly regulated spots and a non-regulated control spot were excised for proteomic analysis. Reversed-phase HPLC for peptide separation was conducted prior online coupling to nano-ESI mass spectrometric detection. Therefore, an U3000 nanoHPLC system (Dionex) with precolumn concentration was used featuring a precolumn (100 µm inner diameter, 1.5 cm length) and a main separation column (75 µm inner diameter, 30 cm length) both being prepared in-house using Kinetix resin (2.6 µm particle size, 100 Å pore size, Phenomenex). Gradient elution was performed using a linear acetonitril gradient from 5% to 60% solvent B in 30 min followed by a column regeneration step for 5 min at 95% solvent B prior reequilibration at 5% solvent B before the next run. Solvent A was 0.1% formic acid in water and solvent B was 84% acetonitril, 0.1% formic acid in water. Mass spectrometric detection of peptides was performed with an LTQ FT ultra-system (Thermo Fisher Scientific) equipped with a nano-ESI source. Using distal coated fused silica tips as emitter (New Objective), spray voltage was set to 1.8 kV. A survey scan

(m/z 350-2,000, resolution 100,000) was followed by six MS/MS scans fragmenting the six most abundant doubly or triply charged precursor ions. Dynamic exclusion of precursors was set to 30 sec after one fragmentation. Raw data were converted to *.mgf format using extract_msn software (v4.0; Thermo Fisher Scientific). Database searches were conducted using Mascot 2.3 (MatrixScience) against a human subset (20,403 sequences) of the SwissProt database (495,880 sequences, 10th July 2009). Search parameter settings used trypsin as protease, a maximum of one allowed missed cleavages, carbamidomethylation (C) as fixed modification and oxidation (M) as variable modification. Mass deviance allowed for precursor and fragment ion masses were 5 ppm and 0.5 Da, respectively. For reliable identification of a protein, at least two individual peptides had to be identified per protein with a $p > 0.05$ value (chance of 5% for random hits) and a Mascot identity threshold of 20. All significant hits were revised manually and functionally assigned using GO-annotations and the GSEA pathway analysis tool (http://www.broad.mit.edu/gsea).

3.2.30 Study population, ET samples and tissue microarray (TMA)

The institutional review boards (IRB) of the Technische Universität München (Germany) and the Universities of Basel (Switzerland), Düsseldorf and Münster (both Germany) approved the current study. 114 archival paraffin-embedded primary ET samples prior to treatment with confirmed histological diagnosis (reference pathology) were obtained from the Departments of Pathology of the TU München and University of Düsseldorf and of the Bone Tumor Reference Center at the Institute of Pathology of the University of Basel. Representative formalin-fixed, paraffin-embedded tumor blocks were selected for either TMA construction at the Department of Pathology of the University of Düsseldorf (66 samples) or open procedures at the Departments of Pathology of the TU München (6 samples) and the University of Basel (42 samples). Each TMA slide contained reference tissues of ET xenografts with known STEAP1

expression as internal controls (Figure 2). Pertinent clinical data of patients were compiled from two sources: first, the EWING trial center of the University Hospital Münster (93 patients either enrolled in the CESS 81, CESS 86, EICESS 92 or EURO-E.W.I.N.G. 99 trials) and second, the Institute of Pathology of the University of Basel (21 patients). Informed consent was obtained from all patients and/or their legal guardians. The study population included 60 males and 54 females with a median age of 16.9 years (range 0.6 to 59.8 years). Acquisition of patient material, TMA construction and analysis of patient data was performed in cooperation with Dr. Daniel Baumhoer (University of Basel), Prof. Dr. Karl-Ludwig Schäfer (University of Düsseldorf) and Dr. Andreas Ranft (EWING trial center, University of Münster).

3.2.31 Immunohistochemistry (IHC) and evaluation of immunoreactivity

Histological analyses were performed in cooperation with Prof. Dr. Irene Esposito, Dr. Michaela Aichler, and Dr. Patricia da Silva-Buttkus (Institute of Pathology, Klinikum rechts der Isar, TU München; and Institute of Pathology, Helmholtz-Zentrum München). IHC analyses were done on formalin fixed, paraffin-embedded, pre-chemotherapy primary tumors. All tissue slides were collected at the Department of Pathology of the TU München for immediate IHC staining. For IHC 4 µm sections were cut and stained by an automated immunostainer with an iView DAB detection kit (Ventana Medical System) according to the company's protocol.

The following primary antibody was used: STEAP1 (1:50; H-105, sc-25514, Santa Cruz). Antigen retrieval was performed by microwave treatment in Dako target retrieval solution, citrate, and pH 6.0. Sections were counterstained with hematoxylin. For internal controls, tumors of xenografted ET cell lines with known STEAP1 mRNA and protein expression levels were used (Figure 2). Semi-quantitative evaluation of STEAP1 immunostaining was carried out in a blinded manner by a pathologist (Prof. Dr. Irene Esposito, Institute of Pathology, TU München) and two scientists experienced

in histopathology (Dr. Patricia da Silva-Buttkus, Dr. Michaela Aichler, both Institute of Pathology, Helmholtz-Zentrum München) after having examined at least three high-power fields (40x) of one section for each sample. The intensity of membranous and cytoplasmic STEAP1 immunoreactivity of the ET cells was determined as grade 0 = none, grade 1 = faint, grade 2 = moderate, and grade 3 = strong (Figure 3).

Intensity scoring was independently recorded and in case of disagreement determined by consensus. For better statistical discrimination samples were classified into two groups as previously described [103, 104]: samples with grade 0 and 1 were classified as STEAP1-low and those with grade 2 and 3 as STEAP1-high. The percentage of necrotic area was calculated as necrotic area over tumor area using slides stained with hematoxylin and eosin (HE).

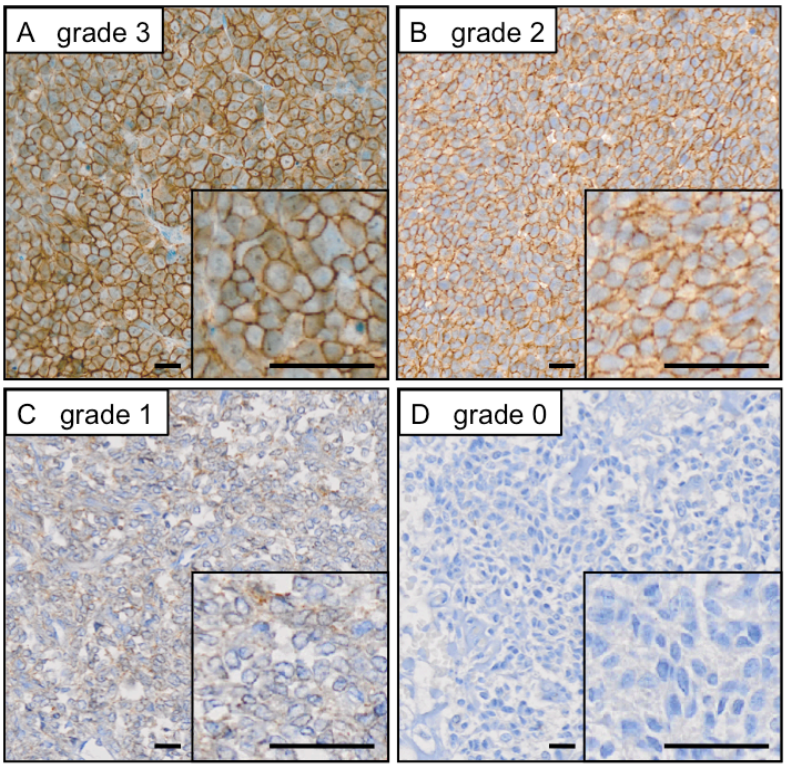

Figure 3: Examples of heterogeneous STEAP1 immunoreactivity:
All samples depicted were located on the same TMA slide and stained simultaneously by an automated immunostainer. Membranous STEAP1 immunoreactivity (brown color) was scored according to reference ET with known STEAP1 expression levels with grade 3 = strong (A), grade 2 = moderate (B), grade 1 = faint (C), and grade 0 = no immunoreactivity (D). Grades 3 and 2 were classified as STEAP1-high and grades 1 and 0 as STEAP1-low. Scale bars = 20 µm for overview and 80 µm for detail images.

3.2.32 Analysis of cellular iron content

72h after transfection with siRNA $3x10^6$ SB-KMS-KS1 and SK-N-MC cells were lysed by homogenization with a 30G needle and subjected to a commercial colorimetric iron detection assay according to the manufacturer's protocol (Biovision Iron Assay Kit; Biovision Research). Absorbance was measured at 593 nm with a Biowave II WPA photometer (Biochrom).

3.2.33 ELISpot analysis for detection of interferon secretion

Procedures were essentially done as previously described [105] and performed in collaboration with Dr. Uwe Thiel (Children's Cancer Research Center, Klinikum rechts der Isar, TU München). Antibody used: interferon alpha pan ELISpot kit (HRP) reactive with all interferon alpha subtypes except subtype 21 (#3425-2H; Mabtech).

Spots were counted on an AID-ELIRIFL04 ELISpot reader (Autoimmun Diagnostika). Positive controls: peripheral blood mononuclear cells (PBMCs) isolated by centrifugation over Ficoll-Paque (GE Healthcare) from healthy donors were either treated with siRNA or left untreated. PBMCs were obtained with IRB approval and informed consent from the DRK-Blutspendedienst Baden-Württemberg-Hessen in Ulm, Germany.

3.2.34 Statistical analyses

Statistical analyses were performed with SPSS 19 (IBM Corporation) and SAS 9.2 (SAS Institute). Overall survival (OS) was estimated by the Kaplan-Meier method. OS time was defined as the interval between the date of diagnosis and the date of last follow-up or death. Living patients were censored at the date of most recent consultation. Group comparisons were calculated by log-rank test.

Multivariate analyses were performed applying the Cox proportional hazard method. Differences in proportions between groups were evaluated by chi-square test, Fisher

exact test, unpaired two-tailed student's t-test or independent one-sample t-test. Significance of correlations was calculated with the Pearson correlation test. Significance level was set at $p < 0.05$ for two-sided testing. No alpha corrections were performed for multiple testing. Patient outcome was analyzed on an exploratory basis.

4 Results

4.1 Analysis of STEAP1 *in vitro* and in ET xenografts

4.1.1 *STEAP1* is induced by EWS/FLI1 and highly expressed in ET

Previously, Staege *et al.* identified STEAP1 to be part of a specific ET expression signature [4]. To substantiate this observation, archival ET microarray data were matched against those of neuroblastomas and a normal body map composed of normal fetal and adult tissues.

As seen from Figure 4A and 4B STEAP1 is highly expressed in ET but only minimally expressed in neuroblastomas and benign tissues. High STEAP1 expression in ET was confirmed by qRT-PCR and WB (Figure 4C).

To test whether EWS/ETS transcription factors can induce STEAP1, human MSCs were transfected with *EWS/FLI1*-containing vectors, which led to a 5-6-fold increase of STEAP1 expression in two MSCs lines (L87 and V54.2) (Figure 4D).

Conversely, RNAi-mediated EWS/FLI1-silencing in ET cells reduced STEAP1 expression (Figure 4E). Moreover, the *STEAP1* promoter contains two evolutionarily conserved ETS binding sites [-1465 and -250 bp upstream of the transcriptional start site (TSS)], which proved to be enriched for FLI1 in chromatin immunoprecipitation (ChIP) (Figure 4F).

In a next step, STEAP1 overexpression was confirmed in primary ET on protein level. Prostate cancer samples were used as positive controls due to their known overexpression of STEAP1 [48]. Figure 4G demonstrates that among a series of tumors, which are usually included in the histological differential diagnosis of ET [106, 107], only ET display very high STEAP1 levels.

Consistently, the analysis of a sarcoma gene expression library (137 sarcomas; 14 entities) [108] revealed that STEAP1 discriminates ET from other sarcomas (sensitivity 89.5%, specificity 82.2%).

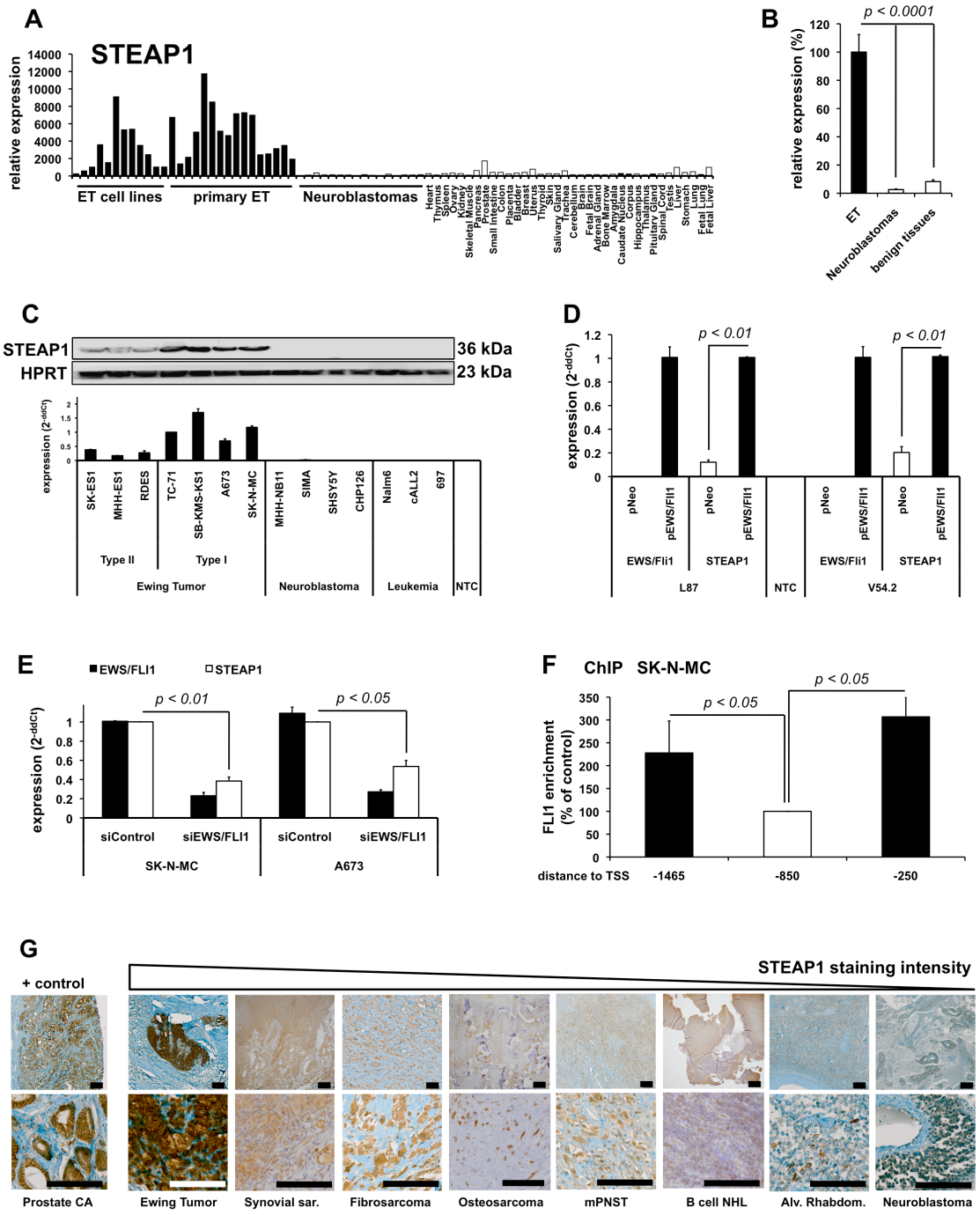

Figure 4: *STEAP1* is induced by EWS/FLI1 and highly expressed in ET:
A and B: STEAP1 expression measured by microarrays of 26 ET and 16 neuroblastomas (GSE1824, GSE1825, GSE15757) compared to 36 benign tissues (GSE2361). Mean±SEM. C: Quantification of STEAP1 by qRT-PCR and WB in ET (type 1 and 2 translocation), neuroblastoma and leukemia cell lines. Mean±SEM of three experiments (duplicates/group). Loading control: hypoxanthine phosphoribosyl-transferase 1 (HPRT); NTC: no-template-control. D: Analysis of STEAP1 and EWS/FLI1 by qRT-PCR in MSCs (L87 and V54.2) transfected with pMSCVews/fli1 (pEWS/FLI1) or empty vector (pNEO). Mean±SEM of three experiments/cell line (duplicates/group). E: Expression of STEAP1 and EWS/FLI1 in ET after EWS/FLI1-silencing. Mean±SEM of two experiments/cell line (duplicates/group). F: ChIP of the *STEAP1* promoter: FLI1 is enriched at the ETS consensus sites at -250 and -1465 bp upstream of the TSS. The -850 bp region is devoid of the ETS recognition sequences and served as negative control. Mean±SEM of three ChIPs; t-test. G: IHC for STEAP1 of prostate cancer, ET, synovial sarcoma, sclerosing epithelioid fibrosarcoma, osteosarcoma, malignant peripheral nerve sheath tumor (mPNST), B cell non-Hodgkin lymphoma (NHL), alveolar rhabdomyosarcoma, and neuroblastoma. Scale bars = 500 and 125 µm.

4.1.2 Silencing of STEAP1 neither affects neuroendothelial phenotype nor alters cellular migration and adhesion *in vitro*

Since ET display a dual neuroectodermal and endothelial (hereafter for brevity termed “neuroendothelial”) phenotype that is induced and maintained by oncogenic EWS/ETS signaling via mostly unknown downstream mediators [4], the author checked whether EWS/FLI1-driven STEAP1 expression influences ET morphology.

As seen from Figure 5A STEAP1-silencing in RDES cells, which possess strong tube-formation abilities on Matrigel, did not inhibit endothelial differentiation. In contrast, knockdown of EWS/FLI1 dramatically abolished tube-formation indicating that other EWS/FLI1-driven factors mediate the endothelial phenotype of ET.

Moreover, STEAP1-silencing neither significantly regulated established endothelial (EMP1, EPHB2) nor neuronal (NGFR, ALCAM, GAP43, GFAP) markers [46] (Figure 5B). Because STEAP1 is a transmembrane protein, the author assessed whether STEAP1-silencing impacts cellular migration and adhesion.

As seen in Figure 5C, STEAP1 knockdown did not alter migration. Furthermore, neither numerical nor morphological changes of focal adhesions were detected by IF of vinculin (Figure 5D), an established surrogate marker for intact focal adhesions [92]. Consistently, neither an influence of STEAP1 on the expression of a series of integrin and adhesion molecules (Figure 5E) nor on the functional adhesive abilities of ET cells was found (Figure 5F).

4.1.3 Knockdown of STEAP1 inhibits proliferation, invasion, anchorage-independent colony-formation, tumorigenicity and metastasis of ET cells

Since STEAP1 is overexpressed in ET, it was tested whether RNAi-mediated STEAP1-silencing impacts the ET phenotype. By using an xCELLigence instrument, a reduced proliferation of ET cells upon STEAP1 knockdown was observed (Figure 6A).

Moreover, STEAP1-silencing inhibited cellular invasiveness through Matrigel as measured by a Matrigel-covered Transwell system (BD Biosciences) (Figure 6B).

To evaluate the effect of long-term knockdown of STEAP1, STEAP1 shRNA expressing infectants of two ET cell lines (SK-N-MC and SB-KMS-KS1) were generated. Constitutive STEAP1-silencing reduced colony-formation of ET cells in methylcellulose in a dose-dependent manner (Figure 6C and Table 1).

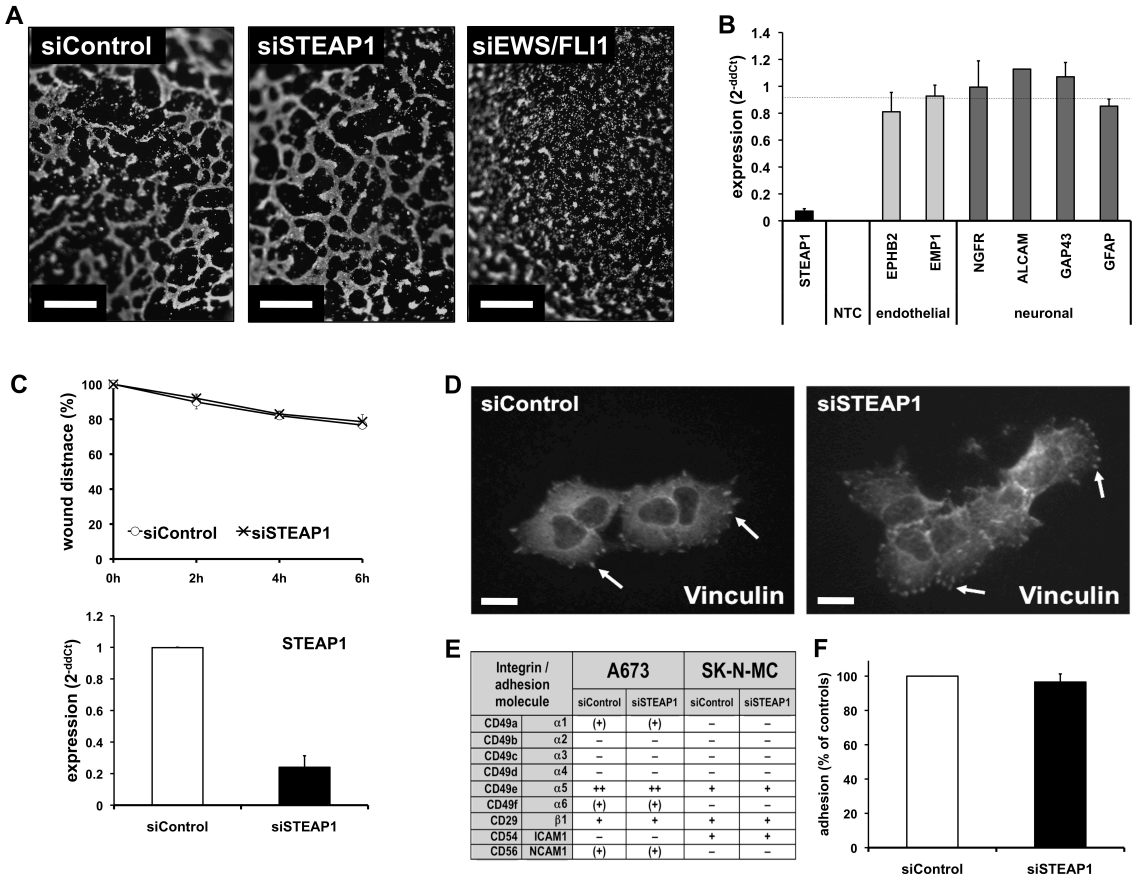

Integrin / adhesion molecule		A673		SK-N-MC	
		siControl	siSTEAP1	siControl	siSTEAP1
CD49a	α1	(+)	(+)	–	–
CD49b	α2	–	–	–	–
CD49c	α3	–	–	–	–
CD49d	α4	–	–	–	–
CD49e	α5	++	++	+	+
CD49f	α6	(+)	(+)	–	–
CD29	β1	+	+	+	+
CD54	ICAM1	–	–	+	+
CD56	NCAM1	(+)	(+)	–	–

Figure 5: STEAP1 neither affects neuroendothelial phenotype nor alters migration and adhesion:
A: Analysis of tube-formation of RDES ET cells on Matrigel after STEAP1 or EWS/FLI1 silencing (scale bar = 100 µm; representative images of three experiments). B: Gene expression analysis by qRT-PCR of endothelial (EPHB2, EMP1) and neuronal markers (NGFR, ALCAM, GAP43, GFAP) after STEAP1 knockdown in SB-KMS-KS1 (mean±SD; controls are set as 1; similar results have been obtained with A673 and SK-N-MC cells; not shown).
C: Migration of confluent A673 cells with/without STEAP1 knockdown (wound distance in % of siControl as mean±SD). D: IF of A673 cells after STEAP1 knockdown stained with an anti-vinculin-antibody (scale bar = 5 µm; representative images of three experiments).
E: Flow-cytometric analysis of integrin and adhesion molecule expression after STEAP1-silencing in A673 and SK-N-MC cells. Semiquantitative evaluation: – = no, (+) = faint, + = moderate, and ++ = strong expression. Similar results have been obtained with TC-71 and SB-KMS-KS1 cells (not shown).
F: Adhesion to plastic surface of A673 cells after STEAP1-silencing. Representative data are mean±SD of two experiments. Similar results have been obtained with SB-KMS-KS1 (not shown).

Consistently, these infectants exhibited delayed tumor growth in Rag2$^{-/-}\gamma_c^{-/-}$ mice (Figure 6D and 6E). The persistence of the STEAP1 knockdown was confirmed *ex vivo* in each xenograft by qRT-PCR (Figure 6D).

Comparing the xenografts with and without STEAP1-silencing no changes for the apoptosis-marker caspase-3 or for tumor-infiltrating macrophages (tested by MAC3; not shown) were found by IHC. In addition, no differences in vascularization, quantified by staining for the endothelial marker CD31 (not shown), and in intratumoral necrosis were observed (Figure 6F).

Similar to local tumor growth, experimental metastasis into the liver was diminished after STEAP1 knockdown (Figure 6G). Although SK-N-MC and SB-KMS-KS1 cell lines showed a high propensity to metastasize into livers, kidney metastases were only noted in mice injected with control cells (pSIcontrol) (not shown).

Taken together, these results suggest that STEAP1 supports growth and invasiveness of ET.

Table 1: Summary of results of colony forming assays:
Each experiment was performed in duplicate and repeated at least twice with each infectant; t-test was applied to test significance of inhibition of colony formation upon STEAP1 knockdown.

		pSIcontrol		pSIsteap1		colonies (% of control)	SD (%)	STEAP1 knockdown		
cell line	clone no.	colonies (mean)	SD	colonies (mean)	SD			% of control	SD (%)	*p* value
SK-N-MC	A	281	9	153.5	7.5	54.6	4.9	46	0.6	0.004
	B	676.5	61.5	195.5	5.5	28.8	2.8	39.7	0.2	0.008
	C	416.5	43.5	75.5	0.5	18.12	0.26	36.4	0.5	0.008
SB-KMS-KS1	A	816.5	68.5	324	7	39.7	2.2	53.8	2.9	0.0094
	B	806	6	334	22	41.4	6.6	44.7	0.3	0.0011
	C	580	15	122	10	21	8.2	37	0.6	0.00084

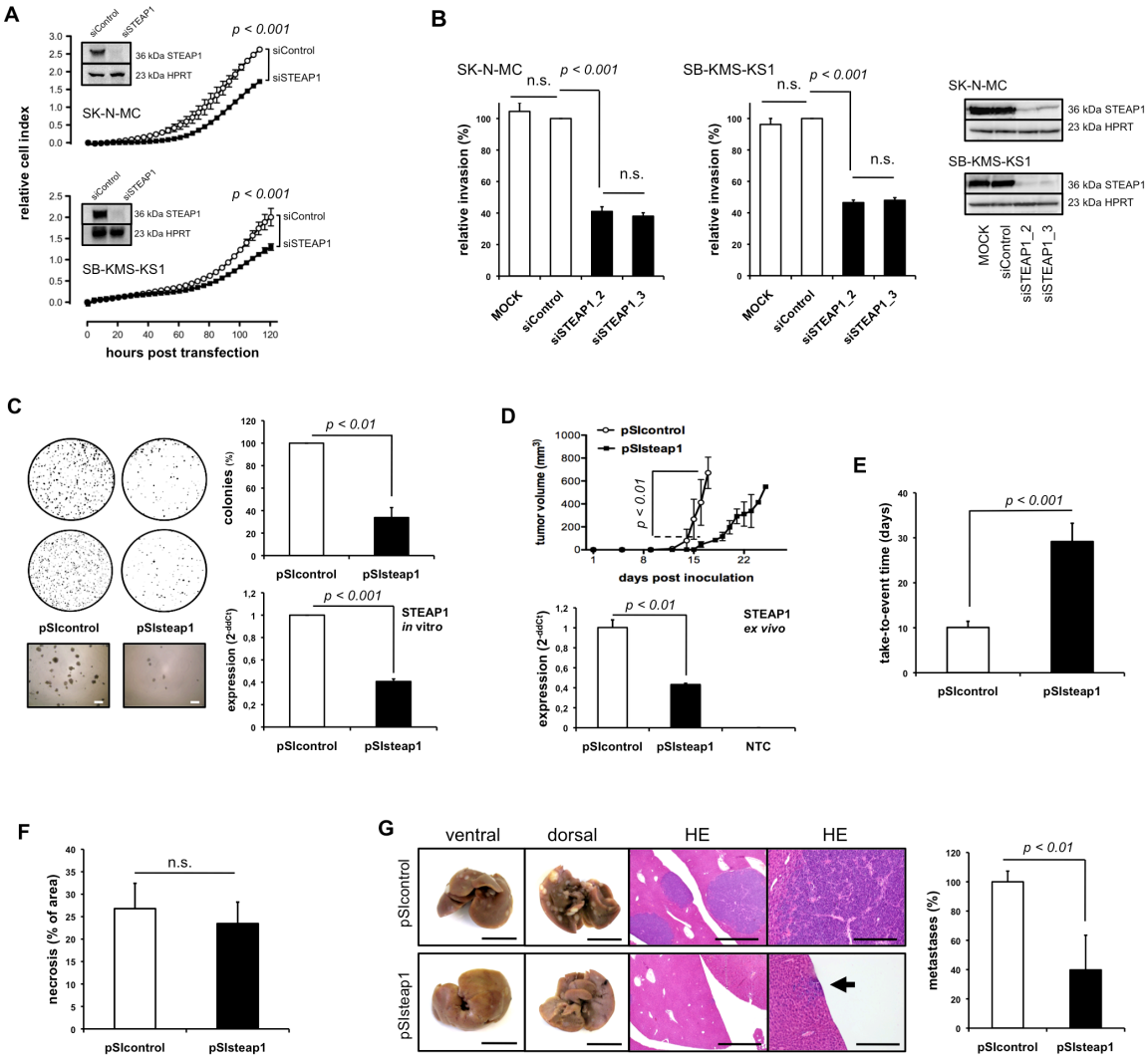

Figure 6: Knockdown of STEAP1 inhibits proliferation, invasion, anchorage-independent colony-formation, tumorigenicity and metastasis of ET cells:
A: Analysis of proliferation of transfected ET cells with xCELLigence. Cellular impedance is displayed as relative cell index. Mean±SEM of two experiments/cell line (heptaplicates/group). WB analysis was performed 100h after transfection with siRNA. B: Analysis of invasiveness of SK-N-MC and SB-KMS-KS1 (transfected with siRNA 48h before seeding). WB shows efficacy of STEAP1 knockdown. Mean±SEM of three experiments (pentaplicates/group).
C: Anchorage-independent colony-formation of SK-N-MC with constitutive STEAP1 knockdown (pSIsteap1). Scale bars 1,000 µm. Mean±SEM of three experiments (duplicates/group).
D: Tumorigenicity of SK-N-MC infectants (5 mice/group) and *ex vivo* confirmation of STEAP1 knockdown by qRT-PCR. Mean±SEM. E: Combined analysis of tumor growth as take-to-event time of three experiments (14 mice pSIcontrol; 18 mice pSIsteap1). Mean±SEM. "Take" is defined as the day when the tumor exceeded 2 mm and "event" as the day when the tumor exceeded 10 mm in diameter.
F: Quantification of necrotic area (14 xenografts/group). Mean±SEM of three experiments. G: Evaluation of metastatic potential of pSIsteap1 infectants (intravenously injected; 4 mice/group). All macroscopically visible metastases were counted and their small-round-blue phenotype was confirmed by histology (scale bar = 10 mm for macroscopy, 1,000 µm and 100 µm for histology; arrow: micro-metastasis). Mean±SEM; t-test.

4.1.4 STEAP1 expression neither impacts cell survival nor cell cycle progression, but correlates with invasiveness

As STEAP1 knockdown appeared to inhibit cell proliferation, it was tested whether this effect is caused by changes in cell survival and/or cell cycle progression. As seen from Figure 7A, both parameters were not affected by STEAP1 knockdown. However, conversely to the data obtained from STEAP1 knockdown experiments (Figure 6), STEAP1 overexpression in slightly STEAP1 expressing ET cells increased invasiveness and proliferation (Figure 7D and 7E). Moreover, endogenous STEAP1 levels correlated with invasiveness of different ET cell lines (Figure 7F).

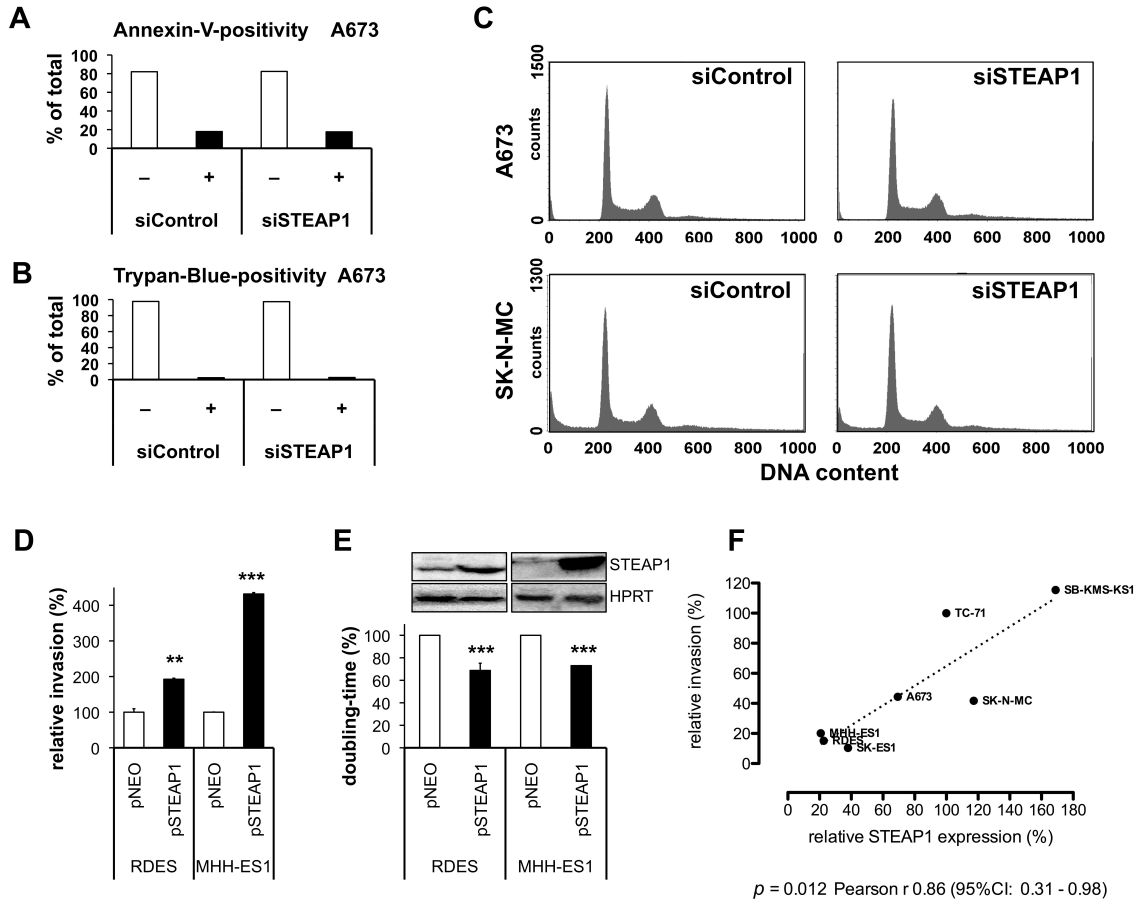

Figure 7: STEAP1 expression neither impacts cell survival nor cell cycle progression, but correlates with invasiveness:
A: Apoptosis rates of A673 cells (annexin-V) 48h after transfection (+/– = annexin-V-positive/negative). B: Trypan-Blue staining of A673 cells 48h after transfection (+/– = Trypan-Blue-positive/negative).C: Cell cycle analysis 48h after transfection. Representative images from three independent experiments/cell line. D and E: Invasiveness and doubling-time of RDES and MHH-ES1 cells with STEAP1 overexpression (pSTEAP1) compared to controls (pNEO). Mean±SEM; duplicates/group; t-test. F: Invasiveness of 7 different ET cell lines in correlation to their STEAP1 expression (compare to Figure 4C). TC-71 was set as 100% (duplicates/cell line). Invasiveness normalized for proliferation. ** $p < 0.01$, *** $p < 0.001$; t-test.

4.1.5 STEAP1-silencing leads to adaptations in oxidative stress response systems

To gain functional insight into how STEAP1 influences ET malignancy, whole-transcriptome microarrays (GSE26422) were performed in order to identify concordantly regulated genes in A673 and SK-N-MC cells after STEAP1-silencing (min. mean log2 fold change ±0.32; max. variation of 40% across siRNAs). STEAP1 knockdown differentially regulates 87 genes (41 up and 46 down; Figure 8A and Table Appendix 9.1). STEAP1-dependent gene regulation was confirmed by qRT-PCR with selected genes after STEAP1 knockdown (Figure 8B).

Among the 40 top-regulated genes 20% were assigned to the ubiquitin-proteasome-system (UPS) according to their GO-annotations, suggesting that STEAP1 might play a role in protein modification that requires enhanced proteasomal decay. Consistently, gene-set enrichment analysis (GSEA) revealed that STEAP1-silencing regulates gene-sets involved in oxidative stress responses, type-II-conjugation and proteolysis (Table 2), which are part of the oxidative stress phenotype seen in cancer [109, 110].

In support of the prediction that changes in oxidative stress responses influence overall proteome composition, STEAP1 knockdown altered the protein levels of 121 spots (81 spots up- and 40 spots downregulated) out of 845 detected spots in 2D gelelectrophoresis of SK-N-MC cells [min. linear fold change ±2 in three independent experiments as assessed by densitometric analysis with PDquest Advanced (BioRad); $p < 0.05$]. The 24 most significantly regulated spots and one non-regulated control spot were excised for proteomic analysis.

By mass spectrometry 132 different proteins were identified of which 17% were assigned to protein transport and folding, 13% to invasion and 11% to the redox-system according to their GO-annotations (Figure 8C). Among these proteins are several redox-enzymes such as peroxiredoxins and superoxide dismutases, which are

deregulated in a large cohort of cancers [66, 111]. Moreover, endosomal redox-stress response proteins [112, 113] were identified including T-complex chaperones, heat-shock proteins, protein-disulfide isomerases as well as co-chaperones. Furthermore, mediators of post-transcriptional mRNA-processing such as heterogeneous nuclear ribonucleoproteins, THO complex proteins and eukaryotic translation initiation factors were identified (Table Appendix 9.2).

Notably, also deregulations of four out of six key modules of the hexameric proteasomal ATPase (PSMC3, PSMC4, PSMC5, and PSMC6) were identified in regulated spots by proteomic means as well as key modules of the proteolytic cavities of the proteasome and immunoproteasome (PSMA3, PSMB5, PSMB8, and PSMB9), which are critical for protein quality control upon oxidative stress [114]. These data were confirmed by GSEA pathway analysis (Table 3).

In summary, these analyses suggest that STEAP1-silencing leads to adaptations in oxidative stress response systems, which is compatible with the hypothesis that STEAP1 is associated with the oxidative stress phenotype of ET.

Table 2: GSEA of differentially regulated genes after STEAP1-silencing:
Gene-sets are displayed according to their enrichment score that reflects the degree to which the gene-set is overrepresented at the extremes (top or bottom) of the entire ranked gene list yielded by microarray analysis. The normalized enrichment score (NES) accounts for different sizes of the interrogated gene-sets [96].

Gene-set	Status[a]	Function	NES	*p* value
SERINE_TYPE_ENDOPEPTIDASE_ACTIVITY	positive	proteolysis	1.967	< 0.01
GENTILE_UV_RESPONSE_CLUSTER_D8	positive	ox-stress-resp[b]	1.887	< 0.01
SERINE_TYPE_PEPTIDASE_ACTIVITY	positive	proteolysis	1.835	< 0.01
SERINE_HYDROLASE_ACTIVITY	positive	proteolysis	1.756	< 0.01
GNF2_PRDX2	positive	ox-stress-resp[b]	1.699	0.023
GLUTATHIONE_TRANSFERASE_ACTIVITY	negative	ox-stress-resp[b]	-1.654	0.019
REACTOME_PHASE_II_CONJUGATION	negative	protein modification	-1.667	0.017
GCM_ERCC4	negative	ox-stress-resp[b]	-1.681	< 0.01
NEWMAN_ERRC6_TARGETS_UP	negative	ox-stress-resp[b]	-1.726	0.021

[a] positive = upregulation after STEAP1-silencing; negative = downregulation after STEAP1-silencing
[b] oxidative stress response

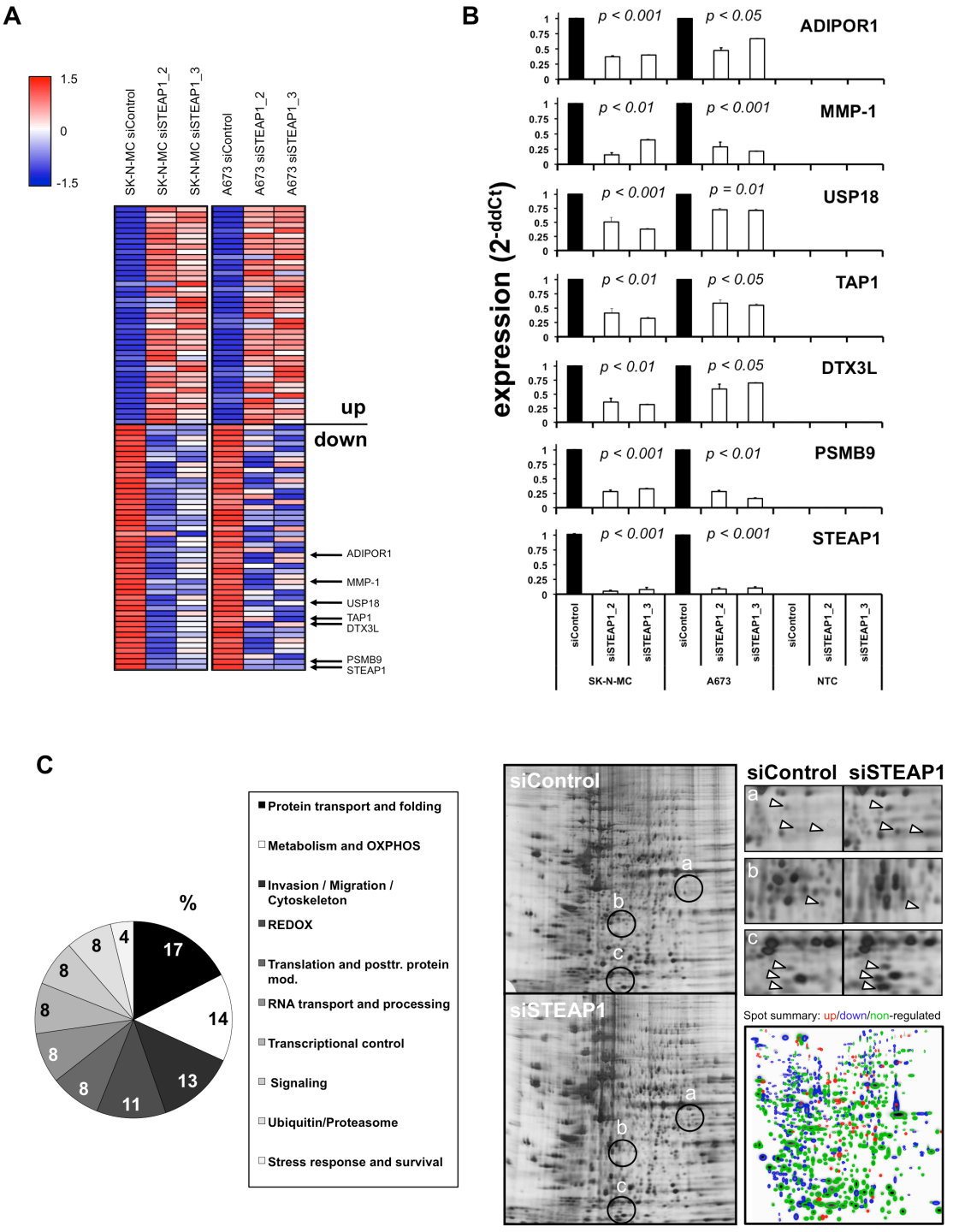

Figure 8: STEAP1-silencing leads to adaptations in oxidative stress response systems:
A: Heat-maps of differentially expressed genes after STEAP1-silencing (normalized median centered log2-values) including genes selected for validation (arrows). B: Validation of differential gene expression by qRT-PCR. ADIPOR1: adiponectin receptor 1; MMP-1: matrix metallopeptidase 1; USP18: ubiquitin specific peptidase 18; TAP1: transporter 1, ATP-binding cassette, sub-family B; DTX3L: E3 ubiquitin-protein ligase deltex 3-like; PSMB9: proteasome subunit beta 9. Mean±SEM of at least two experiments/cell line (duplicates/group); t-test. C: Left: Distribution of functional GO-annotations of differentially expressed proteins in SK-N-MC as identified by 2D gelelectrophoresis and mass spectrometry 72h after RNAi. Right: Representative 2D gels of siControl and siSTEAP1, micrographs showing regulated spots (arrows), and the computational overlay summary of up-, down- and non-regulated spots of three experiments.

Table 3: GSEA pathway analysis of differentially regulated proteins as identified by 2D gelelectrophoresis and mass spectrometry:

Gene-set name[a]	Function	K[b]	k[c]	k/K	*p* value
REACTOME_CHAPERONIN_MEDIATED_PROTEIN_FOLDING	Chaperonin-mediated protein folding	50	7	0.14	< 0.001
REACTOME_PREFOLDIN_MEDIATED_TRANSFER_OF_SUBSTRATE_TO_CCT_TRIC	Chaperonin-mediated protein folding	28	7	0.25	< 0.001
REACTOME_FORMATION_OF_TUBULIN_FOLDING_INTERMEDIATES_BY_CCT_TRIC	Chaperonin-mediated protein folding	22	6	0.27	< 0.001
KEGG_PROTEASOME	Proteasomal protein decay	48	6	0.13	< 0.001
REACTOME_SCF_BETA_TRCP_MEDIATED_DEGRADATION_OF_EMI1	Ubiquitin ligase-mediated protein processing	48	6	0.13	< 0.001
REACTOME_SCF_SKP2_MEDIATED_DEGRADATION_OF_P27_P21	Ubiquitin ligase-mediated protein processing	52	6	0.12	< 0.001
REACTOME_ASSOCIATION_OF_TRIC_CCT_WITH_TARGET_PROTEINS_DURING_BIOSYNTHESIS	Chaperonin-mediated protein folding	29	5	0.17	< 0.001
REACTOME_METABOLISM_OF_PROTEINS	Translation, post-translational modification and protein folding	215	12	0.06	0.024

[a] REACTOME, BIOCARTA and KEGG pathway gene-sets were used for analysis

[b] K = number of genes in gene-set

[c] k = number of genes in overlap

4.1.6 STEAP1 expression is not linked with iron uptake and reduction, but influences key components of the UPS

Others have shown that certain STEAPs can impact iron uptake and reduction in HEK-293T cells [50]. However, as expected from the microarray data of the current study, the author did not find evidence for STEAP1 to impact iron uptake and reduction in ET cells using a colorimetric assay kit for assessment of the cellular ferrous and total iron content (Figure 9A). Because STEAP1 knockdown appeared to be associated with the downregulation of genes involved in the UPS, it was tested whether the artificial overexpression in ET cells does also affect the expression levels of these genes. As seen from Figure 9B STEAP1 overexpression leads to a significant upregulation of these genes further indicating that STEAP1 is involved in the regulation of components of the UPS (Figure 9C), rather than being involved in cellular iron metabolism.

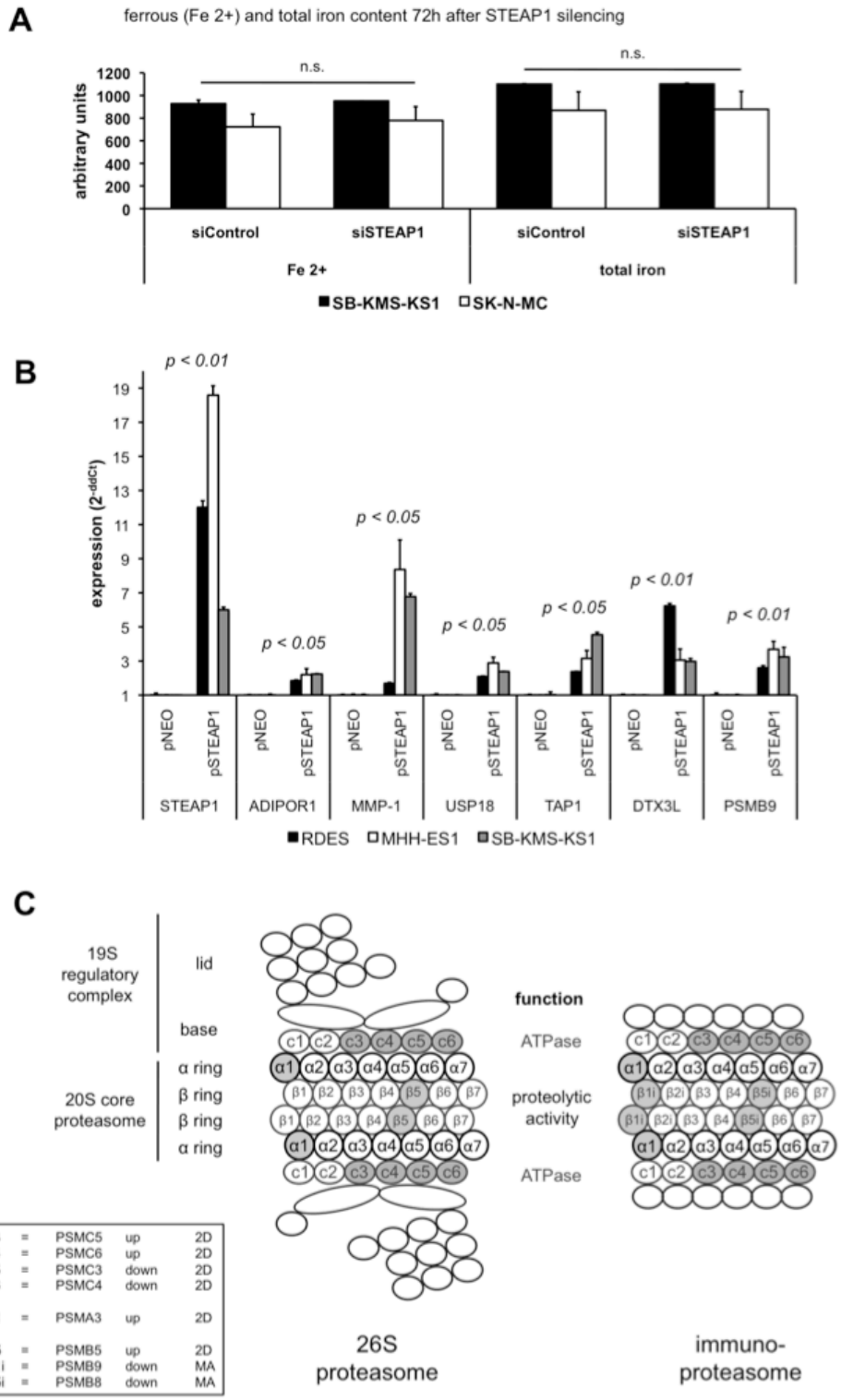

Figure 9: **STEAP1 expression is not linked with iron uptake and reduction, but influences key components of the UPS:**
A: Analysis of iron content. Mean±SEM of two independent experiments/cell line (duplicates/group); t-test. B: Expression of STEAP1-regulated genes after forced STEAP1 overexpression (pSTEAP1) (duplicates/group). Controls (pNEO) were set as 1. Mean±SEM; t-test. C: Schematic illustration of the organization of the 26S proteasome and immunoproteasome. Only the β1, β2 and β5 and the β1i, β2i and β5i monomers have proteolytic activity [115]. Shaded circles: modules affected by STEAP1-silencing. Mode of detection: 2D = 2D gelelectrophoresis; MA = microarrays.

4.1.7 STEAP1-silencing regulates redox-sensitive miRNAs

To test whether STEAP1 might contribute to the transcriptional regulation of miRNAs that in turn may regulate transcripts and/or proteins identified by microarrays and mass spectrometry, transiently transfected ET cells were subjected to microarray analysis for differential miRNA expression. STEAP1-silencing led to a differential expression of 93 miRNAs (min. log2 fold change ±0.25 across cell lines, $p < 0.05$, t-test) (Figure 10 and Table Appendix 9.3). The top 10 up- and downregulated miRNAs were then screened for their corresponding top 10% of potential target transcripts as judged by analysis of a public miRNA database and the corresponding mirSVR scores (see methods). These top-ranked 10% putative target transcripts were compared with the identified STEAP1-regulated transcripts and proteins and are listed in Figure 10. Several of these miRNAs further proved to be potentially regulated by ROS as they were found to be highly sensitive to ROS in published experiments of others [116-122] (literature search closed at end of March 2011). Taken together, these data indicate that STEAP1 might regulate part of its downstream targets on posttranscriptional level, possibly by redox-mediated regulation of the corresponding redox-sensitive miRNAs.

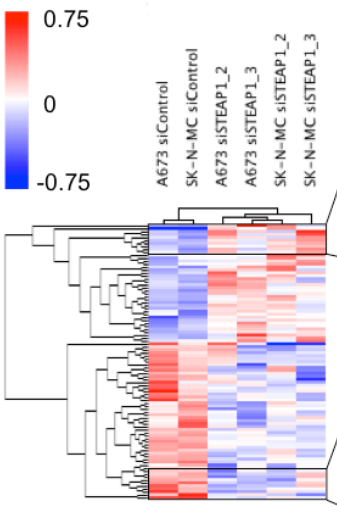

Probe Set ID	mean log2 FC	Targets 2D proteins	Targets Microarrays
hsa-miR-877_st	0.77	*none*	HERC5
hsa-miR-744_st	**0.71**	PPM1G	*none*
hsa-miR-216a_st	0.50	CCT5	GBP1; PSMB8
hsa-miR-653_st	0.44	CASP7	*none*
hsa-miR-520d-5p_st	0.44	HNRNPA2B1; LMNB1	*none*
hsa-miR-671-5p_st	**0.41**	*none*	*none*
hsa-miR-377_st	**0.36**	ANXA2; HNRNPA2B1; HNRNPH3	GBP1
hsa-miR-1825_st	**0.36**	ACTG1	FABP3
hsa-miR-130b_st	**0.35**	CBFB; HSPA8; LMNB1	LIPA; IRF1
hsa-miR-154_st	0.34	*none*	IFIT2

Probe set ID	mean log2 FC	Targets 2D proteins	Targets Microarrays
hsa-miR-214_st	**-0.37**	APITD1; PGRMC2; RAE1; RPSA	FBLN5
hsa-miR-338-3p_st	-0.40	*none*	PLG; TAX1BP3
hsa-miR-371-5p_st	-0.40	ENOPH1; PSMC6	CYBRD1; RCAN2; RNF146
hsa-miR-331-5p_st	-0.41	*none*	*none*
hsa-miR-602_st	-0.42	*none*	*none*
hsa-miR-892b_st	-0.43	IDH2	PELI2; RNF146
hsa-miR-1224-3p_st	-0.47	HNRNPK; PGRMC2	PROS1
hsa-miR-802_st	-0.48	CCT6A; CNBP; STMN1	*none*
hsa-miR-1247_st	-0.48	ARF1	PLG; TAX1BP3
hsa-miR-204_st	**-0.58**	ACAT1; RBMX	DCUN1D3

Figure 10: STEAP1-silencing regulates redox-sensitive miRNAs:
Left: heat-map showing 93 differentially regulated miRNAs in A673 and SK-N-MC 68h after transfection. Right: tables showing the probe set IDs of the top-ranked miRNAs and their putative corresponding targets. “None” indicates that among all putative miRNA targets none was identified among the top-ranked 10% according to the mirSVR scoring algorithm. Redox-sensitive miRNAs are printed in bold font.

4.1.8 STEAP1 expression is associated with ROS levels of ET cells

In a next step, it was assessed whether the long-term knockdown of STEAP1 can alter ROS levels. Indeed, constitutive STEAP1-silencing decreased ROS levels (Figure 11A), whereas STEAP1 overexpression increased ROS levels (Figure 11B) as quantified by dihydroethidium (DHE) fluorescence. Moreover, STEAP1 knockdown reduced mitochondrial ROS without changing mitochondrial mass as quantified by Mitosox Red and Mitotracker Green staining, respectively (Figure 11C and 11D). Consistently, STEAP1 knockdown decreased the cellular pool of oxidized glutathione (glutathione-disulfide; GSSG), but increased the amount of reduced glutathione (GSH)

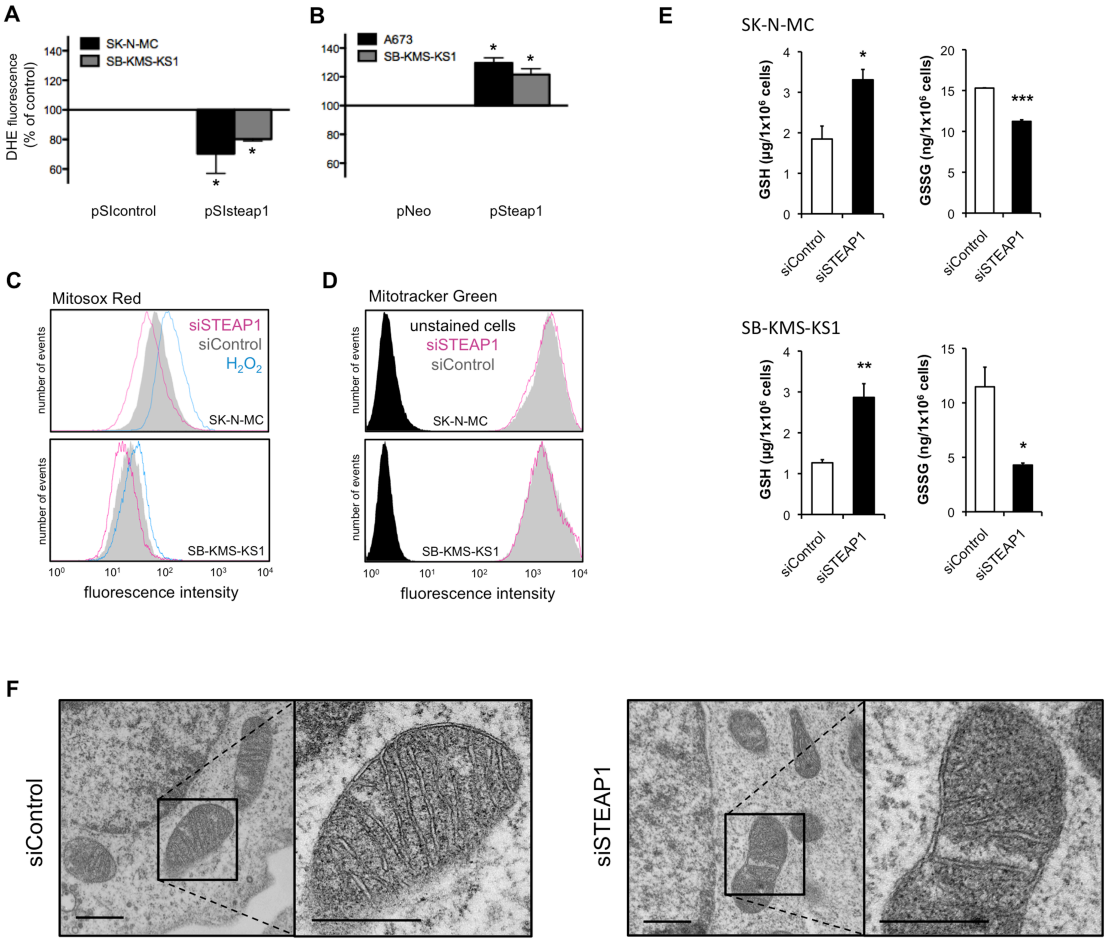

Figure 11: STEAP1 expression is associated with ROS levels of ET cells:
A and B: Measurement of ROS with DHE after constitutive STEAP1-silencing (pSIsteap1) or overexpression (pSteap1). Mean±SEM of three experiments/cell line (octaplicates/group). Controls set as 100%. C and D: Flow-cytometric measurements of mitochondrial ROS (Mitosox Red) and mitochondrial mass (Mitotracker Green). For positive control (Mitosox Red) cells were treated with 100 µM hydrogen peroxide (H_2O_2; blue). E: Analysis of GSH and GSSG. Mean±SEM of two experiments/cell line. F: Electron micrographs of SK-N-MC cells (scale bars = 0.4 µm). * $p < 0.05$, ** $p < 0.01$, *** $p < 0.001$; t-test.

(Figure 11E). No morphological changes of ET cells and their mitochondria were detected by electron microscopy upon STEAP1 knockdown (Figure 11F). Interestingly, reassessment of the microarray data revealed that STEAP1 is most prominently expressed in ET among other NOX and STEAPs (Figure 12).

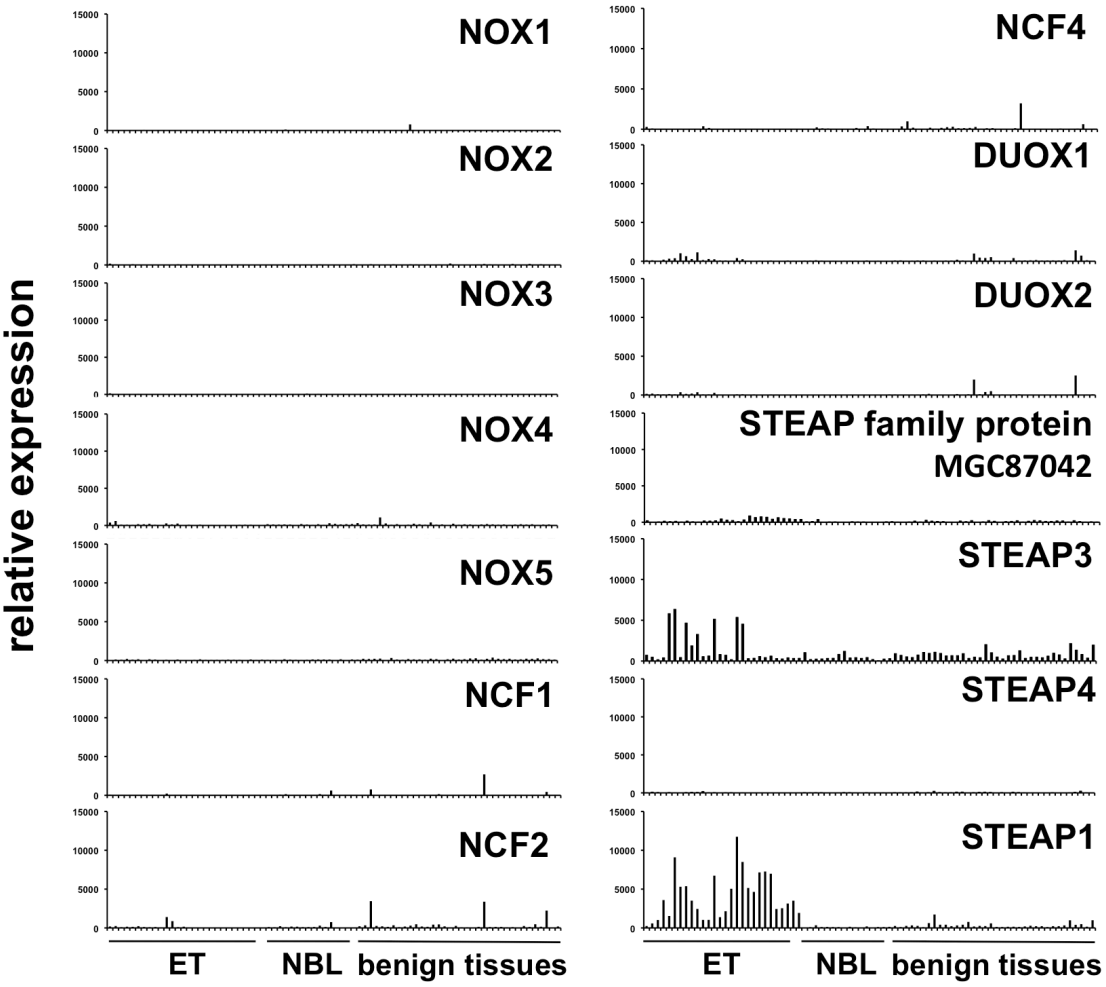

Figure 12: STEAP1 is highly expressed in ET compared to other NOX and STEAPs:
Microarray data of STEAPs, homologous NOX, and other proteins frequently involved in ROS metabolism in cancers [66]. NCF = neutrophil cytosolic factor; DUOX = dual oxidase. NBL = neuroblastomas.

4.1.9 ROS are critical for ET proliferation and invasiveness

The presented data above and recent discussion in the literature [78] indicate that ROS might promote ET aggressiveness. In accordance, treatment of ET cells with the antioxidant N-acetyl-cysteine (NAC) reduced colony-formation, proliferation and invasiveness of ET cells in a dose-dependent manner (Figure 13A to 13C).

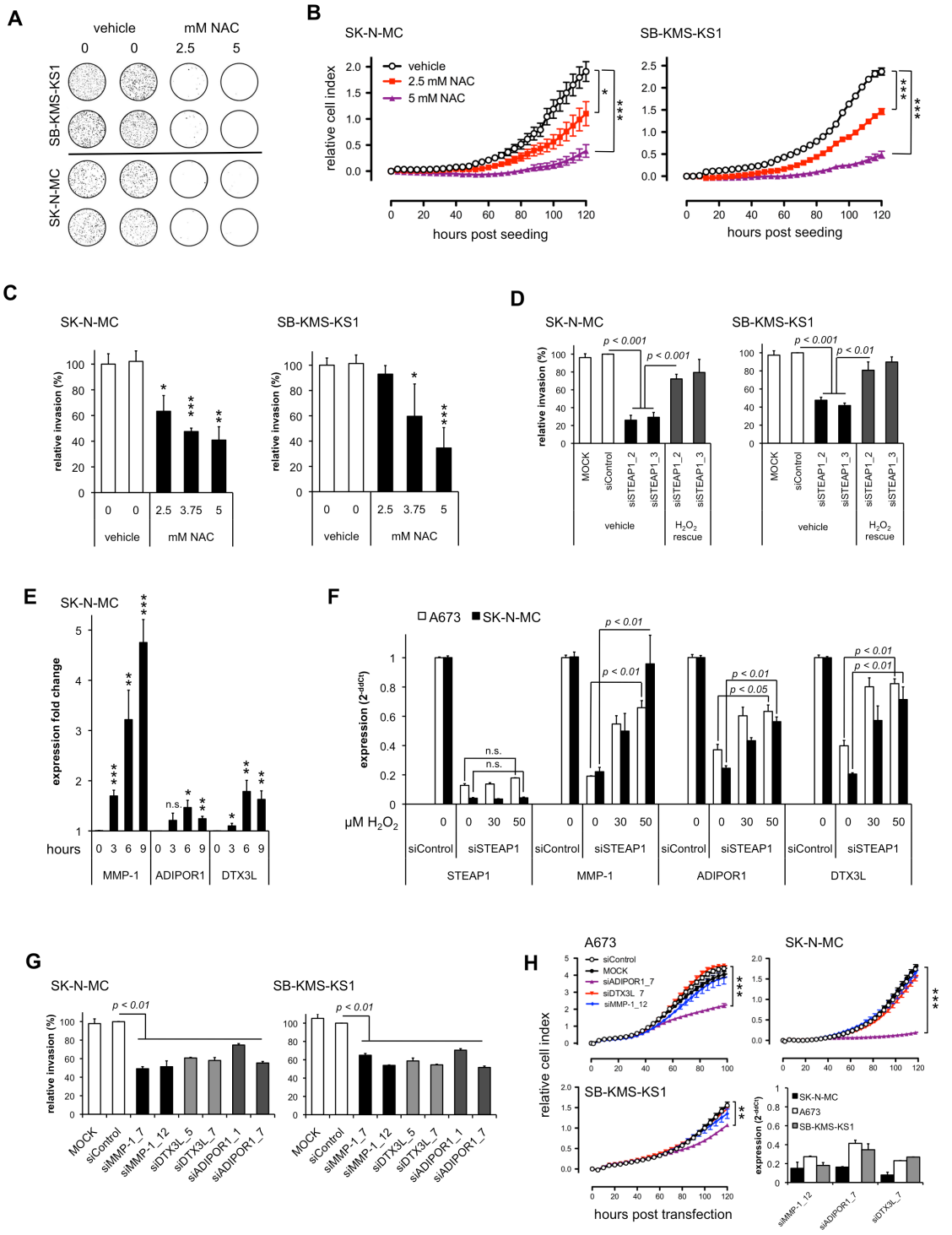

Figure 13: ROS are critical for ET proliferation and invasiveness:
A: Colony-formation after treatment with NAC or vehicle (H_2O) (duplicates/group). B: Proliferation after NAC-treatment. Mean±SEM of two experiments/cell line (quadruplicates/group). C: Invasiveness of ET cells treated with NAC. Mean±SEM of two experiments/cell line (pentaplicates/group). D: Invasiveness of ET cells with/without H_2O_2 rescue (periodical H_2O_2-treatment; cumulative 40 µM). Mean±SEM of two experiments/cell line (pentaplicates/group). E: Gene expression in SK-N-MC treated with 50 µM H_2O_2 for 0-9h. Mean±SEM of five experiments (duplicates/group). F: Analysis gene expression 6h after H_2O_2-treatment. Mean±SEM of at least two experiments/cell line (duplicates/group). G: Invasiveness of ET cells transfected 48h before. Mean±SEM of two experiments/cell line (pentaplicates/group) H: Proliferation of SK-N-MC and SB-KMS-KS1. Knockdown was confirmed by qRT-PCR (controls set as 1). Mean±SEM of two experiments/cell line (heptaplicates/group). * $p < 0.05$, ** $p < 0.01$, *** $p < 0.001$; t-test.

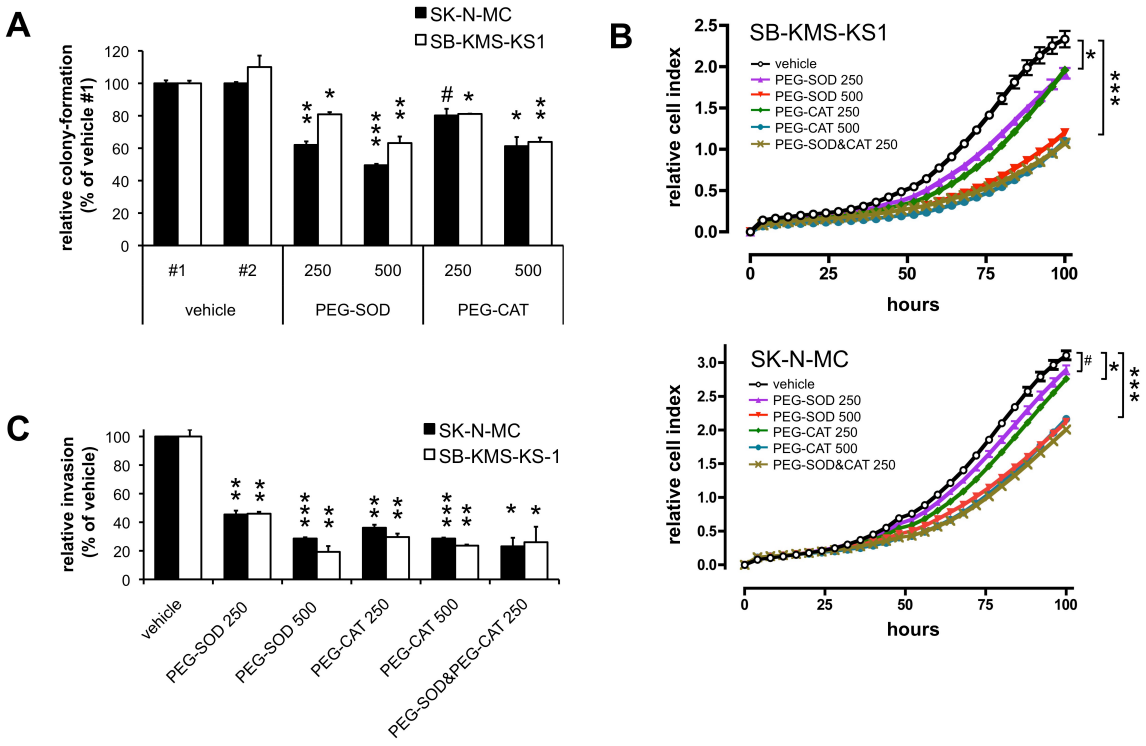

Figure 14: PEG-SOD and PEG-CAT inhibit colony-formation, proliferation and invasiveness of ET: A: Analysis of colony-formation in methylcellulose of SK-N-MC and SB-KMS-KS1 cells treated with 250 U/ml and 500 U/ml PEG-SOD or PEG-CAT or vehicle (PBS), respectively. B: Analysis of proliferation of ET cells treated with 250 U/ml and 500 U/ml PEG-SOD or PEG-CAT or vehicle, respectively. Mean±SEM; t-test. C: Analysis of invasiveness after treatment with 250 U/ml and 500 U/ml PEG-SOD or PEG-CAT or vehicle, respectively. Mean±SEM; # = borderline significant. * $p < 0.05$, ** $p < 0.01$, *** $p < 0.001$; t-test.

Similar results have been obtained with pegylated-superoxide dismutase (PEG-SOD) and pegylated-catalase (PEG-CAT) (Figure 14). Conversely, treatment of STEAP1 silenced ET cells with hydrogen peroxide (H_2O_2) rescued the invasive phenotype of STEAP1 knockdown cells (Figure 13D). The author next tested if STEAP1 regulated genes may be part of the oxidative stress phenotype observed. The proteins MMP-1, ADIPOR1 and DTX3L were chosen for follow-up due to their high expression in ET and their known involvement in oxidative stress responses [111, 123, 124].

Expression of MMP-1, ADIPOR1 and DTX3L appeared to be ROS-sensitive in ET cells as H_2O_2-treatment induced their expression in a time-dependent manner (Figure 13E). Moreover, H_2O_2-treatment rescued MMP-1, ADIPOR1 and DTX3L, but not STEAP1 expression in a dose-dependent manner implying that STEAP1 is upstream of ROS-signaling while the other genes are potentially downstream (Figure 13F). Interestingly,

silencing of these genes reduced invasiveness through Matrigel (Figure 13G), whereas only ADIPOR1 knockdown significantly reduced ET proliferation (Figure 13H). In summary, these data suggest that oxidative stress may support ET aggressiveness possibly in part via enhanced expression of MMP-1, ADIPOR1 and DTX3L.

4.1.10 STEAP1 knockdown inhibits STAT1 activation

Using GSEA to search for common transcription factor motifs within the 87 differentially regulated genes after STEAP1-silencing, the signal transducer and activator of transcription 1 (STAT1) (p = 0.07) and its downstream cofactors [125] interferon response factors (IRF) 1, 2, 7, and 8 ($p < 0.05$) were identified as the top-ranked putative STEAP1 targets. Consistently, interrogation of the GSEA Molecular Signatures Database (C2; v3.0) with these 87 genes revealed a strong overrepresentation of gene-sets involved in interferon signaling accompanying STEAP1 expression (Figure 15A and 15B).

Interestingly, STAT1, which is a downstream-effector of ROS and interferons [126], is predominantly expressed in ET among other STAT proteins (Figure 15C). Of note, STAT1-silencing reduced like STEAP1-silencing the expression of STEAP1-target genes, but left STEAP1 expression unaffected.

Moreover, the downregulation of these genes could (apart from MMP-1 in two of three cell lines tested) not be rescued by H_2O_2-treatment, suggesting that STAT1 may be downstream of ROS and STEAP1 (Figure 15D, compare Figure 13F). Indeed, STEAP1-silencing results in less phosphorylated STAT1, which can be rescued by exogenous H_2O_2 and interferon gamma (Figure 15E). However, ET cells virtually do not produce endogenously interferons and STEAP1-silencing neither alters their expression nor their secretion as seen by microarray (Figure 15F) and ELISpot analysis (Figure 16).

In summary, these data indicate that STEAP1 and ROS may in part mediate their transcriptional effects via interferon-independent activation of STAT1 (Figure 15G).

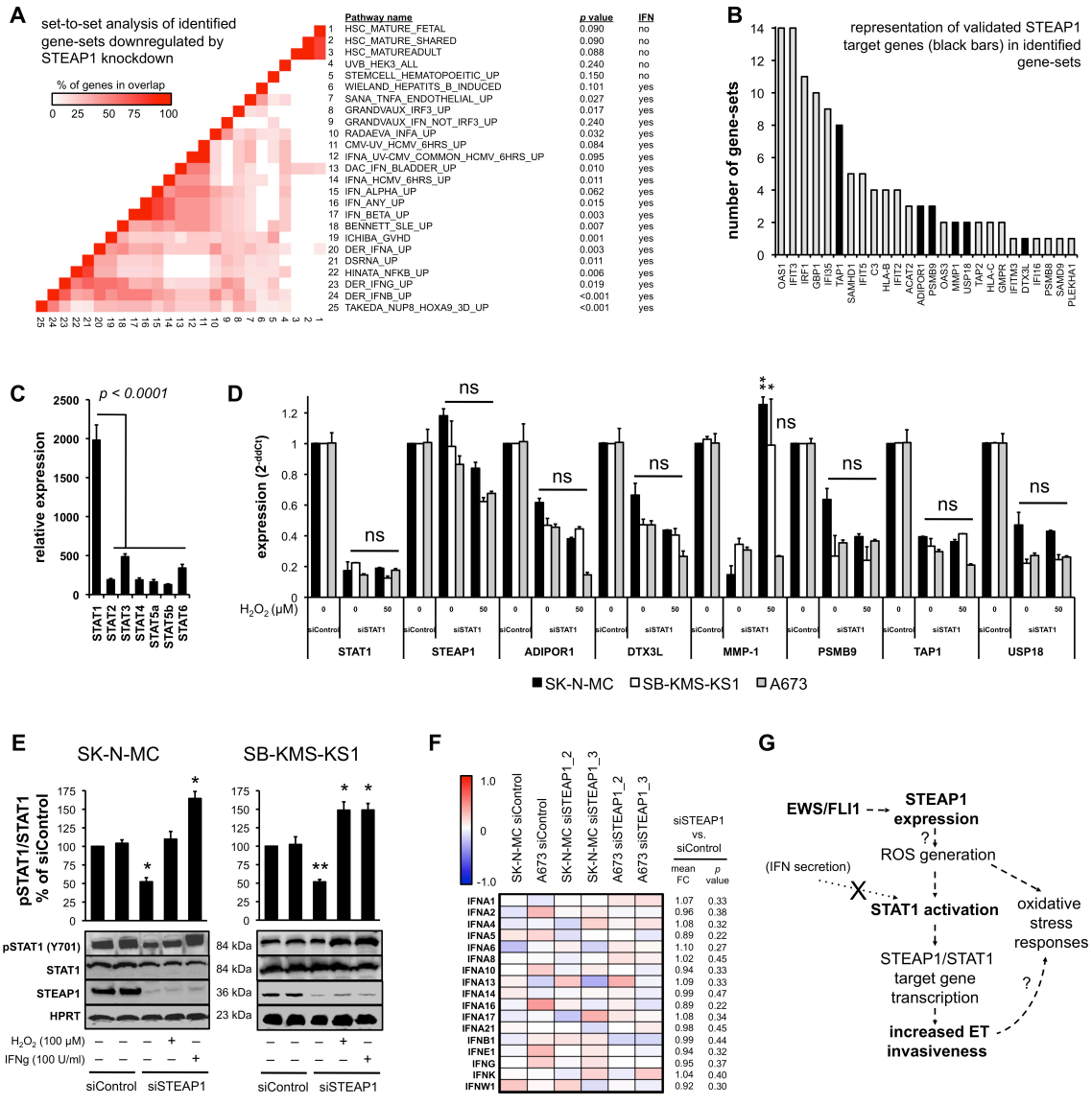

Figure 15: STEAP1 knockdown inhibits STAT1 activation:
A: Matrix-diagram of the GSEA leading-edge set-to-set analysis showing enrichment of interferon(IFN)-related gene-sets. NES: normalized enrichment score. B: Gene-in-subset analysis reveals representation of validated STEAP1 target genes (black bars) within leading-edge genes. C: Expression (Mean±SEM) of different STATs in 26 ET-microarrays. D: Expression analysis of STEAP1 target genes by qRT-PCR 48h after STAT1-silencing and H_2O_2-treatment (50 µM for 6h). E: WB and densitometric analysis of phospho-STAT1 (Y701) in ET cells 48h after RNAi and H_2O_2 (100 µM) or interferon-gamma (IFNg; 100 U/ml) stimulation. F: Heat-map showing expression of interferon genes in ET cells with/without STEAP1-silencing. G: Simplified model of STEAP1-mediated target gene regulation. * $p < 0.05$, ** $p < 0.01$; t-test.

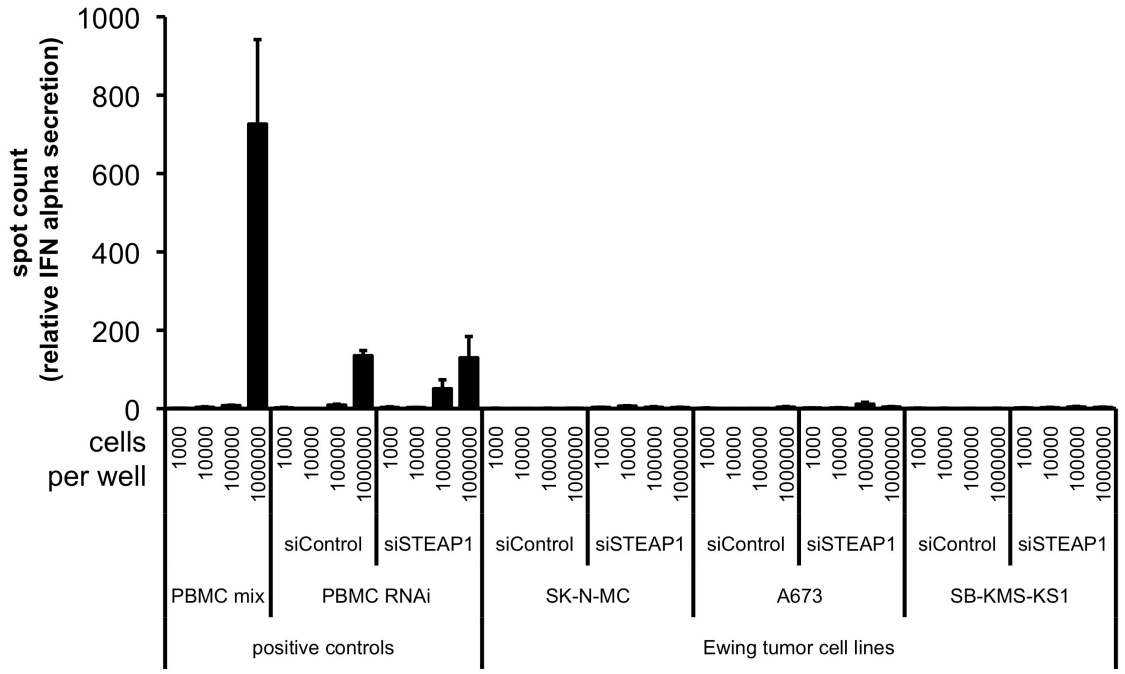

Figure 16: **ET virtually do not secrete interferon alpha:**
ELISpot analysis for quantification of functional interferon alpha secretion of SK-N-MC, A673 and SB-KMS-KS1 cells 72h after transfection with siRNA. Cells were seeded in triplicate at densities of $1x10^3$, $1x10^4$, $1x10^5$, and $1x10^6$ cells/well. For positive controls single-donor peripheral blood mononuclear cells (PBMCs) treated with siRNA or pooled PBMCs (three donors = PBMC mix) without siRNA treatment were used. Mean±SEM.

4.2 Analysis of STEAP1 in clinical ET samples

4.2.1 STEAP1 is expressed in most clinical ET and predominantly locates to plasma membranes

First the expression pattern of STEAP1 in ET was assessed. Of the 114 ET available for IHC 100 displayed detectable STEAP1 expression (87.7%, grades 1-3), albeit with evidently heterogeneous levels. Examples of the differential membranous STEAP1 immunoreactivity are given in Figure 3. 53.5% (*n* = 61) of the samples were scored as membranous STEAP1-high (46.5% membranous STEAP1-low, respectively) and 25.4% (*n* = 29) as cytoplasmic STEAP1-high (74.6% cytoplasmic STEAP1-low) (Table Appendix 9.4). In most samples classified as membranous STEAP1-high, the ET cells stained positive at their entire plasma membrane without defined apical or

basal accentuation (Figure 3). Interestingly, whereas 24.6% (28 of 114) of the cases showed maximum membranous STEAP1 expression (grade 3), only 1 of the 114 samples (0.88%) displayed maximum (grade 3) cytoplasmic STEAP1 expression. Furthermore, there was no correlation of membranous and cytoplasmic STEAP1 expression (p = 1.0 in two-sided Fisher exact test). Taken together, these data demonstrate that the majority of clinical ET express STEAP1 and that STEAP1 is mostly either predominantly located at the plasma membrane or within the cytoplasm as the fraction of membranous and cytoplasmic STEAP1-high ("double-positive") cases was relatively small (16 of 114; 14%).

4.2.2 Membranous and cytoplasmic STEAP1 expression and overall survival

In a second step, membranous or cytoplasmic STEAP1 expression or a combination of both parameters were correlated with outcome of ET patients. Patient characteristics are given in Table 4.

Univariate analysis on the predictive value of membranous and cytoplasmic STEAP1 immunoreactivity showed a lower overall survival (OS) rate in patients bearing ET classified as membranous STEAP1-low (5-year OS = 0.57; n = 53) when compared to membranous STEAP1-high cases (5-year OS = 0.79; n = 61) (p = 0.021), whereas cytoplasmic STEAP1-high expression (n = 29) was not associated with a strong effect (p = 0.212) (Figure 17A and 17B).

Combining both factors into (A) membranous STEAP1-low and cytoplasmic STEAP1-low or -high (n = 53), (B) membranous STEAP1-high and cytoplasmic STEAP1-low (n = 45), and (C) membranous and cytoplasmic STEAP1-high (n = 16) further differentiated the groups according to the OS: the 5-year OS was 0.57 (SE = 0.07) for A; 0.74 (SE = 0.07) for B, and 0.93 (SE = 0.06) for C (p = 0.038) (Figure 17C).

Table 4: Patient characteristics:
* These parameters relate to subsets of the study population.

Variable	Label	*n*	%
Sex	male	60	52.6
	female	54	47.4
Age at diagnosis	<15 years	46	40.4
	≥15 years	68	59.6
Risk group	M0 (no metastases)	83	72.8
	M1 (lung metastases)	20	17.5
	M2 (other +/- lung met.)	11	9.7
Site	axial	66	57.9
	non-axial	48	42.1
Tumor volume*	<200 ml	55	71.4
	≥200 ml	22	28.6
Histological response*	good (<10% viable cells)	46	78.0
	poor (≥10% viable cells)	13	22.0
Membranous STEAP1 expression	low	53	46.5
	high	61	53.5
Cytoplasmic STEAP1 expression	low	85	74.6
	high	29	25.4

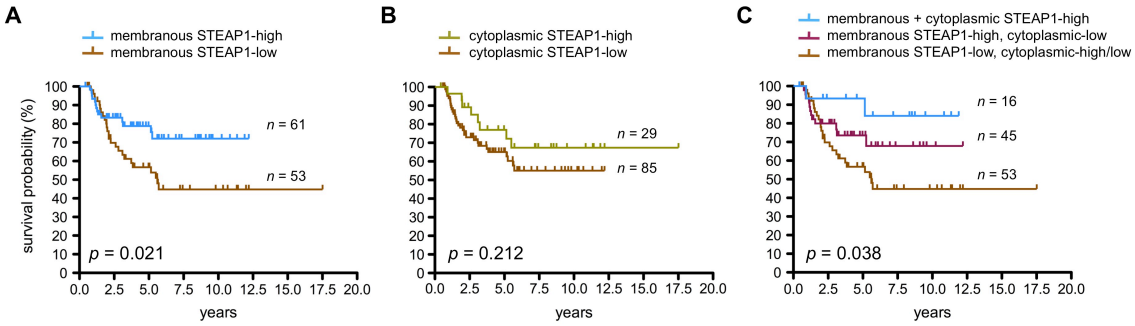

Figure 17: STEAP1 expression correlates with OS:
A: Kaplan-Meier estimates for OS probability for membranous STEAP1 expression. B: Kaplan-Meier estimates for OS probability for cytoplasmic STEAP1 expression. C: Kaplan-Meier estimates for OS probability for combined membranous and cytoplasmic STEAP1-high expression (blue), membranous STEAP1-high and cytoplasmic STEAP1-low expression (magenta), and membranous STEAP1-low and cytoplasmic STEAP1-low or -high expression (brown). Log-rank test.

4.2.3 Multivariate analysis

Next, the impact of risk stratification in patients with STEAP1-high versus STEAP1-low ET was analyzed to rule out a possible bias by favorable risk factor patterns in STEAP1-high cases. The multivariate analysis served to identify underlying factors that could influence prognosis. The known prognostic factors metastatic stage

at diagnosis (M0, M1, M2), site (axial versus non-axial), and age (<15 versus ≥15 years) were included into the multivariate analysis [31, 32, 34]. 83 patients (72.8%) had localized disease (M0), 20 patients (17.5%) had pulmonary metastases (M1), and 11 patients (9.6%) had disseminated disease including metastases other to the lungs (M2). 66 patients (57.9%) presented with an axial site, and 48 patients (42.1%) had a non-axial site. 46 patients (40.4%) were aged under 15 years, 68 patients (59.6%) were aged above 15 years at time of diagnosis. The major risk factor was metastatic disease at diagnosis [M0: Hazard ratio (HR) = 1.00; M1: HR = 2.19; M2: HR = 4.38; p = 0.002]. Membranous STEAP1-low expression (HR = 1.76; p = 0.094), age (>15 years, HR = 1.69; p = 0.135), and primary axial tumor site (HR 1.30; p = 0.435) showed only a tendency or no major impact on survival (n = 114; Table 5).

In a second step the major group of patients with localized disease (M0; n = 83) was analyzed. Here, membranous STEAP1-low expression (HR = 2.59; p = 0.036) and age (>15 years; HR = 3.39; p = 0.030) were major risk factors on survival in relation to primary axial tumor site (HR 1.76; p = 0.218) (Table 6). Tumor volume: A tumor volume categorization (<200 ml versus ≥200 ml) was only available in 77 patients. 55 patients (71.4%) had a tumor volume <200 ml, and 22 patients (28.6%) had a tumor volume >200 ml. Multivariate analysis in this sub-cohort of 77 patients adding tumor volume as known prognostic factor [31, 32, 34] confirmed metastatic disease at diagnosis (p = 0.002) and membranous STEAP1-low expression (HR = 2.65; p = 0.036) as major risk factors.

Table 5: Summary of results of the multivariate analysis in all patients:

Variable	Label	Risk ratio (95% CI)	*p*
Risk group	M0 (no metastases)	1	0.002
	M1 (lung metastases)	2.19 (1.04-4.61)	0.039
	M2 (other +/- lung met.)	4.38 (1.83-10.5)	0.001
Membranous STEAP1 expression	low	1.76 (0.91-3.48)	0.094
Age	≥15 years	1.69 (0.85-3.37)	0.135
Site	axial	1.30 (0.68-2.48)	0.435

Table 6: Summary of results of the multivariate analysis in patients with localized disease:

Variable	Label	Risk ratio (95% CI)	*p*
Membranous STEAP1 expression	low	2.59 (1.07-6.29)	0.036
Age	≥15 years	3.39 (1.13-10.2)	0.030
Site	axial	1.76 (0.72-4.31)	0.218

4.2.4 Association of STEAP1 expression with histological response to chemotherapy

Since high membranous STEAP1 expression correlated with an improved OS in ET, it was tested whether these tumors also responded better to treatment as estimated by Salzer-Kuntschik regression states [127]. For 59 patients (51.8%) data was available for histological response following induction chemotherapy without concurrent early radiotherapy. 46 patients (78%) showed a good histological response (<10% viable tumor cells), and 13 patients (22%) a poor histological response (≥10% viable tumor cells). 80.6% of the patients with membranous STEAP1-high expression showed a good histological response compared to 73.9% of the patients with membranous STEAP1-low expression (p = 0.748). Similarly to their excellent OS, patients with combined membranous and cytoplasmic STEAP1-high expression showed the best rate of good histological response (91.7%) within our cohort (p = 0.473) (Table 7).

Table 7: Summary of results of correlation of STEAP1 with tumor regression grade:

		Histological response		
Variable	Label	good	poor	*p*
Membranous STEAP1 expression	low	17 (73.9%)	6 (26.1%)	
	high	29 (80.6%)	7 (19.4%)	0.748
Membranous + cytoplasmic STEAP1 expression	low + low/high	17 (73.9%)	6 (26.1%)	
	high + low	18 (75.0%)	6 (25.0%)	
	high + high	11 (91.7%)	1 (8.3%)	0.473

To test whether differential STEAP1 expression may indeed alter response to chemotherapy *in vitro*, ET cells with a transient STEAP1 knockdown were treated with chemotherapeutics and their rates of necrosis were assessed by flow cytometry. Treatment of STEAP1-silenced SK-N-MC and SB-KMS-KS1 ET cells with 1 µM doxorubicin for 24h exhibited lower rates of necrosis compared to ET cells with high STEAP1 expression ($p < 0.01$; t-test, $n \geq 4$) (Figure 18), indicating that low STEAP1 expression confers ET cells with a more resistant phenotype to chemotherapy. Similar results were obtained by treatment of SK-N-MC cells with etoposide, whereas no effect of etoposide (1-10 µM) was observed in SB-KMS-KS1 cells, which appeared to be rather resistant to etoposide (not shown).

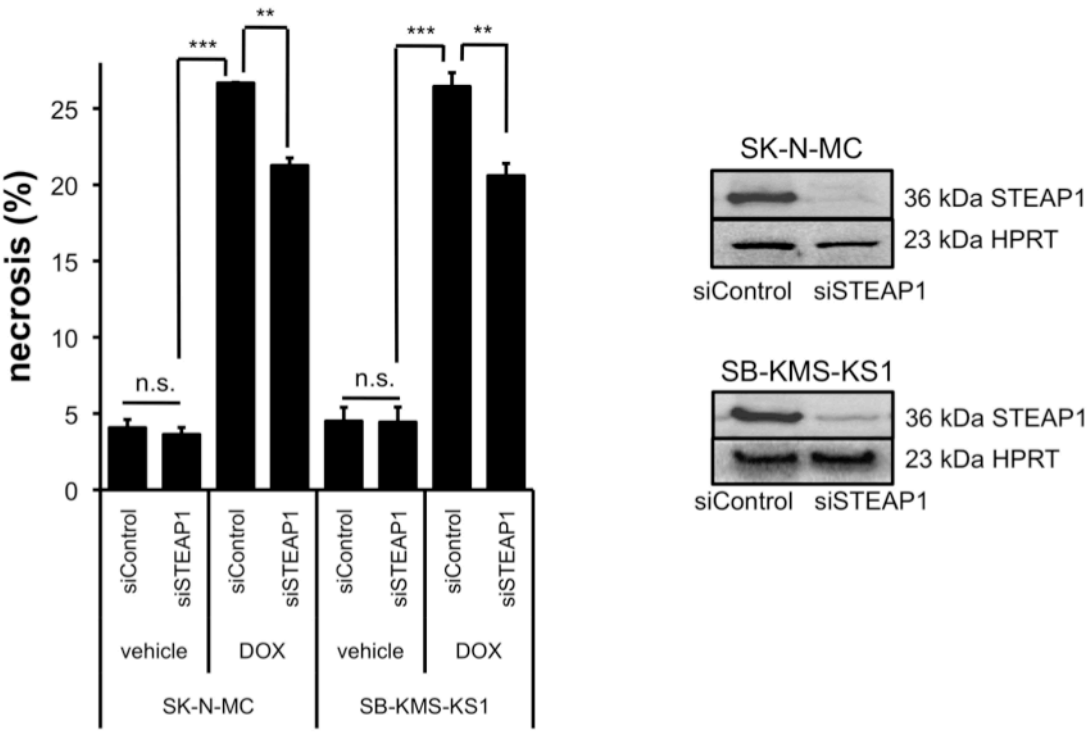

Figure 18: STEAP1 expression correlates with response to chemotherapy *in vitro*:
72h after transfection with siRNA, SK-N-MC and SB-KMS-KS1 cells were incubated for 24h with doxorubicin (DOX; 1 µM) or vehicle (H_2O) and afterwards stained with the necrosis marker 7-AAD. Rates of necrosis were assessed by flow cytometry. At least 30,000 events were recorded. Mean±SEM of at least four independent experiments. Knockdown efficacy was determined by WB. ** $p < 0.01$, *** $p < 0.001$; t-test.

5 Discussion

The current study assessed the involvement of STEAP1 in the invasive and oxidative stress phenotype of ET and whether STEAP1 may serve as a marker for outcome prediction of ET. It could be demonstrated that *STEAP1* gene expression is inducible by EWS/FLI1 transcription factors and important for ET malignancy. Moreover, the data presented in this Ph.D. thesis support a model wherein STEAP1 expression is linked to the maintenance of oxidative stress of ET cells and to increased ET aggressiveness, possibly mediated via STAT1. The results show that STEAP1 is highly expressed in ET compared to benign tissues and a series of other sarcomas implying that STEAP1 could be used in routine pathology as an additional marker for ET diagnosis.

To the best of the author's knowledge, this is the first study evaluating the potential of STEAP1 in IHC on outcome prediction of cancer patients. Regarding independent risk factors in the patient cohort reported in this Ph.D. thesis, especially high membranous STEAP1 expression, but not its exclusive cytoplasmic expression, had a strong impact on OS, which retained its significance in multivariate analysis.

Moreover, combined membranous and cytoplasmic STEAP1-high expression showed a trend toward an improved tumor response as estimated with Salzer-Kuntschik regression states. Even though this sub-sample tendency has to be validated in a larger cohort, it is noteworthy that high STEAP1 expression appears to improve response of ET cell lines to chemotherapy *in vitro*. Hence, it is tempting to speculate that STEAP1 may exert a biological function that sensitizes ET cells to drugs such as doxorubicin and etoposide, which are essential components of current ET treatment protocols [128]. In further support of this notion is the study of Peters *et al.* demonstrating that STEAP1 is significantly overexpressed in carboplatin-sensitive

compared to carboplatin-resistant human ovarian cancers (fold change = 3.7, $p < 0.01$) [129].

On the molecular level, STEAP1 is homologous to NOX [51, 52], which are involved in cellular ROS-production and frequently overexpressed in cancers [52, 130]. Thus, a contribution of STEAP1 to ROS-production appears reasonable. Consistently, recent evidence showed that experimental overexpression of STEAP1 in thyroid epithelial cells increases intracellular ROS levels [67]. Pharmacologically, multiple studies demonstrated that certain chemotherapeutics such as doxorubicin and etoposide become more effective with increased intracellular ROS levels [83]. Moreover, radiotherapy is known to be more effective in killing cancer cells when applied in the presence of ROS-generating radio-sensitizers [84, 131, 132].

Therefore, the observed survival benefit seen in STEAP1-high ET patients may be caused by elevated intracellular ROS levels, which are potentially associated with functional STEAP1 expression.

The fact that high cytoplasmic STEAP1 expression only correlated with improved survival when combined with high membranous STEAP1 expression suggests that the putative function of STEAP1 predominantly depends on its membranous localization and that a synergistic effect may only arise if STEAP1 is highly abundant in both cellular compartments. In line with this hypothesis, many oxidoreductases such as those of the NOX family dramatically increase their rates of ROS-production when they translocate from the cytoplasm to the plasma membrane, while the reason for this increase in activity remains largely unknown [133]. Moreover, it has been shown that experimental inhibition of NOX in glioblastoma and neuroblastoma confers chemoresistance [134] and conversely, that overexpression of NOX (such as NOX2) potentiates the toxic effect of doxorubicin on cardiac muscle [135]. Taken together, these data suggest that ROS-generating oxidoreductases can enhance the susceptibility of a given tissue to chemotherapeutics.

As outlined above, primary metastasis of ET is the most adverse clinical parameter indicative for dismal prognosis with a 5-year relapse-free survival of about 21% compared to 55% in patients with localized disease [31, 32]. Strikingly, the observed survival benefit of combined membranous and cytoplasmic STEAP1-high expression compared to exclusive cytoplasmic and/or no STEAP1 expression is similarly strong as the dramatic difference in survival indicated by metastatic versus localized disease. Hence, the data presented suggest that high STEAP1 expression may be a feature of an independent risk group of ET patients, who specifically might benefit from adapted radio-chemotherapy protocols.

Because many proteins induced by EWS/FLI1 contribute to neuroendothelial differentiation of ET [4, 46], it was assessed if STEAP1-silencing alters gene expression of neuroendothelial markers and inhibits angiogenic tube-formation. However, no involvement of STEAP1 in these processes was found. Furthermore, STEAP1 neither regulates integrins and adhesion molecules nor alters morphology and abundance of focal adhesions or migration of ET cells. Nevertheless, STEAP1 expression was reported to correlate with chondrogenic differentiation and cellular adhesion of MSCs, which is possibly caused by cell-specific factors [54, 136].

Recent *in silico* data suggested that STEAP1 might play a role in apoptosis and necrosis [51, 52]. However, no increase of cell death markers was observed in the untreated *in vitro* and *in vivo* models described in this Ph.D. thesis. These findings on STEAP1 are in contrast to those of others made for STEAP3: Re-expression of STEAP3 in prostatic and hepatocellular carcinoma induces apoptosis. These cancers downregulate STEAP3 during tumor progression, but gradually overexpress STEAP1 [137-141], suggesting that despite their high structural similarities [50] STEAP3 rather acts as a tumor-suppressor and rather STEAP1 as an oncogene.

In accordance, the preclinical data presented here indicate that STEAP1 is important for anchorage-independent colony-formation and invasiveness of ET cells *in vitro* and for tumorigenicity and metastasis *in vivo*. Moreover, it was shown that STEAP1 expression correlates with increased cellular ROS levels, which in turn induce the redox-sensitive and pro-invasive genes *MMP-1*, *DTX3L* and *ADIPOR1*. In analogy to these observations, Pan *et al.* found that STEAP1 overexpression promotes ROS-mediated hyperproliferation of thyroid epithelial cells [67].

Although ROS participate in oncogenic signaling and although elevated ROS are a salient feature of many aggressive cancers [76, 77], abrupt disturbances in the delicate ROS-balance can lead to protein misfolding, accumulation of dysfunctional proteins and activation of cellular stress responses [113]. In accordance, STEAP1-silencing provokes transcriptional and post-transcriptional adaptations of oxidative stress responses comprising the redox-, chaperone-, endopeptidase-, and ubiquitin-proteasome-system (UPS). These observations are compatible with the hypothesis that STEAP1 is associated with an enhanced oxidative stress phenotype in ET. Consistently, it was found that STEAP1 expression positively correlates with cytoplasmic and mitochondrial ROS levels, which possibly might explain the good response of ET cell lines to chemotherapy *in vitro* and of clinical ET *in vivo*.

As mitochondrial morphology remained unaffected, the author of this Ph.D. thesis supposes that mitochondrial ROS levels change concomitantly with cytoplasmic ROS levels upon STEAP1-silencing – a mechanism also seen in the context of other oxidoreductases (such as NOX2), which is termed “ROS-cross-talk” [142]. In this cross-talk NOX-derived ROS are amplified by mitochondrial ROS in a positive feedback-loop whose molecular mechanism and physiological significance are still poorly defined [142].

The role of STEAP1 in ROS-modulation is further supported by *in silico* predictions and crystallography of STEAPs defining them as heme-containing redox-enzymes [47, 51].

Less aggressive ROS are well known to interact with heme-iron of heme-containing proteins [66]. Here a non-enzymatic two-electron oxidation of heme generates ferryl-heme and an unstable free radical that may be released as more aggressive ROS in a site-specific manner depending on the localization of the protein [143, 144]. As STEAP1 contains a ferric oxidoreductase, it is tempting to speculate that STEAP1 might generate ROS by itself [50, 67]. However, although STEAP1 target genes appear to be downstream of ROS, it remains possible that part of STEAP1-induced ROS merely accompany upstream events involved in the STEAP1 phenotype, which needs to be assessed in future experiments.

So far, multiple studies provided evidence that permanently elevated ROS levels activate pro-metastatic and pro-proliferative signaling in cancer [76, 78, 79]. In agreement, the present work shows that antioxidants reduce colony-formation, proliferation and invasion of ET cells, suggesting that ET may benefit from an activated oxidative stress phenotype. Among STEAP1 regulated genes, the author focused on *MMP-1*, *ADIPOR1*, and *DTX3L*, because their encoded corresponding proteins are implicated in ROS-signaling. For instance, MMP-1 has been shown to be highly ROS-inducible [111, 145] and its overexpression increases invasiveness and metastasis of a variety of cancers [146]. ADIPOR1 is the cognate receptor for the growth factor adiponectin, which stimulates proliferation of hematopoietic stem cells [147]. Although the precise function of the ubiquitin ligase DTX3L is still not defined, recent work demonstrates that DTX3L monoubiquitylates histone H4 lysine 91 and thereby protects DNA from ROS-induced oxidative stress [124].

The results described in this Ph.D. thesis show that the above mentioned genes are highly inducible by ROS and possibly regulated by STAT1. STAT1 has been traditionally viewed as a mere interferon signal-transducer, but recently been linked with aggressiveness, therapy-resistance, and oxidative stress responses of several cancers [148, 149]. In accordance, this study proves that the coordinated expression of

MMP-1, ADIPOR1 and DTX3L fosters the invasive and proliferative phenotype of ET. In other reports, STAT1 was shown as a major transcription factor in ET triggering apoptosis of ET cells after stimulation with interferon beta *in vitro* and in a xenograft mouse model [150, 151]. Sancéau *et al.* demonstrated that interferon stimulation led to an upregulation of the interferon target gene 2'5'-oligo(A)synthetase 1 (OAS1) [150], which was found to be one of the putative STEAP1 target genes as identified by microarrays of the current study (see Figure 15B and Appendix Table 9.1).

However, the author of this Ph.D. thesis did not observe any signs of apoptosis upon STEAP1 down- or upregulation and did not detect any considerable interferon production or secretion of untreated ET cells. These data imply that STEAP1 might exert a different effect on STAT1 compared to canonical interferon-mediated STAT1 activation. Furthermore, the concentrations of interferon beta used by Sancéau *et al.* were extremely high (up to 5,000 U/ml) [150] compared to those of interferon gamma used in this Ph.D. thesis (100 U/ml), possibly accounting for the observed cell death rather than promoting growth-fostering effects of STAT1 activation. Interestingly, two independent studies showed that STAT3 is constitutively activated in 50-58% of clinical ET [152, 153]. Moreover, experimental inhibition of STAT3 in ET cell lines led to a strong induction of apoptosis [152]. These data imply that activated STAT proteins like STAT3 may confer a pro-survival signal on ET. However, expression of activated STAT3 in ET was associated with improved outcome of ET patients [153]. These data are of special interest in the context of this Ph.D. thesis since STEAP1 overexpression (and STAT1 activation) on the one hand confers untreated ET cells with a more proliferative and invasive phenotype and on the other hand is associated with improved outcome of ET patients, which were treated with multimodal therapy regimens.

In light of these considerations it appears plausible that especially patients with ET that feature combined high membranous and cytoplasmic STEAP1 immunoreactivity might constitute a specific subgroup of ET patients, who eventually might benefit from

adapted conventional therapy regimens employing more ROS-dependent chemotherapeutics such as doxorubicin and etoposide, while reducing the dosages of non-ROS-dependent drugs. Moreover, as STEAP1 is a surface protein being only minimally expressed in normal tissues, it could be possible to generate monoclonal anti-STEAP1-antibodies tagged with ROS-dependent chemotherapeutics or radionuclides, which would enlarge the current options of targeted therapy of ET.

6 Conclusions, limitations and perspectives

6.1 Conclusions

In summary, this work provides for the first time evidence that an activated oxidative stress phenotype increases ET malignancy. This study demonstrates that STEAP1 overexpression promotes anchorage-independent colony-formation, proliferation, invasiveness, tumorigenicity and metastasis of ET. Because STEAP1 is overexpressed in a wide variety of carcinomas, its oncogenic function may have general relevance for tumor progression and targeted therapy.

Although the author is fully aware of the retrospective nature of the presented TMA patient study and its associated limitations, STEAP1 may constitute a promising new biomarker for outcome prediction of ET patients, which is readily available due to standardized assessment by IHC. The results presented in this Ph.D. thesis have been published in international peer-reviewed journals [154, 155].

6.2 Limitations and perspectives

The results presented in this Ph.D. thesis shed light on the relevance of STEAP1 expression for the ET phenotype and on its potential value as a novel biomarker for outcome prediction of ET patients. However, there are still unresolved questions, which need to be addressed in future studies to fully understand the role of STEAP1 in ET:

1) This work shows that STEAP1 is associated with the oxidative stress phenotype of ET and suggests that STEAP1 is likely to be an upstream regulator of intracellular ROS. However, further studies are needed to confirm this observation. For instance, yeast-two-hybrid experiments appear useful to identify hitherto unknown binding-partners of STEAP1, as many ROS generating enzymes are part of large

macromolecular complexes [156]. If STEAP1 indeed proves to have binding partners, one would need to assess whether the specific knockdown of one or more of them simultaneously can modulate ROS levels as well.

Moreover, it is important to identify critical domains and/or residues (e.g. the transmembrane domains and the ferric oxidoreductase domain) within the STEAP1 protein that are responsible for ROS modulation. Therefore, genetic deletion mutants of STEAP1 need to be constructed and expressed in a reliable reporter system to check which deletion, and hence, which domain(s) within STEAP1 might be essential for its ability to modulate ROS in ET.

2) This study pointed out the involvement of STAT1 in STEAP1- and ROS-mediated regulation of target genes, which are part of the invasive phenotype observed.

As STEAP1 regulates more than 80 genes, about 90 miRNAs and at least 130 proteins, it appears plausible that STAT1 might not be the only downstream signaling molecule targeted by STEAP1. Hence, future studies have to screen for additional pathways involved in the STEAP1 phenotype in order to fully understand the mode of STEAP1 target gene regulation.

3) In this study the author focused on the functional follow-up of three prominent STEAP1 target genes namely *ADIPOR1*, *MMP-1* and *DTX3L*.

Even though these genes proved to be important for STEAP1-mediated phenotypic changes like proliferation and invasiveness, many other features like colony-formation and *in vivo* growth and metastasis of ET need to be tested as well. This also applies to other STEAP1 target genes.

4) Although the results of the retrospective TMA study presented in this Ph.D. thesis are based on the evaluation of 114 patients, which is a quite considerably high number

of patient samples given that ET is a very rare disease, the author recommends to validate this observation in a prospective study in a larger cohort of patients, in order to reduce the possibility of biases, which are typically associated with retrospective studies of limited sample size.

5) The results of the TMA study and functional analyses of STEAP1-silenced ET cells suggest that STEAP1 expression correlates with response of ET to chemotherapy, possibly by enhanced ROS levels.

However, the sample size of the TMA study for which tumor-regression states were available was too low to achieve statistical significance. Hence, this issue should be further validated in a prospective study. In addition, more experiments are needed to assess whether STEAP1-mediated ROS are indeed causative for the differential rates of chemoresponse seen in ET cells, e.g. by chemotherapeutic treatment of mice with xenografted STEAP1-high and STEAP1-low ET cells, respectively.

7 Summary

Ewing tumors (ET) comprise the second most common type of bone-associated sarcomas in children and adolescents and are characterized by oncogenic EWS/FLI1 fusion proteins and early metastasis. Using comprehensive microarray analyses and RNA interference this study identified the six-transmembrane epithelial antigen of the prostate 1 (STEAP1) – a membrane-bound mesenchymal stem cell marker of unknown function – as a highly expressed protein in ET compared to benign tissues and shows its regulation by EWS/FLI1. Knockdown of STEAP1 reduced proliferation, anchorage-independent colony-formation as well as invasiveness of ET cells *in vitro* and decreased tumor growth and metastasis of ET xenografts *in vivo*. Moreover, transcriptome and proteome analyses as well as functional studies revealed that STEAP1 expression correlates with oxidative stress responses and elevated levels of reactive oxygen species (ROS) that in turn are able to regulate redox-sensitive and pro-invasive genes via interferon-independent activation of signal transducer and activator of transcription 1 (STAT1).

As compelling evidence suggests that elevated levels of intracellular oxidative stress can on the one hand contribute to enhanced aggressiveness of numerous cancers, but on the other hand can increase the susceptibility of cancer cells toward chemotherapeutics and radiotherapy, membranous and cytoplasmic STEAP1 expression was analyzed in 114 primary pre-chemotherapy ET by immunohistochemistry and compared with clinical parameters and patient outcome.

This analysis showed that 87.7% of the samples displayed detectable STEAP1 expression. High membranous and cytoplasmic STEAP1 expression was found in 53.5% and 25.4%, respectively, without correlation of both parameters. Especially combined high membranous and cytoplasmic STEAP1 expression, but also exclusive membranous STEAP1 immunoreactivity correlated with improved overall survival (p =

0.021). Accordingly, low membranous STEAP1 expression was identified as an independent risk factor in multivariate analysis (HR 2.65, p = 0.036), whereas very high STEAP1 expression was associated with excellent overall survival and an increased susceptibility of ET cell lines toward chemotherapy.

In synopsis, these data suggest that STEAP1 is associated with the invasive behavior and oxidative stress phenotype of ET and point to a hitherto unanticipated oncogenic function of STEAP1 in ET. In addition, this study proves that high membranous STEAP1 expression can predict improved patient outcome, possibly caused by enhanced ROS-mediated chemosensitivity, and thus may help to define a specific sub-group of ET patients, who might benefit from adapted conventional therapy regimens and targeted delivery of ROS-dependent therapeutics to their STEAP1 expressing tumor cells.

8 References

1. Glass AG, Fraumeni JF, Jr.: **Epidemiology of bone cancer in children**. *J Natl Cancer Inst* 1970, **44**(1):187-199.

2. Bernstein M, Kovar H, Paulussen M, Randall RL, Schuck A, Teot LA, Juergens H: **Ewing's sarcoma family of tumors: current management**. *Oncologist* 2006, **11**(5):503-519.

3. Ewing J: **Diffuse endothelioma of the bone**. *Proc NY Pathol Soc* 1921, **21**:17-24.

4. Staege MS, Hutter C, Neumann I, Foja S, Hattenhorst UE, Hansen G, Afar D, Burdach SE: **DNA microarrays reveal relationship of Ewing family tumors to both endothelial and fetal neural crest-derived cells and define novel targets**. *Cancer Res* 2004, **64**(22):8213-8221.

5. Kovar H: **Context matters: the hen or egg problem in Ewing's sarcoma**. *Semin Cancer Biol* 2005, **15**(3):189-196.

6. Schleiermacher G, Peter M, Oberlin O, Philip T, Rubie H, Mechinaud F, Sommelet-Olive D, Landman-Parker J, Bours D, Michon J *et al*: **Increased risk of systemic relapses associated with bone marrow micrometastasis and circulating tumor cells in localized ewing tumor**. *J Clin Oncol* 2003, **21**(1):85-91.

7. Castex MP, Rubie H, Stevens MC, Escribano CC, de Gauzy JS, Gomez-Brouchet A, Rey A, Delattre O, Oberlin O: **Extraosseous localized ewing tumors: improved outcome with anthracyclines--the French society of pediatric oncology and international society of pediatric oncology**. *J Clin Oncol* 2007, **25**(10):1176-1182.

8. Thiel U, Wawer A, Wolf P, Badoglio M, Santucci A, Klingebiel T, Basu O, Borkhardt A, Laws HJ, Kodera Y *et al*: **No improvement of survival with reduced- versus high-intensity conditioning for allogeneic stem cell transplants in Ewing tumor patients**. *Ann Oncol* 2011, **22**(7):1614-1621.

9. Delattre O, Zucman J, Plougastel B, Desmaze C, Melot T, Peter M, Kovar H, Joubert I, de Jong P, Rouleau G *et al*: **Gene fusion with an ETS DNA-binding domain caused by chromosome translocation in human tumours**. *Nature* 1992, **359**(6391):162-165.

10. Delattre O, Zucman J, Melot T, Garau XS, Zucker JM, Lenoir GM, Ambros PF, Sheer D, Turc-Carel C, Triche TJ *et al*: **The Ewing family of tumors--a subgroup of small-round-cell tumors defined by specific chimeric transcripts**. *N Engl J Med* 1994, **331**(5):294-299.

11. Le Deley MC, Delattre O, Schaefer KL, Burchill SA, Koehler G, Hogendoorn PC, Lion T, Poremba C, Marandet J, Ballet S *et al*: **Impact of EWS-ETS fusion type on disease progression in Ewing's sarcoma/peripheral primitive neuroectodermal tumor: prospective results from the cooperative Euro-E.W.I.N.G. 99 trial**. *J Clin Oncol* 2010, **28**(12):1982-1988.

12. von Levetzow C, Jiang X, Gwye Y, von Levetzow G, Hung L, Cooper A, Hsu JH, Lawlor ER: **Modeling initiation of ewing sarcoma in human neural crest cells**. *PLoS One* 2011, **6**(4):e19305.

13. Tirode F, Laud-Duval K, Prieur A, Delorme B, Charbord P, Delattre O: **Mesenchymal stem cell features of Ewing tumors**. *Cancer Cell* 2007, **11**(5):421-429.

14. Kauer M, Ban J, Kofler R, Walker B, Davis S, Meltzer P, Kovar H: **A molecular function map of Ewing's sarcoma**. *PLoS One* 2009, **4**(4):e5415.

15. Miyagawa Y, Okita H, Nakaijima H, Horiuchi Y, Sato B, Taguchi T, Toyoda M, Katagiri YU, Fujimoto J, Hata J *et al*: **Inducible expression of chimeric EWS/ETS proteins confers Ewing's family tumor-like phenotypes to human mesenchymal progenitor cells**. *Mol Cell Biol* 2008, **28**(7):2125-2137.

16. Potikyan G, France KA, Carlson MR, Dong J, Nelson SF, Denny CT: **Genetically defined EWS/FLI1 model system suggests mesenchymal origin of Ewing's family tumors**. *Lab Invest* 2008, **88**(12):1291-1302.

17. Gonzalez I, Vicent S, de Alava E, Lecanda F: **EWS/FLI-1 oncoprotein subtypes impose different requirements for transformation and metastatic activity in a murine model**. *J Mol Med* 2007, **85**(9):1015-1029.

18. Riggi N, Cironi L, Provero P, Suva ML, Kaloulis K, Garcia-Echeverria C, Hoffmann F, Trumpp A, Stamenkovic I: **Development of Ewing's sarcoma from primary bone marrow-derived mesenchymal progenitor cells**. *Cancer Res* 2005, **65**(24):11459-11468.

19. Lessnick SL, Dacwag CS, Golub TR: **The Ewing's sarcoma oncoprotein EWS/FLI induces a p53-dependent growth arrest in primary human fibroblasts**. *Cancer Cell* 2002, **1**(4):393-401.

20. Neilsen PM, Pishas KI, Callen DF, Thomas DM: **Targeting the p53 Pathway in Ewing Sarcoma**. *Sarcoma* 2011, **2011**:746939.

21. Huang HY, Illei PB, Zhao Z, Mazumdar M, Huvos AG, Healey JH, Wexler LH, Gorlick R, Meyers P, Ladanyi M: **Ewing sarcomas with p53 mutation or p16/p14ARF homozygous deletion: a highly lethal subset associated with poor chemoresponse**. *J Clin Oncol* 2005, **23**(3):548-558.

22. Randall RL, Lessnick SL, Jones KB, Gouw LG, Cummings JE, Cannon-Albright L, Schiffman JD: **Is There a Predisposition Gene for Ewing's Sarcoma?** *J Oncol* 2010, **2010**:397632.

23. Fraumeni JF, Jr., Glass AG: **Rarity of Ewing's sarcoma among U.S. Negro children**. *Lancet* 1970, **1**(7642):366-367.

24. Jensen RD, Drake RM: **Rarity of Ewing's tumour in Negroes**. *Lancet* 1970, **1**(7650):777.

25. Li FP, Tu JT, Liu FS, Shiang EL: **Rarity of Ewing's sarcoma in China**. *Lancet* 1980, **1**(8180):1255.

26. Ozaki T, Schaefer KL, Wai D, Yokoyama R, Ahrens S, Diallo R, Hasegawa T, Shimoda T, Hirohashi S, Kawai A *et al*: **Population-based genetic alterations in Ewing's tumors from Japanese and European Caucasian patients**. *Ann Oncol* 2002, **13**(10):1656-1664.

27. Hutter RV, Francis KC, Foote FW, Jr.: **Ewing's Sarcoma in Siblings: Report of the Second Known Occurrence**. *Am J Surg* 1964, **107**:598-603.

28. Joyce MJ, Harmon DC, Mankin HJ, Suit HD, Schiller AL, Truman JT: **Ewing's sarcoma in female siblings. A clinical report and review of the literature**. *Cancer* 1984, **53**(9):1959-1962.

29. Winn DM, Li FP, Robison LL, Mulvihill JJ, Daigle AE, Fraumeni JF, Jr.: **A case-control study of the etiology of Ewing's sarcoma**. *Cancer Epidemiol Biomarkers Prev* 1992, **1**(7):525-532.

30. Postel-Vinay S, Véron AS, Tirode F, Pierron G, Reynaud S, Kovar H, Oberlin O, Lapouble E, Ballet S, Lucchesi C *et al*: **Common variants near TARDBP and EGR2 are associated with susceptibility to Ewing sarcoma**. *Nat Genet* 2012, **44**(3):323-327.

31. Haeusler J, Ranft A, Boelling T, Gosheger G, Braun-Munzinger G, Vieth V, Burdach S, van den Berg H, Juergens H, Dirksen U: **The value of local treatment in patients with primary, disseminated, multifocal Ewing sarcoma (PDMES)**. *Cancer* 2010, **116**(2):443-450.

32. Cotterill SJ, Ahrens S, Paulussen M, Jurgens HF, Voute PA, Gadner H, Craft AW: **Prognostic factors in Ewing's tumor of bone: analysis of 975 patients from the European Intergroup Cooperative Ewing's Sarcoma Study Group**. *J Clin Oncol* 2000, **18**(17):3108-3114.

33. de Alava E, Antonescu CR, Panizo A, Leung D, Meyers PA, Huvos AG, Pardo-Mindan FJ, Healey JH, Ladanyi M: **Prognostic impact of P53 status in Ewing sarcoma**. *Cancer* 2000, **89**(4):783-792.

34. Riley RD, Burchill SA, Abrams KR, Heney D, Sutton AJ, Jones DR, Lambert PC, Young B, Wailoo AJ, Lewis IJ: **A systematic review of molecular and biological markers in tumours of the Ewing's sarcoma family**. *Eur J Cancer* 2003, **39**(1):19-30.

35. Bui MM, Han G, Acs G, Reed D, Gonzalez RJ, Pasha TL, Zhang PJ: **Connexin 43 is a potential prognostic biomarker for ewing sarcoma/primitive neuroectodermal tumor**. *Sarcoma* 2011, **2011**:971050.

36. Lopez-Guerrero JA, Machado I, Scotlandi K, Noguera R, Pellin A, Navarro S, Serra M, Calabuig-Farinas S, Picci P, Llombart-Bosch A: **Clinicopathological significance of cell cycle regulation markers in a large series of genetically confirmed Ewing's sarcoma family of tumors**. *Int J Cancer* 2011, **128**(5):1139-1150.

37. Ginsberg JP, de Alava E, Ladanyi M, Wexler LH, Kovar H, Paulussen M, Zoubek A, Dockhorn-Dworniczak B, Juergens H, Wunder JS *et al*: **EWS-FLI1**

and EWS-ERG gene fusions are associated with similar clinical phenotypes in Ewing's sarcoma. *J Clin Oncol* 1999, **17**(6):1809-1814.

38. Grunewald TG, Herbst SM, Heinze J, Burdach S: **Understanding tumor heterogeneity as functional compartments--superorganisms revisited**. *J Transl Med* 2011, **9**:79.

39. Lee CK, Lord SJ, Coates AS, Simes RJ: **Molecular biomarkers to individualise treatment: assessing the evidence**. *Med J Aust* 2009, **190**(11):631-636.

40. Nishio K, Arao T, Shimoyama T, Fujiwara Y, Tamura T, Saijo N: **Translational studies for target-based drugs**. *Cancer Chemother Pharmacol* 2005, **56 Suppl 1**:90-93.

41. Kovar H, Aryee D, Zoubek A: **The Ewing family of tumors and the search for the Achilles' heel**. *Curr Opin Oncol* 1999, **11**(4):275-284.

42. Uren A, Toretsky JA: **Ewing's sarcoma oncoprotein EWS-FLI1: the perfect target without a therapeutic agent**. *Future Oncol* 2005, **1**(4):521-528.

43. Scotlandi K, Picci P: **Targeting insulin-like growth factor 1 receptor in sarcomas**. *Curr Opin Oncol* 2008, **20**(4):419-427.

44. Prieur A, Tirode F, Cohen P, Delattre O: **EWS/FLI-1 silencing and gene profiling of Ewing cells reveal downstream oncogenic pathways and a crucial role for repression of insulin-like growth factor binding protein 3**. *Mol Cell Biol* 2004, **24**(16):7275-7283.

45. Erkizan HV, Kong Y, Merchant M, Schlottmann S, Barber-Rotenberg JS, Yuan L, Abaan OD, Chou TH, Dakshanamurthy S, Brown ML *et al*: **A small molecule blocking oncogenic protein EWS-FLI1 interaction with RNA helicase A inhibits growth of Ewing's sarcoma**. *Nat Med* 2009, **15**(7):750-756.

46. Richter GH, Plehm S, Fasan A, Rossler S, Unland R, Bennani-Baiti IM, Hotfilder M, Lowel D, von Luettichau I, Mossbrugger I *et al*: **EZH2 is a mediator of EWS/FLI1 driven tumor growth and metastasis blocking endothelial and neuro-ectodermal differentiation**. *Proc Natl Acad Sci U S A* 2009, **106**(13):5324-5329.

47. Sendamarai AK, Ohgami RS, Fleming MD, Lawrence CM: **Structure of the membrane proximal oxidoreductase domain of human Steap3, the dominant ferrireductase of the erythroid transferrin cycle**. *Proc Natl Acad Sci U S A* 2008, **105**(21):7410-7415.

48. Hubert RS, Vivanco I, Chen E, Rastegar S, Leong K, Mitchell SC, Madraswala R, Zhou Y, Kuo J, Raitano AB *et al*: **STEAP: a prostate-specific cell-surface antigen highly expressed in human prostate tumors**. *Proc Natl Acad Sci U S A* 1999, **96**(25):14523-14528.

49. Ohgami RS, Campagna DR, Greer EL, Antiochos B, McDonald A, Chen J, Sharp JJ, Fujiwara Y, Barker JE, Fleming MD: **Identification of a**

ferrireductase required for efficient transferrin-dependent iron uptake in erythroid cells. *Nat Genet* 2005, **37**(11):1264-1269.

50. Ohgami RS, Campagna DR, McDonald A, Fleming MD: **The Steap proteins are metalloreductases**. *Blood* 2006, **108**(4):1388-1394.

51. Sanchez-Pulido L, Rojas AM, Valencia A, Martinez AC, Andrade MA: **ACRATA: a novel electron transfer domain associated to apoptosis and cancer**. *BMC Cancer* 2004, **4**:98.

52. von Rozycki T, Yen MR, Lende EE, Saier MH, Jr.: **The YedZ family: possible heme binding proteins that can be fused to transporters and electron carriers**. *J Mol Microbiol Biotechnol* 2004, **8**(3):129-140.

53. Knutson MD: **Steap proteins: implications for iron and copper metabolism**. *Nutr Rev* 2007, **65**(7):335-340.

54. Vaghjiani RJ, Talma S, Murphy CL: **Six-transmembrane epithelial antigen of the prostate (STEAP1 and STEAP2)-differentially expressed by murine and human mesenchymal stem cells**. *Tissue Eng Part A* 2009, **15**(8):2073-2083.

55. Valenti MT, Dalle Carbonare L, Donatelli L, Bertoldo F, Giovanazzi B, Caliari F, Lo Cascio V: **STEAP mRNA detection in serum of patients with solid tumours**. *Cancer Lett* 2009, **273**(1):122-126.

56. Cheung IY, Feng Y, Danis K, Shukla N, Meyers P, Ladanyi M, Cheung NK: **Novel markers of subclinical disease for Ewing family tumors from gene expression profiling**. *Clin Cancer Res* 2007, **13**(23):6978-6983.

57. Hayashi T, Oue N, Sakamoto N, Anami K, Oo HZ, Sentani K, Ohara S, Teishima J, Matsubara A, Yasui W: **Identification of transmembrane protein in prostate cancer by the Escherichia coli ampicillin secretion trap: expression of CDON is involved in tumor cell growth and invasion**. *Pathobiology* 2011, **78**(5):277-284.

58. Challita-Eid PM, Morrison K, Etessami S, An Z, Morrison KJ, Perez-Villar JJ, Raitano AB, Jia XC, Gudas JM, Kanner SB *et al*: **Monoclonal antibodies to six-transmembrane epithelial antigen of the prostate-1 inhibit intercellular communication in vitro and growth of human tumor xenografts in vivo**. *Cancer Res* 2007, **67**(12):5798-5805.

59. Hayashi S, Kumai T, Matsuda Y, Aoki N, Sato K, Kimura S, Kitada M, Tateno M, Celis E, Kobayashi H: **Six-transmembrane epithelial antigen of the prostate and enhancer of zeste homolog 2 as immunotherapeutic targets for lung cancer**. *J Transl Med* 2011, **9**:191.

60. Alves PM, Faure O, Graff-Dubois S, Cornet S, Bolonakis I, Gross DA, Miconnet I, Chouaib S, Fizazi K, Soria JC *et al*: **STEAP, a prostate tumor antigen, is a target of human CD8+ T cells**. *Cancer Immunol Immunother* 2006, **55**(12):1515-1523.

61. Azumi M, Kobayashi H, Aoki N, Sato K, Kimura S, Kakizaki H, Tateno M: **Six-transmembrane epithelial antigen of the prostate as an immunotherapeutic target for renal cell and bladder cancer**. *J Urol* 2010, **183**(5):2036-2044.

62. Kim S, Lee JB, Lee GK, Chang J: **Vaccination with recombinant adenoviruses and dendritic cells expressing prostate-specific antigens is effective in eliciting CTL and suppresses tumor growth in the experimental prostate cancer**. *Prostate* 2009, **69**(9):938-948.

63. Kobayashi H, Nagato T, Sato K, Aoki N, Kimura S, Murakami M, Iizuka H, Azumi M, Kakizaki H, Tateno M *et al*: **Recognition of prostate and melanoma tumor cells by six-transmembrane epithelial antigen of prostate-specific helper T lymphocytes in a human leukocyte antigen class II-restricted manner**. *Cancer Res* 2007, **67**(11):5498-5504.

64. Machlenkin A, Paz A, Bar Haim E, Goldberger O, Finkel E, Tirosh B, Volovitz I, Vadai E, Lugassy G, Cytron S *et al*: **Human CTL epitopes prostatic acid phosphatase-3 and six-transmembrane epithelial antigen of prostate-3 as candidates for prostate cancer immunotherapy**. *Cancer Res* 2005, **65**(14):6435-6442.

65. Rodeberg DA, Nuss RA, Elsawa SF, Celis E: **Recognition of six-transmembrane epithelial antigen of the prostate-expressing tumor cells by peptide antigen-induced cytotoxic T lymphocytes**. *Clin Cancer Res* 2005, **11**(12):4545-4552.

66. Lambeth JD: **NOX enzymes and the biology of reactive oxygen**. *Nat Rev Immunol* 2004, **4**(3):181-189.

67. Pan YZ, Li Y, Guo LR, Zhao YY, Zhao XJ: **[Influence of expression of six transmembrane epithelial antigen of the prostate-1 on intracellular reactive oxygen species level and cell growth: an in vitro experiment]**. *Zhonghua Yi Xue Za Zhi* 2008, **88**(9):641-644.

68. Wellen KE, Thompson CB: **Cellular metabolic stress: considering how cells respond to nutrient excess**. *Mol Cell* 2010, **40**(2):323-332.

69. Sundaresan M, Yu ZX, Ferrans VJ, Irani K, Finkel T: **Requirement for generation of H2O2 for platelet-derived growth factor signal transduction**. *Science* 1995, **270**(5234):296-299.

70. Owusu-Ansah E, Banerjee U: **Reactive oxygen species prime Drosophila haematopoietic progenitors for differentiation**. *Nature* 2009, **461**(7263):537-541.

71. Ufer C, Wang CC, Borchert A, Heydeck D, Kuhn H: **Redox control in mammalian embryo development**. *Antioxid Redox Signal* 2010, **13**(6):833-875.

72. Santos CX, Tanaka LY, Wosniak J, Laurindo FR: **Mechanisms and implications of reactive oxygen species generation during the unfolded protein response: roles of endoplasmic reticulum oxidoreductases,**

mitochondrial electron transport, and NADPH oxidase. *Antioxid Redox Signal* 2009, **11**(10):2409-2427.

73. Wu WS: **The signaling mechanism of ROS in tumor progression**. *Cancer Metastasis Rev* 2006, **25**(4):695-705.

74. Fang J, Nakamura H, Iyer AK: **Tumor-targeted induction of oxystress for cancer therapy**. *J Drug Target* 2007, **15**(7-8):475-486.

75. Seifried HE, McDonald SS, Anderson DE, Greenwald P, Milner JA: **The antioxidant conundrum in cancer**. *Cancer Res* 2003, **63**(15):4295-4298.

76. Szatrowski TP, Nathan CF: **Production of large amounts of hydrogen peroxide by human tumor cells**. *Cancer Res* 1991, **51**(3):794-798.

77. Grek CL, Tew KD: **Redox metabolism and malignancy**. *Curr Opin Pharmacol* 2010, **10**(4):362-368.

78. Smith DG, Magwere T, Burchill SA: **Oxidative stress and therapeutic opportunities: focus on the Ewing's sarcoma family of tumors**. *Expert Rev Anticancer Ther* 2011, **11**(2):229-249.

79. Luo J, Solimini NL, Elledge SJ: **Principles of cancer therapy: oncogene and non-oncogene addiction**. *Cell* 2009, **136**(5):823-837.

80. Woo HA, Yim SH, Shin DH, Kang D, Yu DY, Rhee SG: **Inactivation of peroxiredoxin I by phosphorylation allows localized H(2)O(2) accumulation for cell signaling**. *Cell* 2010, **140**(4):517-528.

81. Finkel T: **Signal transduction by reactive oxygen species**. *J Cell Biol* 2011, **194**(1):7-15.

82. Diehn M, Cho RW, Lobo NA, Kalisky T, Dorie MJ, Kulp AN, Qian D, Lam JS, Ailles LE, Wong M *et al*: **Association of reactive oxygen species levels and radioresistance in cancer stem cells**. *Nature* 2009, **458**(7239):780-783.

83. Mailloux RJ, Adjeitey CN, Harper ME: **Genipin-induced inhibition of uncoupling protein-2 sensitizes drug-resistant cancer cells to cytotoxic agents**. *PLoS One* 2010, **5**(10):e13289.

84. Sun Y, St Clair DK, Xu Y, Crooks PA, St Clair WH: **A NADPH oxidase-dependent redox signaling pathway mediates the selective radiosensitization effect of parthenolide in prostate cancer cells**. *Cancer Res* 2010, **70**(7):2880-2890.

85. Mateescu B, Batista L, Cardon M, Gruosso T, de Feraudy Y, Mariani O, Nicolas A, Meyniel JP, Cottu P, Sastre-Garau X *et al*: **miR-141 and miR-200a act on ovarian tumorigenesis by controlling oxidative stress response**. *Nat Med* 2011, **17**(12):1627-1635.

86. Dunst J, Schuck A: **Role of radiotherapy in Ewing tumors**. *Pediatr Blood Cancer* 2004, **42**(5):465-470.

87. Giard DJ, Aaronson SA, Todaro GJ, Arnstein P, Kersey JH, Dosik H, Parks WP: **In vitro cultivation of human tumors: establishment of cell lines derived from a series of solid tumors**. *J Natl Cancer Inst* 1973, **51**(5):1417-1423.

88. Schlesinger HR, Gerson JM, Moorhead PS, Maguire H, Hummeler K: **Establishment and characterization of human neuroblastoma cell lines**. *Cancer Res* 1976, **36**(9 pt.1):3094-3100.

89. Douglass EC, Valentine M, Etcubanas E, Parham D, Webber BL, Houghton PJ, Houghton JA, Green AA: **A specific chromosomal abnormality in rhabdomyosarcoma**. *Cytogenet Cell Genet* 1987, **45**(3-4):148-155.

90. Goldman JP, Blundell MP, Lopes L, Kinnon C, Di Santo JP, Thrasher AJ: **Enhanced human cell engraftment in mice deficient in RAG2 and the common cytokine receptor gamma chain**. *Br J Haematol* 1998, **103**(2):335-342.

91. Klein A, Guhl E, Zollinger R, Tzeng YJ, Wessel R, Hummel M, Graessmann M, Graessmann A: **Gene expression profiling: cell cycle deregulation and aneuploidy do not cause breast cancer formation in WAP-SVT/t transgenic animals**. *J Mol Med (Berl)* 2005, **83**(5):362-376.

92. Grunewald TG, Kammerer U, Schulze E, Schindler D, Honig A, Zimmer M, Butt E: **Silencing of LASP-1 influences zyxin localization, inhibits proliferation and reduces migration in breast cancer cells**. *Exp Cell Res* 2006, **312**(7):974-982.

93. Grunewald TG, Kammerer U, Winkler C, Schindler D, Sickmann A, Honig A, Butt E: **Overexpression of LASP-1 mediates migration and proliferation of human ovarian cancer cells and influences zyxin localisation**. *Br J Cancer* 2007, **96**(2):296-305.

94. Tsai CA, Chen YJ, Chen JJ: **Testing for differentially expressed genes with microarray data**. *Nucleic Acids Res* 2003, **31**(9):e52.

95. Sturn A, Quackenbush J, Trajanoski Z: **Genesis: cluster analysis of microarray data**. *Bioinformatics* 2002, **18**(1):207-208.

96. Subramanian A, Tamayo P, Mootha VK, Mukherjee S, Ebert BL, Gillette MA, Paulovich A, Pomeroy SL, Golub TR, Lander ES *et al*: **Gene set enrichment analysis: a knowledge-based approach for interpreting genome-wide expression profiles**. *Proc Natl Acad Sci U S A* 2005, **102**(43):15545-15550.

97. Betel D, Koppal A, Agius P, Sander C, Leslie C: **Comprehensive modeling of microRNA targets predicts functional non-conserved and non-canonical sites**. *Genome Biol* 2010, **11**(8):R90.

98. Diebold I, Djordjevic T, Petry A, Hatzelmann A, Tenor H, Hess J, Gorlach A: **Phosphodiesterase 2 mediates redox-sensitive endothelial cell proliferation and angiogenesis by thrombin via Rac1 and NADPH oxidase 2**. *Circ Res* 2009, **104**(10):1169-1177.

99. Traenka C, Remke M, Korshunov A, Bender S, Hielscher T, Northcott PA, Witt H, Ryzhova M, Felsberg J, Benner A *et al*: **Role of LIM and SH3 Protein 1 (LASP1) in the Metastatic Dissemination of Medulloblastoma**. *Cancer Res* 2010, **70**(20):8003-8014.

100. Helson L, Das SK, Hajdu SI: **Human neuroblastoma in nude mice**. *Cancer Res* 1975, **35**(9):2594-2599.

101. Chappell D, Dorfler N, Jacob M, Rehm M, Welsch U, Conzen P, Becker BF: **Glycocalyx protection reduces leukocyte adhesion after ischemia/reperfusion**. *Shock* 2009, **34**(2):133-139.

102. Grunewald TG, von Luettichau I, Welsch U, Dorr HG, Hopner F, Kovacs K, Burdach S, Rabl W: **First report of ectopic ACTH syndrome and PTHrP-induced hypercalcemia due to a hepatoblastoma in a child**. *Eur J Endocrinol* 2010, **162**(4):813-818.

103. Frietsch JJ, Grunewald TG, Jasper S, Kammerer U, Herterich S, Kapp M, Honig A, Butt E: **Nuclear localisation of LASP-1 correlates with poor long-term survival in female breast cancer**. *Br J Cancer* 2010, **102**(11):1645-1653.

104. Grunewald TG, Kammerer U, Kapp M, Eck M, Dietl J, Butt E, Honig A: **Nuclear localization and cytosolic overexpression of LASP-1 correlates with tumor size and nodal-positivity of human breast carcinoma**. *BMC Cancer* 2007, **7**:198.

105. Thiel U, Pirson S, Muller-Spahn C, Conrad H, Busch DH, Bernhard H, Burdach S, Richter GH: **Specific recognition and inhibition of Ewing tumour growth by antigen-specific allo-restricted cytotoxic T cells**. *Br J Cancer* 2011, **104**(6):948-956.

106. Lessnick SL, Dei Tos AP, Sorensen PH, Dileo P, Baker LH, Ferrari S, Hall KS: **Small round cell sarcomas**. *Semin Oncol* 2009, **36**(4):338-346.

107. Schmidt D, Harms D, Burdach S: **Malignant peripheral neuroectodermal tumours of childhood and adolescence**. *Virchows Arch A Pathol Anat Histopathol* 1985, **406**(3):351-365.

108. Baird K, Davis S, Antonescu CR, Harper UL, Walker RL, Chen Y, Glatfelter AA, Duray PH, Meltzer PS: **Gene expression profiling of human sarcomas: insights into sarcoma biology**. *Cancer Res* 2005, **65**(20):9226-9235.

109. Acharya A, Das I, Chandhok D, Saha T: **Redox regulation in cancer: a double-edged sword with therapeutic potential**. *Oxid Med Cell Longev* 2010, **3**(1):23-34.

110. Landriscina M, Maddalena F, Laudiero G, Esposito F: **Adaptation to oxidative stress, chemoresistance, and cell survival**. *Antioxid Redox Signal* 2009, **11**(11):2701-2716.

111. Nelson KK, Ranganathan AC, Mansouri J, Rodriguez AM, Providence KM, Rutter JL, Pumiglia K, Bennett JA, Melendez JA: **Elevated sod2 activity augments matrix metalloproteinase expression: evidence for the**

involvement of endogenous hydrogen peroxide in regulating metastasis. *Clin Cancer Res* 2003, **9**(1):424-432.

112. Buchberger A, Bukau B, Sommer T: **Protein quality control in the cytosol and the endoplasmic reticulum: brothers in arms**. *Mol Cell* 2010, **40**(2):238-252.

113. Gorlach A, Klappa P, Kietzmann T: **The endoplasmic reticulum: folding, calcium homeostasis, signaling, and redox control**. *Antioxid Redox Signal* 2006, **8**(9-10):1391-1418.

114. Seifert U, Bialy LP, Ebstein F, Bech-Otschir D, Voigt A, Schroter F, Prozorovski T, Lange N, Steffen J, Rieger M *et al*: **Immunoproteasomes preserve protein homeostasis upon interferon-induced oxidative stress**. *Cell* 2010, **142**(4):613-624.

115. Kloetzel PM: **Generation of major histocompatibility complex class I antigens: functional interplay between proteasomes and TPPII**. *Nat Immunol* 2004, **5**(7):661-669.

116. Simone NL, Soule BP, Ly D, Saleh AD, Savage JE, Degraff W, Cook J, Harris CC, Gius D, Mitchell JB: **Ionizing radiation-induced oxidative stress alters miRNA expression**. *PLoS One* 2009, **4**(7):e6377.

117. Pulkkinen K, Malm T, Turunen M, Koistinaho J, Yla-Herttuala S: **Hypoxia induces microRNA miR-210 in vitro and in vivo ephrin-A3 and neuronal pentraxin 1 are potentially regulated by miR-210**. *FEBS Lett* 2008, **582**(16):2397-2401.

118. Marsit CJ, Eddy K, Kelsey KT: **MicroRNA responses to cellular stress**. *Cancer Res* 2006, **66**(22):10843-10848.

119. Dave RS, Khalili K: **Morphine treatment of human monocyte-derived macrophages induces differential miRNA and protein expression: impact on inflammation and oxidative stress in the central nervous system**. *J Cell Biochem* 2010, **110**(4):834-845.

120. Li G, Luna C, Qiu J, Epstein DL, Gonzalez P: **Alterations in microRNA expression in stress-induced cellular senescence**. *Mech Ageing Dev* 2009, **130**(11-12):731-741.

121. Lin Y, Liu X, Cheng Y, Yang J, Huo Y, Zhang C: **Involvement of MicroRNAs in hydrogen peroxide-mediated gene regulation and cellular injury response in vascular smooth muscle cells**. *J Biol Chem* 2009, **284**(12):7903-7913.

122. Wang Z, Liu Y, Han N, Chen X, Yu W, Zhang W, Zou F: **Profiles of oxidative stress-related microRNA and mRNA expression in auditory cells**. *Brain Res* 2010, **1346**:14-25.

123. Iwabu M, Yamauchi T, Okada-Iwabu M, Sato K, Nakagawa T, Funata M, Yamaguchi M, Namiki S, Nakayama R, Tabata M *et al*: **Adiponectin and**

AdipoR1 regulate PGC-1alpha and mitochondria by Ca(2+) and AMPK/SIRT1. *Nature* 2010, **464**(7293):1313-1319.

124. Yan Q, Dutt S, Xu R, Graves K, Juszczynski P, Manis JP, Shipp MA: **BBAP monoubiquitylates histone H4 at lysine 91 and selectively modulates the DNA damage response**. *Mol Cell* 2009, **36**(1):110-120.

125. Honda K, Takaoka A, Taniguchi T: **Type I interferon [corrected] gene induction by the interferon regulatory factor family of transcription factors**. *Immunity* 2006, **25**(3):349-360.

126. Simon AR, Rai U, Fanburg BL, Cochran BH: **Activation of the JAK-STAT pathway by reactive oxygen species**. *Am J Physiol* 1998, **275**(6 Pt 1):C1640-1652.

127. Salzer-Kuntschik M, Brand G, Delling G: **[Determination of the degree of morphological regression following chemotherapy in malignant bone tumors]**. *Pathologe* 1983, **4**(3):135-141.

128. Mackintosh C, Ordonez JL, Garcia-Dominguez DJ, Sevillano V, Llombart-Bosch A, Szuhai K, Scotlandi K, Alberghini M, Sciot R, Sinnaeve F *et al*: **1q gain and CDT2 overexpression underlie an aggressive and highly proliferative form of Ewing sarcoma**. *Oncogene* 2012, **31**(10):1287-1298.

129. Peters D, Freund J, Ochs RL: **Genome-wide transcriptional analysis of carboplatin response in chemosensitive and chemoresistant ovarian cancer cells**. *Mol Cancer Ther* 2005, **4**(10):1605-1616.

130. Kamata T: **Roles of Nox1 and other Nox isoforms in cancer development**. *Cancer Sci* 2009, **100**(8):1382-1388.

131. Diepart C, Karroum O, Magat J, Feron O, Verrax J, Calderon PB, Gregoire V, Leveque P, Stockis J, Dauguet N *et al*: **Arsenic trioxide treatment decreases the oxygen consumption rate of tumor cells and radiosensitizes solid tumors**. *Cancer Res* 2012, **72**(2):482-490.

132. Girdhani S, Bhosle SM, Thulsidas SA, Kumar A, Mishra KP: **Potential of radiosensitizing agents in cancer chemo-radiotherapy**. *J Cancer Res Ther* 2005, **1**(3):129-131.

133. Leto TL, Morand S, Hurt D, Ueyama T: **Targeting and regulation of reactive oxygen species generation by Nox family NADPH oxidases**. *Antioxid Redox Signal* 2009, **11**(10):2607-2619.

134. Barth BM, Gustafson SJ, Young MM, Fox TE, Shanmugavelandy SS, Kaiser JM, Cabot MC, Kester M, Kuhn TB: **Inhibition of NADPH oxidase by glucosylceramide confers chemoresistance**. *Cancer Biol Ther* 2010, **10**(11):1126-1136.

135. Zhao Y, McLaughlin D, Robinson E, Harvey AP, Hookham MB, Shah AM, McDermott BJ, Grieve DJ: **Nox2 NADPH oxidase promotes pathologic cardiac remodeling associated with Doxorubicin chemotherapy**. *Cancer Res* 2010, **70**(22):9287-9297.

136. Solchaga LA, Penick K, Goldberg VM, Caplan AI, Welter JF: **Fibroblast Growth Factor-2 Enhances Proliferation and Delays Loss of Chondrogenic Potential in Human Adult Bone Marrow-Derived Mesenchymal Stem Cells**. *Tissue Eng Part A* 2010, **16**(3):1009-1019.

137. Passer BJ, Nancy-Portebois V, Amzallag N, Prieur S, Cans C, Roborel de Climens A, Fiucci G, Bouvard V, Tuynder M, Susini L *et al*: **The p53-inducible TSAP6 gene product regulates apoptosis and the cell cycle and interacts with Nix and the Myt1 kinase**. *Proc Natl Acad Sci U S A* 2003, **100**(5):2284-2289.

138. Zhang X, Steiner MS, Rinaldy A, Lu Y: **Apoptosis induction in prostate cancer cells by a novel gene product, pHyde, involves caspase-3**. *Oncogene* 2001, **20**(42):5982-5990.

139. Lu Y, Zhang X, Beheshti B, Zhang J: **Adenoviral-mediated pHyde gene transfer and cisplatin additively inhibit human prostate cancer growth by enhancing apoptosis**. *Prostate* 2009, **69**(3):234-248.

140. Caillot F, Daveau R, Daveau M, Lubrano J, Saint-Auret G, Hiron M, Goria O, Scotte M, Francois A, Salier JP: **Down-regulated expression of the TSAP6 protein in liver is associated with a transition from cirrhosis to hepatocellular carcinoma**. *Histopathology* 2009, **54**(3):319-327.

141. Porkka KP, Nupponen NN, Tammela TL, Vessella RL, Visakorpi T: **Human pHyde is not a classical tumor suppressor gene in prostate cancer**. *Int J Cancer* 2003, **106**(5):729-735.

142. Daiber A: **Redox signaling (cross-talk) from and to mitochondria involves mitochondrial pores and reactive oxygen species**. *Biochim Biophys Acta* 2010, **1797**(6-7):897-906.

143. Galaris D, Skiada V, Barbouti A: **Redox signaling and cancer: the role of "labile" iron**. *Cancer Lett* 2008, **266**(1):21-29.

144. Chevion M: **A site-specific mechanism for free radical induced biological damage: the essential role of redox-active transition metals**. *Free Radic Biol Med* 1988, **5**(1):27-37.

145. Grange L, Nguyen MV, Lardy B, Derouazi M, Campion Y, Trocme C, Paclet MH, Gaudin P, Morel F: **NAD(P)H oxidase activity of Nox4 in chondrocytes is both inducible and involved in collagenase expression**. *Antioxid Redox Signal* 2006, **8**(9-10):1485-1496.

146. Johansson N, Ahonen M, Kahari VM: **Matrix metalloproteinases in tumor invasion**. *Cell Mol Life Sci* 2000, **57**(1):5-15.

147. DiMascio L, Voermans C, Uqoezwa M, Duncan A, Lu D, Wu J, Sankar U, Reya T: **Identification of adiponectin as a novel hemopoietic stem cell growth factor**. *J Immunol* 2007, **178**(6):3511-3520.

148. Khodarev NN, Minn AJ, Efimova EV, Darga TE, Labay E, Beckett M, Mauceri HJ, Roizman B, Weichselbaum RR: **Signal transducer and activator of**

transcription 1 regulates both cytotoxic and prosurvival functions in tumor cells. *Cancer Res* 2007, **67**(19):9214-9220.

149. Schultz J, Koczan D, Schmitz U, Ibrahim SM, Pilch D, Landsberg J, Kunz M: **Tumor-promoting role of signal transducer and activator of transcription (Stat)1 in late-stage melanoma growth**. *Clin Exp Metastasis* 2010, **27**(3):133-140.

150. Sanceau J, Hiscott J, Delattre O, Wietzerbin J: **IFN-beta induces serine phosphorylation of Stat-1 in Ewing's sarcoma cells and mediates apoptosis via induction of IRF-1 and activation of caspase-7**. *Oncogene* 2000, **19**(30):3372-3383.

151. Sanceau J, Poupon MF, Delattre O, Sastre-Garau X, Wietzerbin J: **Strong inhibition of Ewing tumor xenograft growth by combination of human interferon-alpha or interferon-beta with ifosfamide**. *Oncogene* 2002, **21**(50):7700-7709.

152. Behjati S, Basu BP, Wallace R, Bier N, Sebire N, Hasan F, Anderson J: **STAT3 Regulates Proliferation and Immunogenicity of the Ewing Family of Tumors In Vitro**. *Sarcoma* 2012, **2012**:987239.

153. Lai R, Navid F, Rodriguez-Galindo C, Liu T, Fuller CE, Ganti R, Dien J, Dalton J, Billups C, Khoury JD: **STAT3 is activated in a subset of the Ewing sarcoma family of tumours**. *J Pathol* 2006, **208**(5):624-632.

154. Grunewald TG, Diebold I, Esposito I, Plehm S, Hauer K, Thiel U, da Silva-Buttkus P, Neff F, Unland R, Muller-Tidow C *et al*: **STEAP1 is associated with the invasive and oxidative stress phenotype of Ewing tumors**. *Mol Cancer Res* 2012, **10**(1):52-65.

155. Grunewald TG, Ranft A, Esposito I, da Silva-Buttkus P, Aichler M, Baumhoer D, Schaefer KL, Ottaviano L, Poremba C, Jundt G *et al*: **High STEAP1 expression is associated with improved outcome of Ewing's sarcoma patients**. *Ann Oncol* 2012, **23**(8):2185-2190.

156. Petry A, Weitnauer M, Gorlach A: **Receptor activation of NADPH oxidases**. *Antioxid Redox Signal* 2010, **13**(4):467-487.

9 Appendix

9.1 List of differentially regulated genes as identified by microarrays

Genes are ordered by mean log2-transformed fold change (FC). Independent one-sample t-test was applied to determine significance. Genes that have been selected to validate the microarray data with qRT-PCR are printed in bold font.

Gene symbol	Description	FC SK-N-MC	FC A673	mean log2 FC	*p* value
STEAP1	**six transmembrane epithelial antigen of the prostate 1**	**-2.70**	**-1.67**	**-2.18**	**0.0021**
IFIT5	interferon-induced protein with tetratricopeptide repeats 5	-2.58	-0.16	-1.37	0.0834
PSMB9	**proteasome subunit, beta type, 9**	**-2.07**	**-0.57**	**-1.32**	**0.0204**
DTX3L	**deltex 3-like (Drosophila)**	**-2.39**	**-0.24**	**-1.31**	**0.0568**
USP18	**ubiquitin specific peptidase 18**	**-2.48**	**-0.13**	**-1.30**	**0.0700**
SAMD9	sterile alpha motif domain containing 9	-2.22	-0.28	-1.25	0.0689
IFIT3	interferon-induced protein with tetratricopeptide repeats 3	-2.40	-0.09	-1.24	0.0842
TAP1	**transporter 1, ATP-binding cassette, sub-family B**	**-2.22**	**-0.24**	**-1.23**	**0.0521**
GBP1	guanylate binding protein 1, interferon-inducible, 67kDa	-1.97	-0.45	-1.21	0.0302
OAS1	2',5'-oligoadenylate synthetase 1, 40/46kDa	-1.85	-0.49	-1.17	0.0387
OAS3	2'-5'-oligoadenylate synthetase 3, 100kDa	-2.17	-0.14	-1.16	0.0657
IFIT2	interferon-induced protein with tetratricopeptide repeats 2	-2.23	-0.05	-1.14	0.0669
C3	complement component 3	-1.96	-0.32	-1.14	0.0363
IFI35	interferon-induced protein 35	-1.75	-0.48	-1.12	0.0361
IRF1	interferon regulatory factor 1	-1.97	-0.24	-1.10	0.0422
ZNF594	zinc finger protein 594	-1.13	-0.81	-0.97	0.0059
GRAP	GRB2-related adaptor protein	-0.65	-1.25	-0.95	0.0053
UBA7	ubiquitin-like modifier activating enzyme 7	-1.58	-0.26	-0.92	0.0422
EPSTI1	epithelial stromal interaction 1 (breast)	-1.64	-0.17	-0.90	0.0618
ACTA2	actin, alpha 2, smooth muscle, aorta	-1.36	-0.43	-0.90	0.0177
MMP-1	**matrix metallopeptidase 1 (interstitial collagenase)**	**-0.61**	**-1.16**	**-0.89**	**0.0209**
TDO2	tryptophan 2,3-dioxygenase	-1.74	-0.03	-0.88	0.0748
TAP2	transporter 2, ATP-binding cassette, sub-family B	-1.68	-0.08	-0.88	0.0742
APOL2	apolipoprotein L, 2	-1.05	-0.61	-0.83	0.0038
SAMHD1	SAM domain and HD domain 1	-1.35	-0.28	-0.81	0.0391
HLA-B	major histocompatibility complex, class I, B	-1.48	-0.13	-0.81	0.0543
ADIPOR1	**adiponectin receptor 1**	**-1.15**	**-0.44**	**-0.80**	**0.0199**
PLEKHA1	pleckstrin homology domain containing, family A member 1	-1.31	-0.25	-0.78	0.0432
CENPH	centromere protein H	-1.10	-0.46	-0.78	0.0133
LOC92270	hypothetical protein LOC92270	-1.28	-0.22	-0.75	0.0337

Gene symbol	Description	FC SK-N-MC	FC A673	mean log2 FC	*p* value
ZP3	zona pellucida glycoprotein 3 (sperm receptor)	-0.32	-1.17	-0.75	0.0255
HLA-C	major histocompatibility complex, class I, C	-1.33	-0.14	-0.73	0.0498
STAT2	signal transducer and activator of transcription 2, 113kDa	-1.22	-0.19	-0.70	0.0654
PSMB8	proteasome (prosome, macropain) subunit, beta type, 8	-1.39	-0.01	-0.70	0.0691
GMPR	guanosine monophosphate reductase	-1.23	-0.17	-0.70	0.0411
B3GNT7	beta-1,3-N-acetylglucosaminyltransferase 7	-0.34	-1.04	-0.69	0.0145
IFITM3	interferon induced transmembrane protein 3 (1-8U)	-1.10	-0.28	-0.69	0.0445
IFI16	interferon, gamma-inducible protein 16	-1.13	-0.23	-0.68	0.0421
OSMR	oncostatin M receptor	-1.03	-0.29	-0.66	0.0248
GLIPR1	GLI pathogenesis-related 1 (glioma)	-1.00	-0.29	-0.65	0.0180
SMPDL3B	sphingomyelin phosphodiesterase, acid-like 3B	-1.10	-0.18	-0.64	0.0408
HRASLS	HRAS-like suppressor	-1.04	-0.15	-0.59	0.0487
DKFZp434O0320	hypothetical protein DKFZp434O0320	-1.08	-0.11	-0.59	0.0683
RASD2	RASD family, member 2	-1.01	-0.17	-0.59	0.0356
ESRRB	estrogen-related receptor beta	-1.02	-0.10	-0.56	0.0470
LMLN	leishmanolysin-like (metallopeptidase M8 family)	-1.02	-0.07	-0.54	0.0541
OSBPL6	oxysterol binding protein-like 6	0.07	0.57	0.32	0.0555
CST2	cystatin SA	0.62	0.12	0.37	0.0379
ARMCX6	armadillo repeat containing, X-linked 6	0.16	0.60	0.38	0.0522
ARMCX1	armadillo repeat containing, X-linked 1	0.18	0.59	0.38	0.0177
CDR2L	cerebellar degeneration-related protein 2-like	0.65	0.12	0.38	0.0340
GPR44	G protein-coupled receptor 44	0.69	0.09	0.39	0.0466
OR51A4	olfactory receptor, family 5, subfamily AR, member 1	0.60	0.18	0.39	0.0245
ZNF761	zinc finger protein 761	0.08	0.73	0.41	0.0437
OR51S1	olfactory receptor, family 51, subfamily A, member 4	0.65	0.16	0.41	0.0349
HIG2	hypoxia-inducible protein 2	0.26	0.57	0.41	0.0219
TAX1BP3	Tax1 (human T-cell leukemia virus type I) binding protein 3	0.62	0.21	0.41	0.0152
AKNA	AT-hook transcription factor	0.61	0.21	0.41	0.0173
C11orf77	chromosome 11 open reading frame 77	0.25	0.58	0.42	0.0116
CYP26C1	cytochrome P450, family 26, subfamily C, polypeptide 1	0.64	0.20	0.42	0.0160
DEFB109	defensin, beta 109	0.25	0.60	0.42	0.0118
SHOX2	short stature homeobox 2	0.25	0.61	0.43	0.0090
LQK1	LQK1 hypothetical protein short isoform	0.13	0.72	0.43	0.0321
C1QTNF9	C1q and tumor necrosis factor related protein 9	0.27	0.60	0.43	0.0258
ERO1L	ERO1-like (S. cerevisiae)	0.69	0.19	0.44	0.0228
PLG	plasminogen	0.69	0.20	0.45	0.0196
CDSN	corneodesmosin	0.59	0.30	0.45	0.0076
GAS2L3	growth arrest-specific 2 like 3	0.65	0.25	0.45	0.0136
PELI2	pellino homolog 2 (Drosophila)	0.77	0.14	0.46	0.0330
PTGFRN	prostaglandin F2 receptor negative regulator	0.30	0.62	0.46	0.0106

Gene symbol	Description	FC SK-N-MC	FC A673	mean log2 FC	*p* value
TRIM47	tripartite motif-containing 47	0.69	0.24	0.46	0.0145
RNF146	ring finger protein 146	0.25	0.68	0.46	0.0204
ZNF480	zinc finger protein 480	0.81	0.12	0.47	0.0389
RTN4R	reticulon 4 receptor	0.58	0.36	0.47	0.0136
KRTAP10-3	keratin associated protein 10-3	0.32	0.62	0.47	0.0091
FAM90A1	family with sequence similarity 90, member A1	0.59	0.37	0.48	0.0023
LCAP	lung carcinoma-associated protein	0.66	0.31	0.49	0.0073
GNPNAT1	glucosamine-phosphate N-acetyltransferase 1	0.64	0.35	0.49	0.0079
SURF1	surfeit 1	0.36	0.65	0.51	0.0049
FBXW9	F-box and WD repeat domain containing 9	0.63	0.40	0.52	0.0016
GPR153	G protein-coupled receptor 153	0.60	0.45	0.52	0.0016
C19orf12	chromosome 19 open reading frame 12	0.79	0.30	0.55	0.0131
CLN8	ceroid-lipofuscinosis, neuronal 8	0.52	0.59	0.56	0.0024
MAGEL2	MAGE-like 2	0.61	0.54	0.58	0.0002
OCR1	ovarian cancer-related protein 1	0.70	0.48	0.59	0.0019
TMEM70	transmembrane protein 70	0.54	0.68	0.61	0.0005
MEIS3	Meis homeobox 3	0.73	0.73	0.73	0.0003

9.2 List of differentially regulated proteins as identified by mass spectrometry

To differentiate between major and minor protein constituents within a single 2D PAGE spot, the most abundant protein(s) as judged by exponentially modified Protein Abundance Index (emPAI) scoring is/are marked in bold font. This scoring is based on the probability that a highly abundant protein will produce more identifiable spectra (each belonging to the same protein-isoform) than a comparable protein in the same spot. Spot 25 represents a control spot that was not regulated in all three runs. MFC: mean linear fold change; SD: standard deviation.

No	Protein description	Gene ID	Biological function	Status	MFC	SD
1	**Cytochrome b-c1 complex subunit 1, mitochondrial**	**UQCRC1**	**REDOX**	down	-6.9	1.7
	60 kDa heat shock protein, mitochondrial	HSPD1	Protein transport and folding			
	Tetratricopeptide repeat protein 4	TTC4	Invasion / Migration / Cytoskeleton			
	Tubulin beta chain	TUBB2C	Invasion / Migration / Cytoskeleton			
	T-complex protein 1 subunit epsilon	CCT5	Protein transport and folding			
2	**Glyceraldehyde-3-phosphate dehydrogenase**	**GAPDH**	**Metabolism and OXPHOS**	down	-6.7	0.0
	Annexin A2	ANXA2	Invasion / Migration / Cytoskeleton			
	Heterogeneous nuclear ribonucleoproteins A2/B1	HNRNPA2B1	Translation and posttr. protein mod.			
3	**Tropomyosin alpha-4 chain**	**TPM4**	**Invasion / Migration / Cytoskeleton**	up	7.7	1.9
	Tropomyosin alpha-3 chain	**TPM3**	**Invasion / Migration / Cytoskeleton**			
	Tropomyosin beta chain	TPM2	Invasion / Migration / Cytoskeleton			
	Putative tropomyosin alpha-3 chain-like protein	Not kown	Not kown			
	Protein disulfide-isomerase	P4HB	Protein transport and folding			
	Heterogeneous nuclear ribonucleoproteins C1/C2	HNRNPC	Translation and posttr. protein mod.			
	Enolase-phosphatase E1	ENOPH1	Metabolism and OXPHOS			
4	**Peroxiredoxin-2**	**PRDX2**	**REDOX**	down	-6.0	1.4
	THO complex subunit 7 homolog	THOC7	Translation and posttr. protein mod.			
	Core-binding factor subunit beta	CBFB	Transcriptional control			
	T-complex protein 1 subunit gamma	CCT3	Protein transport and folding			
5	**Eukaryotic translation initiation factor 3 subunit I**	**EIF3G**	**Translation and posttr. protein mod.**	down	-6.6	0.4
	Ubiquitin domain-containing protein UBFD1	**UBFD1**	**UPS**			
	Protein disulfide-isomerase A3	PDIA3	Protein transport and folding			
	Peroxiredoxin-2	PRDX2	REDOX			
6	**Alpha-enolase**	**ENO1**	**Metabolism and OXPHOS**	up	14.8	0.6
	Aspartate aminotransferase, cytoplasmic	GOT1	Metabolism and OXPHOS			
7	**Glutamate dehydrogenase 1, mitochondrial**	**GLUD1**	**Metabolism and OXPHOS**	up	9.0	0.6
	Alpha-enolase	ENO1	Metabolism and OXPHOS			

No	Protein description	Gene ID	Biological function	Status	MFC	SD
7	Fascin	FSCN1	Invasion / Migration / Cytoskeleton	up	9.0	0.6
	D-3-phosphoglycerate dehydrogenase	PHGDH	Metabolism and OXPHOS			
	ATP synthase subunit alpha, mitochondrial	ATP5A1	REDOX / OXPHOS			
	T-complex protein 1 subunit zeta	CCT6A	Protein transport and folding			
	Plasminogen activator inhibitor 1 RNA-binding protein	SERBP1	Not kown			
	Putative elongation factor 1-alpha-like 3	EEF1AL3	Pseudogene			
	Elongation factor 1-alpha 1	EEF1A1	Translation and posttr. protein mod.			
	T-complex protein 1 subunit beta	CCT2	Protein transport and folding			
	Inosine-5'-monophosphate dehydrogenase 2	IMPDH2	REDOX			
	Alpha-aminoadipic semialdehyde dehydrogenase	ALDH7A1	REDOX			
8	**Nuclear autoantigenic sperm protein**	**NASP**	**Protein transport and folding**	up	1.9	0.3
	Heterogeneous nuclear ribonucleoprotein K	HNRNPK	Translation and posttr. protein mod.			
	T-complex protein 1 subunit gamma	CCT3	Protein transport and folding			
9	**Succinyl-CoA:3-ketoacid-coenzyme A transferase 1, mitochondrial**	**OXCT1**	**Metabolism and OXPHOS**	down	-7.4	1.6
	Protein disulfide-isomerase A3	**PDIA3**	**Protein transport and folding**			
	T-complex protein 1 subunit beta	CCT2	Protein transport and folding			
	D-3-phosphoglycerate dehydrogenase	PHGDH	Metabolism and OXPHOS			
10	**40S ribosomal protein SA**	**RPSA**	**Translation and posttr. protein mod.**	up	2.4	0.4
11	**Superoxide dismutase [Mn], mitochondrial**	**SOD2**	**REDOX**	up	2.2	0.2
12	Phosphatidylethanolamine-binding protein 1	PEBP1 / RKIP	Signaling	up	2.2	0.5
	Proteasome subunit beta type-5	PSMB5	UPS			
	Peroxiredoxin-1	PRDX1	REDOX			
	Cellular nucleic acid-binding protein	CNBP	Transcriptional control			
	NEDD8-conjugating enzyme Ubc12 1	UBE2M	UPS			
13	Deoxyuridine 5'-triphosphate nucleotidohydrolase, mitochondrial	DUT	Transcriptional control	up	1.7	0.1
	Uncharacterized protein KIAA1143	KIAA1143	not known			
	14-3-3 protein theta	YWHAQ	Signaling			
14	Superoxide dismutase [Cu-Zn]	SOD1	REDOX	up	2.3	0.1
	Stathmin	STMN1	Signaling			
	Translocon-associated protein subunit delta	SSR4	Protein transport and folding			
	ADP-ribosylation factor 3	ARF3	Protein transport and folding			
	ADP-ribosylation factor 1	ARF1	Protein transport and folding			
	Vesicle-trafficking protein SEC22b	SEC22B	Protein transport and folding	up	2.3	0.1
	Nucleoside diphosphate kinase A	NME1	Metabolism and OXPHOS			
	Dermcidin	DCD	Stress response and survival			
15	**Stathmin**	**STMN1**	**Signaling**	up	5.4	0.1
	Peptidyl-prolyl cis-trans isomerase A	PPIA	Protein transport and folding			
	Actin-related protein 2/3 complex subunit 5	ARPC5	Invasion / Migration / Cytoskeleton			
	Centromere protein S	APITD1	Transcriptional control			
	Activated RNA polymerase II transcriptional coactivator p15	SUB1	Transcriptional control			
	Prefoldin subunit 2	PFDN2	Protein transport and folding			
16	**26S protease regulatory subunit S10B**	**PSMC6**	**UPS**	up	3.2	0.4
	Fructose-bisphosphate aldolase A	ALDOA	Metabolism and OXPHOS			
	Isovaleryl-CoA dehydrogenase, mitochondrial	IVD	Metabolism and OXPHOS			
	Mitochondrial import receptor subunit TOM40 homolog	TOMM40	Protein transport and folding			
	Alpha-2-macroglobulin receptor-associated protein	LRPAP1	Protein transport and folding			
	Stathmin OS=Homo sapiens	STMN1	Signaling			

No	Protein description	Gene ID	Biological function	Status	MFC	SD
16	Acetyl-CoA acetyltransferase, mitochondrial	ACAT1	Metabolism and OXPHOS	Up	3.2	0.4
	Heterogeneous nuclear ribonucleoprotein	HNRNPD	RNA transport and processing			
	GMP reductase 2	GMPR2	REDOX			
	mRNA export factor	RAE1	RNA transport and processing			
	Heterogeneous nuclear ribonucleoprotein A3	HNRNPA3	RNA transport and processing			
17	Rho GDP-dissociation inhibitor 1	ARHGDIA	Signaling	up	2.8	0.2
	Tumor protein D52	TPD52	Signaling			
	14-3-3 protein theta	YWHAQ	Signaling			
	Ran-specific GTPase-activating protein	RANBP1	Signaling			
	14-3-3 protein beta/alpha	YWHAB	Signaling			
	Membrane-associated progesterone receptor component 2	PGRMC2	Signaling			
	T-complex protein 1 subunit theta	CCT8	Protein transport and folding			
	Proteasome subunit alpha type-3	PSMA3	UPS			
18	Caspase-7	CASP7	Stress response and survival	down	-2.2	0.0
	L-lactate dehydrogenase B chain	LDHB	REDOX			
	Nicotinate-nucleotide pyrophosphorylase [carboxylating]	QPRT	Metabolism and OXPHOS			
	Inorganic pyrophosphatase 2, mitochondrial	PPA2	Metabolism and OXPHOS			
	STIP1 homology and U box-containing protein 1	STUB1	UPS and CHAPERONE			
	Heterogeneous nuclear ribonucleoprotein H3	HNRNPH3	RNA transport and processing			
19	**Heterogeneous nuclear ribonucleoprotein M**	**HNRNPM**	**RNA transport and processing**	up	2.0	0.1
	Far upstream element-binding protein 1	**FUBP1**	**Transcriptional control**			
	Probable ATP-dependent RNA helicase DDX17	DDX17	RNA transport and processing			
19	Polyadenylate-binding protein 1	PABPC1	RNA transport and processing	up	2.0	0.1
	Interferon regulatory factor 2-binding protein 1	IRF2BP1	Transcriptional control			
	RNA-binding protein 14	RBM14	Transcriptional control			
20	**26S protease regulatory subunit 8**	**PSMC5**	**UPS**	up	1.5	0.0
	Isocitrate dehydrogenase [NADP], mitochondrial	IDH2	REDOX			
	Nucleolysin TIA-1 isoform p40	TIA1	Stress response and survival			
	Multifunctional protein ADE2	PAICS	Metabolism and OXPHOS			
	Cytochrome b-c1 complex subunit 2, mitochondrial	UQCRC2	Metabolism and OXPHOS			
	Heterogeneous nuclear ribonucleoprotein G	RBMX	RNA transport and processing			
	Heterogeneous nuclear ribonucleoprotein	HNRNPD	RNA transport and processing			
	Citrate synthase, mitochondrial	CS	Metabolism and OXPHOS			
	Elongation factor Tu, mitochondrial	TUFM	Translation and posttr. prot. mod.			
	Obg-like ATPase 1	OLA1	REDOX			
	Argininosuccinate synthase	ASS1	Metabolism and OXPHOS			
21	3-hydroxyacyl-CoA dehydrogenase type-2	HSD17B1	REDOX	up	3.7	0.2
	Annexin A1	ANXA1	Invasion / Migration / Cytoskeleton			
	Protein LSM12 homolog	LSM12	Stress response and survival			
22	NADH-ubiquinone oxidoreductase 75 kDa subunit, mitochondrial	NDUFS1	REDOX and OXPHOS	down	-1.7	0.1
	Cytoplasmic dynein 1 intermediate chain 2	DYNC1I2	Invasion / Migration / Cytoskeleton			
	Zinc finger protein 326	ZNF326	Transcriptional control			
	Protein disulfide-isomerase A4	PDIA4	REDOX			
	78 kDa glucose-regulated protein	HSPA5	UPS			
	Heat shock protein HSP 90-beta	HSP90AB1	Protein transport and folding			
	Lamin-B1	LMNB1	Invasion / Migration / Cytoskeleton			
	Heat shock protein HSP 90-alpha	HSP90AA1	Protein transport and folding			
	Nucleolin	NCL	Translation and posttr. protein mod.			

No	Protein description	Gene ID	Biological function	Status	MFC	SD
22	ATP-dependent RNA helicase DDX3X	DDX3X	RNA transport and processing	down	-1.7	0.1
	Protein phosphatase 1G	PPM1G	RNA transport and processing			
23	Thioredoxin domain-containing protein 5	TXNDC5	REDOX	down	-3.3	0.2
	Hsc70-interacting protein	ST13	Protein transport and folding			
	Hsp90 co-chaperone Cdc37	CDC37	Protein transport and folding			
	cAMP-dependent protein kinase type I-alpha regulatory subunit	PRKAR1A	Signaling			
	Dynactin subunit 2	DCTN2	Invasion / Migration / Cytoskeleton			
	Tubulin alpha-1B chain	TUBA1B	Invasion / Migration / Cytoskeleton			
	Hydroxymethylglutaryl-CoA synthase, cytoplasmic	HMGCS1	Metabolism and OXPHOS			
	Tubulin alpha-1C chain	TUBA1C	Invasion / Migration / Cytoskeleton			
	Tubulin alpha-1A chain	TUBA1A	Invasion / Migration / Cytoskeleton			
	Protein disulfide-isomerase A6	PDIA6	Protein transport and folding			
	Polymerase delta-interacting protein 3	POLDIP3	Transcriptional control			
	26S protease regulatory subunit 6A	PSMC3	UPS			
	Zinc finger protein ubi-d4	DPF2	Stress response and survival			
	Putative elongation factor 1-alpha-like 3	EEF1AL3	Pseudogene			
23	Elongation factor 1-alpha 1	EEF1A1	Translation and posttr. protein mod.	down	-3.3	0.2
	Actin-like protein 6A	ACTL6A	Transcriptional control			
	Probable serine carboxypeptidase	CPVL	Protein transport and folding			
	Heat shock cognate 71 kDa protein	HSPA8	Protein transport and folding			
23	Na(+)/H(+) exchange regulatory cofactor NHE-RF1	SLC9A3R1	Signaling	down	-3.3	0.2
	Lupus La protein / Sjogren syndrome antigen B	SSB	RNA transport and processing			
	Eukaryotic translation initiation factor 2 subunit 2-like protein	Not kown	Not kown			
	Eukaryotic translation initiation factor 2 subunit 2	EIF2S2	Translation and posttr. protein mod.			
	Eukaryotic translation initiation factor 3 subunit F	EIF3F	Translation and posttr. protein mod.			
	Lamin-B1	LMNB1	Invasion / Migration / Cytoskeleton			
	26S protease regulatory subunit 6B	PSMC4	UPS			
24	Fructose-bisphosphate aldolase A	ALDOA	Metabolism and OXPHOS	up	2.2	0.1
	26S protease regulatory subunit S10B	PSMC6	UPS			
25	60S acidic ribosomal protein P0	RPLP0	Translation and posttr. protein mod.	no	1.0	0.1
	L-lactate dehydrogenase B chain	LDHB	REDOX			
	Alpha-enolase	ENO1	Metabolism and OXPHOS			
	F-actin-capping protein subunit alpha-1	CAPZA1	Invasion / Migration / Cytoskeleton			
	Eukaryotic translation initiation factor 3 subunit I	EIF3I	Translation and posttr. protein mod.			
	Transaldolase	TALDO1	Metabolism and OXPHOS			
	F-actin-capping protein subunit alpha-2	CAPZA2	Invasion / Migration / Cytoskeleton			
	Pyruvate dehydrogenase E1 component subunit beta, mitochondrial	PDHB	Metabolism and OXPHOS			

9.3 List of differentially regulated miRNAs

Micro RNAs are listed according to their mean log2 fold change (FC) across both cell lines. Only those miRNAs are listed which were at least regulated ±0.27 log2 fold across both cell lines.

Probe set ID	lin. FC A673	lin. FC SK-N-MC	mean lin. FC	mean log2 FC
hsa-miR-877_st	1.65	1.75	1.70	0.77
hsa-miR-744_st	1.94	1.33	1.63	0.71
hsa-miR-216a_st	1.32	1.51	1.41	0.50
hsa-miR-653_st	1.24	1.48	1.36	0.44
hsa-miR-520d-5p_st	1.50	1.22	1.36	0.44
hsa-miR-129-star_st	1.20	1.46	1.33	0.41
hsa-miR-671-5p_st	1.37	1.29	1.33	0.41
hsa-miR-7-1-star_st	1.10	1.47	1.29	0.36
hsa-miR-377_st	1.32	1.25	1.28	0.36
hsa-miR-1825_st	1.46	1.11	1.28	0.36
hsa-miR-130b_st	1.18	1.37	1.28	0.35
hsa-miR-154_st	1.28	1.25	1.26	0.34
hsa-miR-576-5p_st	1.25	1.27	1.26	0.34
hsa-miR-1300_st	1.37	1.15	1.26	0.33
hsa-miR-1245_st	1.26	1.26	1.26	0.33
hsa-miR-624-star_st	1.29	1.22	1.26	0.33
hsa-miR-34b_st	1.16	1.35	1.26	0.33
hsa-miR-548c-3p_st	1.12	1.37	1.24	0.31
hsa-miR-374b_st	1.16	1.32	1.24	0.31
hsa-miR-451_st	1.29	1.18	1.23	0.30
hsa-miR-15b-star_st	1.35	1.10	1.22	0.29
hsa-miR-518f_st	1.23	1.21	1.22	0.29
hsa-miR-135b_st	1.33	1.11	1.22	0.29
hsa-miR-195_st	1.18	1.26	1.22	0.29
hsa-miR-129-3p_st	1.32	1.12	1.22	0.29
hsa-miR-26b-star_st	1.16	1.27	1.22	0.28
hsa-miR-497_st	1.19	1.24	1.21	0.28
hsa-miR-103_st	1.10	1.33	1.21	0.28
hsa-miR-508-5p_st	1.27	1.15	1.21	0.28
hsa-miR-31_st	1.05	1.38	1.21	0.28
hsa-miR-766_st	1.25	1.17	1.21	0.28
hsa-miR-384_st	1.25	1.16	1.21	0.27
hsa-miR-1827_st	1.10	1.31	1.20	0.27
hsa-miR-620_st	1.26	1.14	1.20	0.27
hsa-miR-644_st	1.04	1.36	1.20	0.27
hsa-miR-511_st	1.23	1.17	1.20	0.26
hsa-let-7a_st	1.21	1.18	1.19	0.26
hsa-miR-943_st	1.08	1.31	1.19	0.25
hsa-miR-490-3p_st	1.18	1.21	1.19	0.25
hsa-miR-200b-star_st	1.22	1.16	1.19	0.25
hsa-miR-1299_st	0.88	0.80	0.84	-0.25

Probe set ID	lin. FC A673	lin. FC SK-N-MC	mean lin. FC	mean log2 FC
hsa-miR-619_st	0.78	0.89	0.84	-0.25
hsa-miR-1270_st	0.88	0.79	0.84	-0.26
hsa-miR-27b-star_st	*0.85*	*0.82*	*0.83*	*-0.26*
hsa-miR-1271_st	0.77	0.89	0.83	-0.27
hsa-miR-20a-star_st	0.80	0.87	0.83	-0.27
hsa-miR-199b-3p_st	0.91	0.75	0.83	-0.27
hsa-miR-302d-star_st	0.81	0.85	0.83	-0.27
hsa-miR-214-star_st	0.81	0.85	0.83	-0.27
hsa-miR-526b-star_st	0.83	0.83	0.83	-0.27
hsa-miR-137_st	0.81	0.85	0.83	-0.27
hsa-miR-100_st	0.92	0.74	0.83	-0.27
hsa-miR-337-5p_st	0.85	0.81	0.83	-0.27
hsa-let-7d_st	0.89	0.76	0.83	-0.28
hsa-miR-1302_st	0.79	0.86	0.82	-0.28
hsa-miR-17-star_st	0.87	0.77	0.82	-0.28
hsa-miR-506_st	0.79	0.85	0.82	-0.28
hsa-miR-1229_st	0.79	0.85	0.82	-0.29
hsa-miR-939_st	0.79	0.85	0.82	-0.29
hsa-miR-181d_st	0.88	0.76	0.82	-0.29
hsa-miR-126-star_st	0.83	0.80	0.82	-0.29
hsa-miR-500_st	0.79	0.84	0.82	-0.29
hsa-miR-409-5p_st	0.77	0.85	0.81	-0.30
hsa-miR-10a_st	0.72	0.90	0.81	-0.30
hsa-miR-325_st	0.82	0.79	0.81	-0.31
hsa-miR-423-3p_st	0.80	0.80	0.80	-0.32
hsa-miR-885-5p_st	0.82	0.79	0.80	-0.32
hsa-miR-365_st	0.79	0.82	0.80	-0.32
hsa-miR-145_st	0.77	0.84	0.80	-0.32
hsa-miR-183-star_st	0.73	0.87	0.80	-0.32
hsa-miR-605_st	0.68	0.92	0.80	-0.32
hsa-miR-613_st	0.74	0.85	0.80	-0.33
hsa-miR-654-3p_st	0.78	0.80	0.79	-0.34
hsa-miR-550_st	0.78	0.80	0.79	-0.34
hsa-miR-1307_st	0.73	0.85	0.79	-0.34
hsa-miR-938_st	0.87	0.70	0.78	-0.35
hsa-miR-1236_st	0.90	0.66	0.78	-0.36
hsa-miR-629-star_st	0.79	0.77	0.78	-0.37
hsa-miR-214_st	0.67	0.87	0.77	-0.37
hsa-miR-18a-star_st	0.65	0.88	0.76	-0.39
hsa-miR-500-star_st	0.66	0.87	0.76	-0.39
hsa-miR-338-3p_st	0.62	0.90	0.76	-0.40
hsa-miR-371-5p_st	0.77	0.75	0.76	-0.40
hsa-miR-367-star_st	0.72	0.78	0.75	-0.41
hsa-miR-331-5p_st	0.59	0.91	0.75	-0.41
hsa-miR-7-2-star_st	0.79	0.71	0.75	-0.42
hsa-miR-602_st	0.62	0.87	0.75	-0.42
hsa-miR-892b_st	0.63	0.86	0.74	-0.43
hsa-miR-222-star_st	0.72	0.72	0.72	-0.47
hsa-miR-1224-3p_st	0.82	0.62	0.72	-0.47

Probe set ID	lin. FC A673	lin. FC SK-N-MC	mean lin. FC	mean log2 FC
hsa-miR-802_st	0.89	0.54	0.72	-0.48
hsa-miR-1247_st	0.56	0.87	0.71	-0.48
hsa-miR-204_st	0.66	0.67	0.67	-0.58

9.4 Clinicopathological characteristics of patients included in TMA

ID: patient number; sex: 1 = male, 2 = female; study: 92 = European Intergroup Cooperative Ewing's Sarcoma Study 92, 99 = European Intergroup Cooperative Ewing's Sarcoma Study 99, no entry = patient data from University of Basel, Switzerland; volume: 1 = tumor volume <200 ml, 2 = tumor volume >200 ml; site: location of primary tumor: 1 = pelvis, 2 = head, 3 = spinal column, 4 = thorax, 6 = humerus, 7 = upper extremity other than humerus, 8 = femur, 9 = lower extremity other than femur, 10 = non-osseous location; lung-met. (lung metastasis): 1 = yes, 0 = no; met. other than lungs (extrapulmonal metastasis): 1 = yes, 0 = no; risk group: 0 = no metastasis, 1 = lung metastasis, 2 = extrapulmonal metastasis, 3 = extensive extrapulmonal metastasis; event: 1 = yes, 0 = no; EFS: event free survival (days); OS: overall survival (days), defined as the number of days from day of diagnosis until death or last consultation; STEAP1 cyto.: 1 = cytoplasmic STEAP1-high, 0 = cytoplasmic STEAP1-low; STEAP1 memb.: 1 = membranous STEAP1-high, 0 = membranous STEAP1-low.

ID	sex	study	age	vol.	site	met.	lung-met.	met. other than lung	risk group	event	EFS	alive	OS	STEAP1 cyto.	STEAP1 memb.
1	2	92	24.1		8	0	0	0	1	0	3961	0	3961	1	1
2	1	92	20.89	1	4	1	1	0	2	1	318	1	490	0	1
3	2	92	6.6		1	1	0	1	3	1	227	1	298	0	0
4	2	92	14.53	1	1	1	1	0	2	1	322	1	414	0	1
5	1	92	28.67	1	6	0	0	0	1	1	273	1	769	0	0
6	2	92	17.16		1	0	0	0	1	1	577	1	1128	0	1
7	1	92	33.8		9	1	0	1	3	1	320	1	539	0	0
8	1	99	10.53	1	9	1	1	0	2	1	1596	0	4052	1	0
9	1	99	17.18	1	9	1	1	0	2	0	3469	0	3469	1	1
10	1	99	17.4	1	1	0	0	0	1	0	3210	0	3210	0	0
11	1	99	20.25	2	1	0	0	0	1	1	431	1	564	0	0
12	1	99	21.33	1	6	0	0	0	1	0	3504	0	3504	0	1
13	2	99	35.32		8	1	1	1	3	1	783	0	3128	0	0
14	1	99	18.13	2	4	1	1	0	2	0	2065	0	2065	0	0
15	1	99	31.45	2	1	0	0	0	1	0	1186	0	1186	0	1

ID	sex	study	age	vol.	site	met.	lung-met.	met. other than lung	risk group	event	EFS	alive	OS	STEAP1 cyto.	STEAP1 memb.
16	1	99	31.78	1	4	0	0	0	1	1	487	1	735	0	0
17	1	99	5.07	2	9	0	0	0	1	1	1851	0	2121	0	1
18	1	99	11.72	1	9	0	0	0	1	0	2086	0	2086	0	0
19	1	99	14.81	1	10	1	1	0	2	1	256	1	771	0	0
20	2	99	22.61		1	0	0	0	1	1	422	1	422	0	1
21	2	99	19.59	1	10	0	0	0	1	0	1619	0	1619	0	0
22	2	99	33.88	1	3	0	0	0	1	1	708	0	1337	0	1
23	1	99	12.21	2	1	0	0	0	1	1	701	1	1402	0	0
24	1	99	7.01	1	7	0	0	0	1	0	1819	0	1819	0	1
25	1	99	12.76	1	1	1	1	0	2	1	980	0	1855	0	0
26	1	99	8.06	1	10	0	0	0	1	0	1846	0	1846	0	1
27	1	99	11.82	1	10	0	0	0	1	0	1651	0	1651	0	1
28	2	99	18.84	2	8	0	0	0	1	1	316	1	316	0	1
29	1	99	16.32	2	1	1	1	0	2	0	1736	0	1736	0	0
30	1	99	0.63	1	10	0	0	0	1	0	1665	0	1665	0	0
31	2	99	15.35	1	10	0	0	0	1	0	1681	0	1681	0	0
32	2	99	15.55	2	10	1	1	1	3	0	1496	0	1496	0	1
33	1	99	8.59	1	9	1	1	0	2	0	1137	0	1137	0	1
34	2	99	6.32	1	10	0	0	0	1	0	1526	0	1526	1	0
35	1	99	16.98	1	9	1	1	0	2	0	1435	0	1435	0	0
36	2	99	14.45	1	4	0	0	0	1	0	1465	0	1465	0	1
37	1	99	22.11	1	3	1	1	0	2	1	1364	1	1364	0	0
38	2	99	43.32	1	9	0	0	0	1	0	1216	0	1216	0	0
39	1	99	3.58	2	8	1	1	1	3	1	385	1	397	0	0
40	2	99	9.28	1	10	0	0	0	1	0	1158	0	1158	0	1
41	1	99	13.05	2	3	1	0	1	3	1	296	1	364	0	0
42	2	99	10.49	1	3	0	0	0	1	0	1109	0	1109	0	1
43	2	99	8.62	1	10	0	0	0	1	0	1020	0	1020	0	0
44	1	99	14.08	1	4	0	0	0	1	0	256	0	256	0	0
45	2	99	15.37	2	1	1	1	0	2	0	975	0	975	0	1
46	1	99	12.23	2	8	0	0	0	1	0	1033	0	1033	0	0
47	1	99	48.58	2	1	1	0	1	3	1	384	1	409	0	0
48	2	99	35.08	1	9	0	0	0	1	0	966	0	966	0	1
49	2	99	59.83		10	0	0	0	1	0	965	0	965	0	1
50	1	99	33.63	2	1	1	1	0	2	1	531	1	531	0	0
51	2	99	13.8	1	9	0	0	0	1	0	716	0	716	0	1
52	2	99	6.24	1	10	1	1	0	2	0	721	0	721	0	1
53	2	99	25.04	1	9	0	0	0	1	0	671	0	671	0	1
54	2	99	17.79	2	10	0	0	0	1	0	538	0	538	0	0
55	2	99	28.11		10	0	0	0	1	1	574	1	574	0	1
56	1	99	28	1	2	0	0	0	1	0	644	0	644	0	0
57	1	99	26.01	1	9	0	0	0	1	0	480	0	480	0	1

ID	sex	study	age	vol.	site	met.	lung-met.	met. other than lung	risk group	event	EFS	alive	OS	STEAP1 cyto.	STEAP1 memb.
58	2	99	14	2	1	0	0	0	1	0	706	0	706	0	1
59	1	99	16.35		8	1	1	0	2	1	497	1	704	1	0
60	2	99	27.8	1	9	0	0	0	1	0	569	0	569	0	1
61	2	99	18.29	1	10	0	0	0	1	1	253	1	443	0	1
62	1	99	46.79	1	3	0	0	0	1	0	454	0	454	0	1
63	1	99	25.25	2	1	1	1	1	3	1	340	0	608	0	0
64	2	99	9.73	1	9	1	1	1	3	0	489	0	489	0	1
65	2	99	15.25	2	1	0	0	0	1	0	399	0	399	1	0
66	1	99	14.82	2	9	1	1	0	2	1	407	1	464	0	1
67	1		9.15		4	0	0	0	1	0	157	0	157	1	1
68	2		5.61		4	0	0	0	1	0	139	0	139	1	1
69	2		13.67		1	0	0	0	1	0	2600	0	2600	1	0
70	2		17.81		9	1	0	1	3	1	266	0	266	1	1
71	1		3.48		8	0	0	0	1	1	365	0	424	1	1
72	2		11.74		7	0	0	0	1	0	150	0	150	1	1
73	2		17.69		9	1	1	0	2	1	471	0	471	1	1
74	2		19.46		9	0	0	0	1	0	0	0	0	1	1
75	1		15.34		1	0	0	0	1	0	2161	0	2161	0	1
76	1		16.93		8	0	0	0	1	0	3051	0	3051	1	1
77	2		12.54		1	1	1	0	2	0	3	0	2876	1	1
78	1		29.71		10	0	0	0	1	0	403	0	403	1	0
79	1		4.67		4	0	0	0	1	0	471	0	471	0	0
80	2		12.18		1	0	0	0	1	0	1449	0	1449	0	1
81	2		5.81		7	1	1	1	3	0	1133	1	1133	0	1
82	2		59.79		1	0	0	0	1	0	3420	0	3420	0	1
83	1		15.27		8	0	0	0	1	0	2091	0	2091	1	1
84	2		35.16		1	0	0	0	1	0	1543	0	1543	0	1
85	2		59.37		10	0	0	0	1	0	2685	0	2685	0	1
86	1		26.44		1	0	0	0	1	0	4150	0	4150	1	1
87	1		19.94		4	0	0	0	1	0	4346	0	4346	1	1
88	2		21.49		8	0	0	0	1	0	2645	0	2645	1	0
89	1		51.71		9	0	0	0	1	0	493	0	493	1	0
90	1		25.03		2	0	0	0	1	1	691	1	1181	1	0
91	2		7.37		9	0	0	0	1	0	1426	0	1426	0	1
92	2		17.39		1	0	0	0	1	0	277	1	277	0	1
93	2		10.21		4	0	0	0	1	0	5712	0	5712	1	0
94	1		18.67		9	0	0	0	1	0	2899	0	2899	1	1
95	2		14.7		4	1	1	0	2	1	470	1	830	0	0
96	1		28.4		6	0	0	0	1	0	3322	0	3322	0	1
97	1		24.32		7	0	0	0	1	0	828	0	828	0	1
98	2		7.96		10	0	0	0	1	1	171	0	213	0	0
99	1		13.38		2	0	0	0	1	0	3745	0	3745	0	1

ID	sex	study	age	vol.	site	met.	lung-met.	met. other than lung	risk group	event	EFS	alive	OS	STEAP1 cyto.	STEAP1 memb.
100	2		4.83		9	1	1	1	3	1	252	1	2084	0	0
101	2		8.05		1	0	0	0	1	0	5422	0	5422	1	0
102	1		19.99		2	0	0	0	1	1	440	1	665	0	0
103	2		34.74		6	0	0	0	1	1	816	1	1028	0	0
104	1		28.44		8	0	0	0	1	0	3582	0	3582	0	0
105	1		18.59		1	0	0	0	1	0	4383	0	4383	0	0
106	1		16.33		8	0	0	0	1	0	1882	1	1882	0	0
107	1		18.98		9	1	1	0	2	1	699	1	958	1	1
108	2		16.84		9	1	1	0	2	1	784	1	1132	1	0
109	2	99	6.36		6	0	0	0	1	0	4138	0	4138	0	1
110	1	99	3.88	1	9	0	0	0	1	1	466	1	952	0	1
111	1	99	13.52	1	4	0	0	0	1	0	2342	0	2342	0	1
112	1	99	17.07	1	9	0	0	0	1	0	2903	0	2903	0	0
113	2	99	18.15		9	1	0	1	3	1	271	1	325	1	0
114	1	92	26.21	2	9	0	0	0	1	0	527	0	527	0	0

9.5 List of figures

9.6 List of tables

9.7 List of abbreviations

ALL	acute lymphoblastic leukemia
cDNA	complementary DNA
ChIP	chromatin immunoprecipitation
ET	Ewing tumors
EWS/ETS	Ewing sarcoma breakpoint region 1 / E-twenty-six
EWS/FLI1	Ewing sarcoma breakpoint region 1 / friend leukemia virus integration 1
FMN	flavin mononucleotide
FNO	F420:NADPH oxidoreductase
GO	gene ontology
GSEA	gene-set enrichment analysis
GSH	glutathione
GSSG	glutathione-disulfide
HR	hazard ratio
HRP	horseradish peroxidase
IF	indirect immunofluorescence
IGF1	insulin-like growth factor 1
IHC	immunohistochemistry
IRB	institutional review board
H_2O_2	hydrogen peroxide
KO	knockout
mRNA	messenger RNA
miRNA	micro RNA
MSCs	mesenchymal stem cells
NAC	N-acetyl-cysteine
NAD	nicotinamide adenine dinucleotide
NBL	neuroblastoma
NCI	National Cancer Institute
NOX	NADPH oxidoreductase
NTC	no-template-control
OS	overall survival
PI	propidium iodide
PBMCs	peripheral blood mononuclear cells
qRT-PCR	quantitative Real-Time PCR
RNAi	RNA interference
ROS	reactive oxygen species
RT	room temperature
SD	standard deviation
SDS-PAGE	sodium-dodecylsulfate-polyacrylamid-gelelectrophoresis
SEER	Surveillance Epidemiology and End Results
SEM	standard error of the mean
siRNA	small interfering RNA
shRNA	short hairpin RNA
STEAP	six-transmembrane epithelial antigen of the prostate
STEAPs	STEAP proteins
TMA	tissue microarray
UPS	ubiquitin-proteasome-system
WB	Western blot

10 Acknowledgement

I would like to thank my supervisor Univ.-Prof. Dr. med. Stefan Burdach (Chair of the Department of Pediatrics, Klinikum rechts der Isar, Technische Universität München) for his enthusiastic support throughout my doctorate, his constant motivation to look beyond the already known and his true encouragement to work in my own way.

I am grateful for the fruitful discussions with my advisors Univ.-Prof. Dr. med. Irene Esposito (Department of Pathology, Klinikum rechts der Isar, Technische Universität München) and Prof. Dr. rer. nat. Achim Krüger (Institut für Experimentelle Onkologie und Therapieforschung, Klinikum rechts der Isar, Technische Universität München) and their helpful comments on the manuscripts prior to submission.

I thank Dr. rer. nat. Günther Richter (Department of Pediatrics, Klinikum rechts der Isar, Technische Universität München) for his kind technical and administrative support.

This thesis would not have been possible without the excellent support of my many collaboration partners to which I owe my deepest gratitude. I am especially grateful to Prof. Dr. rer. nat. Elke Butt (Institute for Clinical Biochemistry, University of Würzburg) for her continuous and outstanding biochemical advice and to Dr. phil. Andreas Ranft (Department of Pediatrics, University Hospital of Münster) for his excellent statistical advice.

I would like to show my gratitude to all of my colleagues for their social and technical support. In particular I thank Mrs. Colette Zobywalski for her expert technical assistance and Dr. med. Uwe Thiel (both Department of Pediatrics, Klinikum rechts der Isar, Technische Universität München) for his integrity and sincere friendship.

I thank my best man and true friend Veit R. Buchholz for countless inspiring scientific discussions and proof-reading of my manuscripts prior to submission.

I am indepted to my wife, Dr. med. Barbara Grünewald, who has warmly supported me throughout all my studies, for her love and patience in the past years.

11 Publications derived from this Ph.D. thesis

Original articles (peer-reviewed)

Grunewald TG, Diebold I, Esposito I, Plehm S, Hauer K, Thiel U, da Silva-Buttkus P, Neff F, Unland R, Müller-Tidow C, Zobywalski C, Lohrig K, Lewandrowski U, Sickmann A, Prazeres da Costa O, Görlach A, Cossarizza A, Butt E, Richter GH, Burdach S

"STEAP1 is associated with the invasive and oxidative stress phenotype of Ewing tumors"

Molecular Cancer Research, 2012 Jan;10(1):52-65

Grunewald TG, Ranft A, Esposito I, da Silva-Buttkus P, Aichler M, Baumhoer D, Schaefer KL, Ottaviano L, Poremba C, Jundt G, Juergens H, Dirksen U, Richter GH, Burdach S

"High STEAP1 expression is associated with improved outcome of Ewing's sarcoma patients"

Annals of Oncology, 2012 Aug;23(8):2185-90

Contributions to congresses

Grunewald TG and Burdach S

Poster: "STEAP1 overexpression modulates the invasive and oxidative stress phenotype of Ewing tumor cells and predicts outcome of Ewing tumor patients"

Pediatric Cancer Translational Genomics conference, Phoenix/USA, 02/2012